On the Rigidity of Disordered Networks

by

Varda Faghir Hagh

A Dissertation Presented in Partial Fulfillment
of the Requirements for the Degree
Doctor of Philosophy

Approved July 2018 by the
Graduate Supervisory Committee:

Michael F. Thorpe, Chair
Oliver Beckstein
Ralph V. Chamberlin
Kevin E. Schmidt

ARIZONA STATE UNIVERSITY

December 2018

ABSTRACT

The rigidity of a material is the property that enables it to preserve its structure when deformed. In a rigid body, no internal motion is possible since the degrees of freedom of the system are limited to translations and rotations only. In the macroscopic scale, the rigidity and response of a material to external load can be studied using continuum elasticity theory. But when it comes to the microscopic scale, a simple yet powerful approach is to model the structure of the material and its interparticle interactions as a ball−and−spring network. This model allows a full description of rigidity in terms of the vibrational modes and the balance between degrees of freedom and constraints in the system.

In the present work, we aim to establish a microscopic description of rigidity in *disordered* networks. The studied networks can be designed to have a specific number of degrees of freedom and/or elastic properties. We first look into the rigidity transition in three types of networks including randomly diluted triangular networks, stress diluted triangular networks and jammed networks. It appears that the rigidity and linear response of these three types of systems are significantly different. In particular, jammed networks display higher levels of self-organization and a non-zero bulk modulus near the transition point. This is a unique set of properties that have not been observed in any other types of disordered networks. We incorporate these properties into a new definition of jamming that requires a network to hold one extra constraint in excess of isostaticity and have a finite non-zero bulk modulus. We then follow this definition by using a tuning by pruning algorithm to build spring networks that have both these properties and show that they behave exactly like jammed networks. We finally step into designing new disordered materials with desired elastic properties and show how disordered auxetic materials with a fully convex geometry can be produced.

TABLE OF CONTENTS

CHAPTER Page

LIST OF TABLES

LIST OF FIGURES

Figure Page

Figure Page

Figure Page

Chapter 1

INTRODUCTION

Rigidity of a structure is an important property that prevents it from failure and controls its behavior under external load. To a large extent, the mechanical properties and elastic response of materials can be understood by modeling their interconnected structure as ball−and−spring networks. A ball−and−spring network is a graph-like structure that consists of nodes connected to one another by simple harmonic springs as edges [1] . These edges represent the interactions between the nodes. In principle, each node interacts with its neighboring nodes through a Hookean potential. The range of interactions is usually nearest neighbors, but further neighbors can be included as well. Here, the focus is on the rigidity of disordered networks. Disordered networks are the network representations of non-crystalline solids that do not possess a long range positional order in their structure. Figure 1.1 displays an example of such networks. These types of networks have helped us understand the physics of many amorphous systems such as glasses [2], polymers [3], jamming [4], auxetics [5], and designer materials [6].

This dissertation is organized such that the first chapter introduces the concept of rigidity using two different approaches: *dynamical approach* and *constraint count approach*. In dynamical approach, one studies the time evolution of a structure when it undergoes an external load. In the constraint count approach, the rigidity of a system is defined solely based on the number of degrees of freedom and constraints that

[1] In this Dissertation, we use "node", "site", and "vertex" interchangeably. This also holds for the words "edge" and "bond".

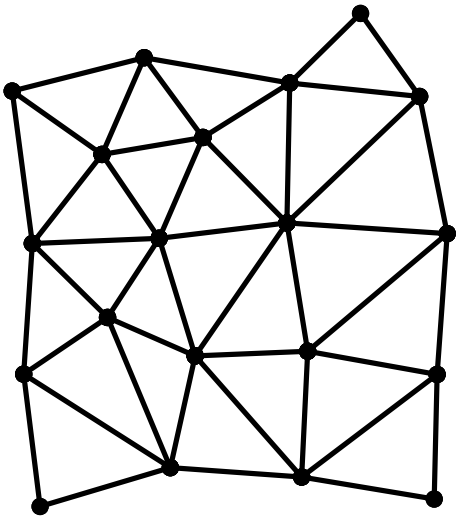

Figure 1.1: A Finite Disordered Network With 20 Nodes and 44 Edges.

balance them. This chapter also reviews the linear response theory and provides the relevant mathematical tools that will be extensively used throughout the dissertation.

The second chapter introduces ideas from percolation theory and studies the critical behavior of two distinct models in detail. This chapter does not address the rigidity directly, but builds a connection between the concepts of loops in bond percolation and stress in rigidity percolation. Thus, it paves the way for understanding the rigidity transition which is the main subject of the following chapter.

In chapter three, we study rigidity transition and linear response of three different types of networks: randomly diluted networks, stress diluted networks, and jamming [7]. This study reveals some fundamental properties of jammed networks in terms of their rigidity, self-organization, and linear response that distinguish them from randomly generated rigid systems. This chapter has helped us understand the structural and mechanical properties of jamming and has led to what comes in chapter four which puts jamming in perspective.

In chapter four, we establish a new definition for jamming based on the rigidity

and linear response of jammed networks. We also introduce a new method to build a jammed packing without employing conventional methods of pushing particles together. The new method starts from a fully triangulated spring network and encodes the jamming properties into the network by pruning its edges in a particular order. The final pruned network can be mapped into a unique circle packing in 2D that has the same bulk properties as a conventional disk packing [8].

The fifth chapter uses the ideas developed in chapter four to create materials with customized mechanical response by removing edges from a triangulated disordered network. In particular, it describes the design of a new type of auxetic structures. These structures are rigid and respond to longitudinal compression in an unusual way [9].

Finally, the conclusion chapter gives a summary of the ideas visited in this dissertation and points out the possible future directions.

1.1 What Is Rigidity?

Rigidity is the ability of a material to sustain its structure while undergoing deformations. With a ball−and−spring model, such deformations can be considered topological, geometrical, or a combination of both. In topological deformations, the connections between the particles are changed; either new bonds are formed between previously non-bonded nodes or an existing bond is broken between two nodes. Geometrical deformations are caused by changes in the positions of nodes through local distortions and/or bulk deformations.

The mechanical response of a spring network to deformations and external load depends on the global and local force balances on the nodes [10]. In general, the mechanical stability of a network is governed by a few key factors, including the

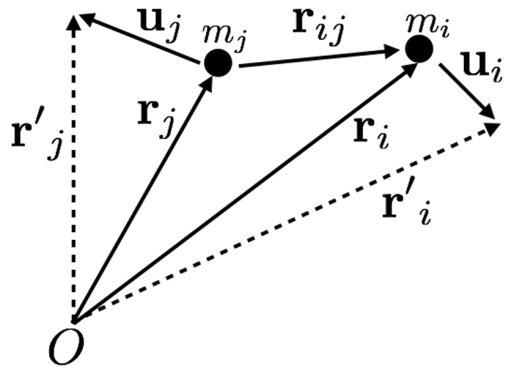

Figure 1.2: Two Nodes i and j are Shown with Masses m_i and m_j, Respectively. Displacing the Particles Changes Their Distance, which for Small Displacements is Equal to the Component of the Displacement which is Parallel to the Vector Connecting i and j. The Point O is the Origin.

positions of its nodes, the number of its edges, and their distributions. Since the edges are considered harmonic springs, a deformation in general leads to changes in the rest lengths of the springs and therefore some energy is stored in the system. Hence, the rigidity of a network can be studied by looking into the changes in the edge lengths after applying a deformation. This is the dynamical approach to the study of rigidity. Before getting into more details about this approach, we should first develop the mathematical tools and definitions that will be needed along the way.

For this purpose, consider N points (nodes) distributed over a $d-$dimensional space, where $\mathbf{r}_i$ denotes the position of point i. The network is formed by placing N_e edges between these nodes. The length l_{ij} of the edge connecting nodes i and j is their Euclidean distance:

$$l_{ij} = |\mathbf{r}_i - \mathbf{r}_j| \tag{1.1}$$

where $|\bullet|$ represents the norm of a vector. If two nodes interact through central forces only (which is the case for spring networks), the force between the nodes will be along the edge that is connecting them or their *contact vector*. The contact vector $\mathbf{n}_{ij}$ is

the unit vector from j to i, defined as:

$$\mathbf{n}_{ij} = \frac{\mathbf{r}_i - \mathbf{r}_j}{l_{ij}} = \frac{\mathbf{r}_{ij}}{l_{ij}}. \tag{1.2}$$

After applying a small deformation, point i is displaced by $\mathbf{u_i}$ and its new position $\mathbf{r'}_i$ is given by (see Figure 1.2):

$$\mathbf{r'}_i = \mathbf{r}_i + \mathbf{u}_i \tag{1.3}$$

Now, if the nodes at the two ends of an edge are both slightly displaced, the displacement vector can be decomposed into two parts, one of which is parallel ($\|$) and the other is perpendicular ($\perp$) to the edge:

$$\mathbf{u}_{ij} = \mathbf{u}_i - \mathbf{u}_j = \mathbf{u}_{ij,\|} + \mathbf{u}_{ij,\perp} = (\mathbf{u}_{ij}.\mathbf{n}_{ij})\mathbf{n}_{ij} + \mathbf{u}_{ij,\perp} \tag{1.4}$$

The vector connecting i and j after they are displaced can be written in terms of these parallel and perpendicular components:

$$\mathbf{r'}_i - \mathbf{r'}_j = (\mathbf{r}_i - \mathbf{r}_j) + (\mathbf{u}_i - \mathbf{u}_j) \tag{1.5}$$

$$= l_{ij}\mathbf{n}_{ij} + \mathbf{u}_{ij} \tag{1.6}$$

$$= l_{ij}\mathbf{n}_{ij} + (\mathbf{u}_{ij}.\mathbf{n}_{ij})\mathbf{n}_{ij} + \mathbf{u}_{ij,\perp} \tag{1.7}$$

$$= (l_{ij} + u_{ij,\|})\mathbf{n}_{ij} + \mathbf{u}_{ij,\perp} \tag{1.8}$$

And the change in the length of the edge between i and j now becomes:

$$\Delta_{ij} = l'_{ij} - l_{ij} = |\mathbf{r'}_i - \mathbf{r'}_j| - |\mathbf{r}_i - \mathbf{r}_j| \tag{1.9}$$

$$= \sqrt{(l_{ij} + u_{ij,\|})^2 + (u_{ij,\perp})^2} - l_{ij} \tag{1.10}$$

which for small displacements ($|u| \ll 1$) can be written as:

$$\Delta_{ij} \approx l_{ij} + u_{ij,\|} + \frac{u_{ij,\perp}^2}{2l_{ij}} - l_{ij} = u_{ij,\|} + \frac{(u_{ij,\perp})^2}{2l_{ij}} + \mathcal{O}(u^3) \tag{1.11}$$

Meaning that the change in the edge length is equal to the the parallel component of displacement to the first order. This allows us to write the change in the length of an edge in terms of the motion of its two ends up to the first order as:

$$\Delta_{ij} = u_{ij,\parallel} = \mathbf{u}_{ij}.\mathbf{n}_{ij} = \mathbf{n}_{ij}.\mathbf{u}_i + \mathbf{n}_{ji}.\mathbf{u}_j \tag{1.12}$$

Note that $\mathbf{n}_{ij} = -\mathbf{n}_{ji}$. A similar equation can be written for any edge in the network. Therefore, this is a system of N_e equations for all the edge lengths. If we define the transpose of the displacement matrix for all the nodes as $\mathbf{u}^T = [\mathbf{u}_1, \mathbf{u}_2, \ldots, \mathbf{u}_N]$, then this set of equations can be written in a matrix form as:

$$\boldsymbol{\Delta} = \mathbf{R}\mathbf{u}, \tag{1.13}$$

where $\mathbf{R}$ is called the *rigidity matrix* and contains geometrical and topological information about the network. The entries of $\mathbf{R}$ are the contact vectors $\mathbf{n}_{ij}$:

$$\mathbf{R} = \begin{array}{c} \\ \vdots \\ (i,j) \\ \vdots \end{array} \begin{array}{c} \begin{array}{ccccccc} 1 & \ldots & i & \ldots & j & \ldots & N \end{array} \\ \begin{pmatrix} \vdots & \ddots & \vdots & \ldots & \vdots & \ddots & \vdots \\ \mathbf{0} & \ldots & \mathbf{n}_{ij} & \ldots & \mathbf{n}_{ji} & \ldots & \mathbf{0} \\ \vdots & \ddots & \vdots & \ldots & \vdots & \ddots & \vdots \end{pmatrix} \end{array} \tag{1.14}$$

Each column corresponds to a node while each row represents an edge. Hence, $\mathbf{R}$ is a $N_e \times dN$ matrix where each row has at most $2d$ non-zero entries. With a total of at most $2dN_e$ non-zero elements, it is a sparse matrix for large N.

Eq. (1.13) relates the changes in the edge lengths to displacements of the nodes through rigidity matrix. In general, displacing the nodes of a network changes the set of its edge lengths. However there might exist motions that leave the edge lengths fixed. A deformation that does not change any edge length is a *degree of freedom* or a *floppy mode* of the network. In other words, a floppy mode is a deformation with no energy cost. For example, consider a finite ball−and−spring network with

free boundary conditions and a prescribed set of edge lengths. If all the nodes are displaced by the same vector, the entire system is translated without any changes in the edge lengths. To see this more clearly, let us assume that all the nodes are translated by vector $\mathbf{u}$. From Eq. (1.13), the change in the edge length between i and j is:

$$\Delta_{ij} = \mathbf{n}_{ij}.\mathbf{u} + \mathbf{n}_{ji}.\mathbf{u} = (\mathbf{n}_{ij} + \mathbf{n}_{ji}).\mathbf{u} = 0, \tag{1.15}$$

which is correct for all the edges since $\mathbf{n}_{ij} = -\mathbf{n}_{ji}$. The net translation is a floppy mode of the system, however a *trivial* one which is due to a rigid motion. Symmetries and boundary conditions can greatly impact the rigidity of a structure and its number of floppy modes. For example in the above example, if one node is fixed in place, the translational symmetry is broken and there will be no translational degrees of freedom. On the other hand, a system with periodic boundary conditions has no rotational degrees of freedom. But if the volume of its unit cell is allowed to change, new floppy modes will be introduced to the system and the rigidity matrix should be modified accordingly.

To explore the effect of these additional floppy modes on the rigidity matrix, consider a network under periodic boundary conditions which tiles the space with a unit cell of N nodes and N_e edges. The edges far from the boundary have a length that equals the Euclidean distance of their ends. But for the nodes that are close to the boundary, the edges connecting them might cross the unit cell boundary and therefore a *minimum image convention* should be used to ensure that bonding is between the nearest neighbors. In this case the edge length norm is modified as:

$$l_{ij} = |\mathbf{r}_i - \mathbf{r}_j + \mathbf{T}_{ij}| \tag{1.16}$$

where $\mathbf{T}$ is a translation vector to find the correct image of node j that gives the proper length for the edge between i and j. Note that for nodes far from boundary

$\mathbf{T}_{ij} = \mathbf{0}$.

There are two types of deformations that can change the edge lengths in a periodic network: (1) changing the positions of the nodes, and (2) changing the shape of the unit cell. If we let the nodes at the two ends of an edge move by $\mathbf{u}_i$ and $\mathbf{u}_j$ respectively, and then let the volume of the unit cell change (which is equivalent to changing the translation vectors) so that $\mathbf{T'}_{ij} = \mathbf{T}_{ij} + \mathbf{v}_{ij}$, the new edge length will be:

$$l'_{ij} = |\mathbf{r}_i - \mathbf{r}_j + \mathbf{T} + \mathbf{u}_i - \mathbf{u}_j + \mathbf{v}_{ij}| \tag{1.17}$$

For small displacements, this l'_{ij} can be expanded to find the change in the length of the i-j edge up to the first order:

$$\Delta_{ij} \approx \mathbf{n}_{ij}.(\mathbf{u}_{ij} + \mathbf{v}_{ij}) \tag{1.18}$$

This equation can be written in a matrix form similar to Eq. (1.13) but with an "augmented" rigidity matrix and a modified displacement matrix $\mathbf{u}^T = [\mathbf{u}_1, \mathbf{u}_2, \ldots, \mathbf{u}_N, \mathbf{v}]$:

$$\boldsymbol{\Delta} = \mathbf{R}\mathbf{u}, \tag{1.19}$$

where the new rigidity matrix has the following form:

$$\mathbf{R} = \begin{array}{c} \\ \vdots \\ (i,j) \\ \vdots \end{array} \begin{array}{c} \begin{array}{ccccccc} 1 & \ldots & i & \ldots & j & \ldots & N \end{array} \\ \left(\begin{array}{ccccccc|c} \vdots & \ddots & \vdots & \ldots & \vdots & \ddots & \vdots & \vdots \\ \mathbf{0} & \ldots & \mathbf{n}_{ij} & \ldots & \mathbf{n}_{ji} & \ldots & \mathbf{0} & \mathbf{n}_{ij} \\ \vdots & \ddots & \vdots & \ldots & \vdots & \ddots & \vdots & \vdots \end{array}\right) \end{array} \quad \text{volume change} \tag{1.20}$$

New degrees of freedom are added as columns but the exact number of columns depend on the allowed variables. For example, in two dimensions there are two repeat vectors and up to three new degrees of freedom are possible when the volume of the unit cell is allowed to change. These include the lengths of two repeat vectors and the angle between them. A more detailed account of the impact of boundary conditions and symmetries on floppy modes is given in section 1.3.

1.2 Dynamical Approach to Rigidity

The static picture developed in previous section is useful for studying the rigidity of spring networks. This representation also allows us to explore the dynamics of these networks. In particular, vibrations of a network and its interaction with elastic waves are of great interest. To study the dynamics, we first write down the Hamiltonian of the system as:

$$\mathcal{H} = \frac{1}{2}\sum_{i=1}^{N} m_i \dot{\mathbf{u}}_i^2 + U(\{\mathbf{u}_i\}). \tag{1.21}$$

where the first term is the kinetic energy and the second term represents the potential energy of the system. In the kinetic energy term, $\dot{\mathbf{u}}_i$ is the velocity vector of node i and m_i is its mass. This term can be fully written in a vector notation. Let $\dot{\mathbf{u}}^T = [\dot{\mathbf{u}}_1, \dot{\mathbf{u}}_2, \ldots, \dot{\mathbf{u}}_N]$ be the velocity vector of all the nodes in the system and $\mathbf{M}$ be the diagonal matrix of masses. The Hamiltonian can now be rewritten as:

$$\mathcal{H} = \frac{1}{2}\dot{\mathbf{u}}^T \mathbf{M} \dot{\mathbf{u}} + U(\{\mathbf{u}_i\}). \tag{1.22}$$

In general, the potential energy U is a function of displacement vector $\mathbf{u}$, but for a central force network we have $U(\{\mathbf{u}_i\}) = U(\{u_i\})$. The energy stored in a typical edge due to a small change in its length can be expanded up to the second order of displacements as:

$$U\left(l' - l\right) = U\left(l\right) + \left.\frac{dU}{dl'}\right|_l \left(l' - l\right) + \frac{1}{2}\left.\frac{d^2U}{dl'^2}\right|_l \left(l' - l\right)^2 + \ldots \tag{1.23}$$

$$\approx U\left(l\right) + U'(l)\left(u_\parallel + \frac{u_\perp^2}{2l}\right) + \frac{1}{2}U''(l)u_\parallel^2 \tag{1.24}$$

using Eq. (1.11). This can be generalized to every edge in the system. The total potential energy is then the sum of stored energy in all the edges. The energy expression in Eq. (1.24) has three main contributors: $U(l)$ which is a constant value and can be arbitrarily set to $U(l) = 0$ by assuming that the system is not initially stressed. $U'(l)$,

which is the first derivative of energy with respect to changes in the edge length (due to displacement of nodes) and represents the forces (*e.g.* friction or pre-stress) in the network. If the system is assumed to be at mechanical equilibrium then $U'(l) = 0$. And finally the harmonic term $U''(l) = k$, where k is the stiffness or force constant or spring constant of the stretched/compressed edge. So using Eq. (1.12) and setting both $U(l)$ and $U'(l)$ terms to zero, the energy stored in an edge up to the second order in displacements is:

$$U_{ij} = \frac{1}{2}U''(l)u_{ij,\parallel}^2 = \frac{1}{2}k_{ij}\Delta_{ij}^2 \tag{1.25}$$

It is sometimes more convenient to represent ij subscripts as a compact index such as $ij \to \alpha$. In this notation, the nodes are labeled by Latin letters while the edges are labeled using the Greek alphabet. Using this new notation, the total potential energy can be written in a matrix form as:

$$\begin{aligned} U &= \frac{1}{2}\sum_{\alpha=1}^{N_e} k_\alpha \Delta_\alpha^2 \\ &= \frac{1}{2}\begin{pmatrix}\Delta_1 \dots \Delta_{N_e}\end{pmatrix}\begin{pmatrix} k_1 & 0 & \dots & 0 \\ 0 & k_2 & \dots & 0 \\ \vdots & \vdots & \ddots & \vdots \\ 0 & 0 & \dots & k_{N_e}\end{pmatrix}\begin{pmatrix}\Delta_1 \\ \vdots \\ \Delta_{N_e}\end{pmatrix} = \frac{1}{2}\mathbf{\Delta}^T\mathbf{K}\mathbf{\Delta}. \end{aligned} \tag{1.26}$$

where $\mathbf{K}$ is a $N_e \times N_e$ diagonal matrix with elements that are equal to the force constants (stiffness of the springs). Replacing $\mathbf{\Delta}$ by Eq. (1.19) gives:

$$U = \frac{1}{2}\mathbf{\Delta}^T\mathbf{K}\mathbf{\Delta} = \frac{1}{2}\mathbf{u}^T\mathbf{R}^T\mathbf{K}\mathbf{R}\mathbf{u} = \frac{1}{2}\mathbf{u}^T\mathbf{H}\mathbf{u} \tag{1.27}$$

where $\mathbf{H} = \mathbf{R}^T\mathbf{K}\mathbf{R}$ is the Hessian or stiffness matrix with elements being the second-derivatives of the potential energy with respect to displacements.

Under a deformation, the elongation or compression of all the edges can be rep-

resented as a matrix called the tension matrix which has the following form:

$$\mathbf{f} = \mathbf{K}\boldsymbol{\Delta} = \mathbf{K}\mathbf{R}\mathbf{u} \tag{1.28}$$

The potential energy can also be written in terms of this tension matrix:

$$U = \frac{1}{2}\mathbf{f}^T\mathbf{K}^{-1}\mathbf{f} \tag{1.29}$$

since $\mathbf{K}^T = \mathbf{K}$. But we will use the form given in Eq. (1.27).

Now, the Hamiltonian in the absence of external forces can be written in a fully vectorial (coordinate-free) form in harmonic approximation:

$$\mathcal{H} = \frac{1}{2}\dot{\mathbf{u}}^T\mathbf{M}\dot{\mathbf{u}} + \frac{1}{2}\mathbf{u}^T\mathbf{H}\mathbf{u}, \tag{1.30}$$

from which the equations of motions for all the nodes can be derived. First, we find the infinitesimal force on particle i:

$$\mathbf{F}_i = -\frac{\partial U}{\partial \mathbf{u}_i} = -\sum_{j=1}^{N}\frac{\partial^2 U}{\partial \mathbf{u}_i \partial \mathbf{u}_j}\mathbf{u}_j = -\sum_{j=1}^{N} H_{ij}\mathbf{u}_j. \tag{1.31}$$

Then using Newton's second law, we can write:

$$\mathbf{F} = \mathbf{M}\ddot{\mathbf{u}} = -\mathbf{H}\mathbf{u} = -\mathbf{R}^T\mathbf{K}\mathbf{R}\mathbf{u} = -\mathbf{R}^T\mathbf{f} \tag{1.32}$$

with $\ddot{\mathbf{u}}$ being the acceleration vector of the system. This is a set of dN equations with wave-like solutions which are equivalent to harmonic oscillations of a many-body system. Assuming that all of the nodes are oscillating with the same angular frequency ω, we propose a solution of the form:

$$\mathbf{u}_j = \mathbf{A}_j e^{i\omega t} e^{-i\mathbf{q}.\mathbf{r}_j} \tag{1.33}$$

where $\mathbf{A}_j$ is the amplitude of vibrations on node j, and $\mathbf{q}$ is the wave-vector which is related to the wavelength λ by $|\mathbf{q}| = 2\pi/\lambda$. To find the normal modes of vibrations,

we insert the proposed wave-like solution into Eq. (1.32) and assume that $\lambda \gg 1$. In this limit, the wavelengths are significantly longer than the spacing between nodes (*i.e.* edge lengths) and the network is considered a continuum with $\mathbf{q} = \mathbf{0}$. Now, we can write:

$$\omega^2 \mathbf{A} = \left(\mathbf{M}^{-1}\mathbf{R}^T\mathbf{K}\mathbf{R}\right)\mathbf{A} = \mathbf{D}\mathbf{A} \tag{1.34}$$

where $\mathbf{D}$ is called the dynamical matrix of the system[2]. The problem is now reduced to an eigenvalue problem where ω^2 is the eigenvalue of $\mathbf{D}$ with eigenvector $\mathbf{A}$ which contains the oscillation amplitudes of all the nodes in the system. Note that the network is assumed to be mechanically stable, hence ω^2 is strictly non-negative but can be zero ($\mathbf{D}$ is positive semi-definite). The eigenvalues are the square of characteristic angular frequency of phonons which is proportional to the energy ($E = \hbar\omega$)[11]. A zero eigenvalue corresponds to a normal mode that has zero energy cost and therefore is a floppy mode of the system.

The eigenvalues can be calculated by diagonalizing the dynamical matrix which is a $dN \times dN$ matrix. Hence for a network with N nodes, there are dN normal mode frequencies. Numerical diagonalization of a large matrix can be difficult; but in the case of spring networks we only consider the short-range harmonic interactions, so the dynamical matrix is extremely sparse. The density of normal mode frequencies is the *density of states* $\mathcal{D}(\omega)$ which is of fundamental importance regarding marginality of the system. This has been studied in more detail in chapter four.

Finally, note that if $\mathbf{q} \neq \mathbf{0}$, then the eigenvalue problem should be modified to include the phase factor in the entries of the rigidity matrix. Since each displacement has a phase factor $e^{-i\mathbf{q}.\mathbf{r}_k}$, then the contact vectors are modified as $\mathbf{n}_{ji} \to \mathbf{n}_{ji}e^{-i\mathbf{q}.\mathbf{r}_j}$. In addition, all the transpose operations should be replaced by their conjugate transpose

[2]Note that for a system where the masses and spring constants are set to unity, as assumed in this Dissertation, the dynamical matrix and Hessian matrix are equal.

operations ($i \to -i$) since the phase factor is a complex number.

1.3 Constraint Count Approach to Rigidity

The stability/rigidity of a structure is determined by whether there are enough constraints to balance out its degrees of freedom or floppy modes. Degrees of freedom in a network are those deformations for which there is no change in the edge lengths and therefore, the stored elastic energy in the system is zero. Using the static and dynamic pictures of deformations developed in previous sections, we can easily find the number of degrees of freedom which depend on symmetry, boundary conditions and constraints present in the system.

Based on Eq. (1.19), we know that the null space of the rigidity matrix corresponds to all motions that do not change any edge lengths or equivalently all the displacements $\mathbf{X}$ for which:

$$\mathbf{\Delta} = \mathbf{RX} = \mathbf{0}. \tag{1.35}$$

where $\mathbf{X}$ is called the (right) null space of the rigidity matrix $\mathbf{R}$. This is a set of N_e linear equations for dN unknown displacements. The rigidity matrix is characterized by its number of linearly independent rows/columns (*i.e* rank($\mathbf{R}$)), and the number of solutions to Eq. (1.35) (*i.e* nullity($\mathbf{R}$)) which is equal to the number of degrees of freedom (F) in the network. Therefore, $F = \text{nullity}(\mathbf{R})$ and $\mathbf{X}$ is a $dN \times 1$ matrix. The rank-nullity theorem [12] requires that[3]:

$$\text{rank}(\mathbf{R}) + F = dN \tag{1.36}$$

The above equation is the result of infinitesimal displacements with no subsequent changes in the edge lengths. The rank of $\mathbf{R}$ or the number of independent rows/columns

[3] Note that equation 1.35 shows that $\mathbf{X}$ is the null space of $\mathbf{H}$ as well, since $\mathbf{HX} = \mathbf{R}^T\mathbf{KRX} = \mathbf{0}$, so nullity($\mathbf{R}$) = nullity($\mathbf{H}$). This means rank($\mathbf{R}$) = rank($\mathbf{R}^T$) = rank($\mathbf{H}$).

greatly depends on the symmetries of the system. So it is generally assumed that the network is *generic*, meaning that no special symmetry is present in the system except the trivial rigid motions such as rotations or translations.

The force balance on the system can also provide additional information about the number of degrees of freedom. If the network is under no external load, the net force on each node should be zero. However, the tension in the edges can be non-zero since:

$$\mathbf{F} = -\mathbf{R}^T\mathbf{f} = \mathbf{0}, \tag{1.37}$$

does not require that $\mathbf{f} = 0$. The solutions of Eq. (1.37) are called *states of self stress* with $\mathbf{f}$ representing the set of non-zero tensions on the edges for which the force balance holds. The rank of $\mathbf{R}^T$ is the same as rank($\mathbf{R}$) and its nullity is equal to the number of states of self stress N_r in the network. Now since $\mathbf{R}^T$ has N_e columns, the rank-nullity theorem reads:

$$\text{rank}(\mathbf{R}) + N_r = N_e. \tag{1.38}$$

Although rank($\mathbf{R}$) is not accessible unless explicitly computed, but by eliminating it from both Eqs. (1.36) and (1.38), the following count is found:

$$F - N_r = dN - N_e. \tag{1.39}$$

The right-hand side of above equation is equal to a *naive* count of degrees of freedom. dN is the total number of translational degrees of freedom for the nodes in the network whereas each edge constrains one degree of freedom. In two dimensions for example, each node has two degrees of freedom corresponding to its two trivial rigid motions and each edge brings one constraint by fixing the distance between these nodes. Any finite 2D network has at least three floppy modes, corresponding to the two global

translations and one global rotation on the plane. If the only remaining allowed motions in a network and every sub-graph of the network are these three floppy modes, and if the network does not have any states of self stress, it is said to be minimally rigid or *locally isostatic*. Whereas if the number of degrees of freedom is large compared to the number of constraints and there is not a macroscopic rigid structure, the network is said to be underconstrained or *floppy*. On the other hand, when there are more constraints than degrees of freedom, a fraction of these constraints will not be necessary to maintain the rigidity of the network. Such constraints are called "redundant" and the system is said to be overconstrained or *stressed*. Each redundant edge creates one state of self stress in the system. Therefore the number of redundant edges can be found by calculating the number of states of self stress which is equal to the number of non-trivial solutions to Eq. (1.37). Since addition of a redundant edge does not reduce the number of degrees of freedom, in counting the number of floppy modes all the redundant edges should be excluded from the list of constraints [13]. This has been applied to the left-hand side of Eq. (1.39).

The count of floppy modes can be written in term of a useful quantity called the mean coordination number. The coordination number is defined as the number of incident edges on a node. When referring to a single node, we use the letter z to denote its coordination number. But when we are talking about an entire network, it is useful to look into its mean coordination $\langle z \rangle$ which is defined as:

$$\langle z \rangle = \frac{2N_e}{N} \tag{1.40}$$

The factor 2 comes in because each edge is a shared constraint between two nodes. Using Eq. (1.40), we can write Eq. (1.39) as:

$$F - N_r = dN - N_e = (d - \frac{\langle z \rangle}{2})N \tag{1.41}$$

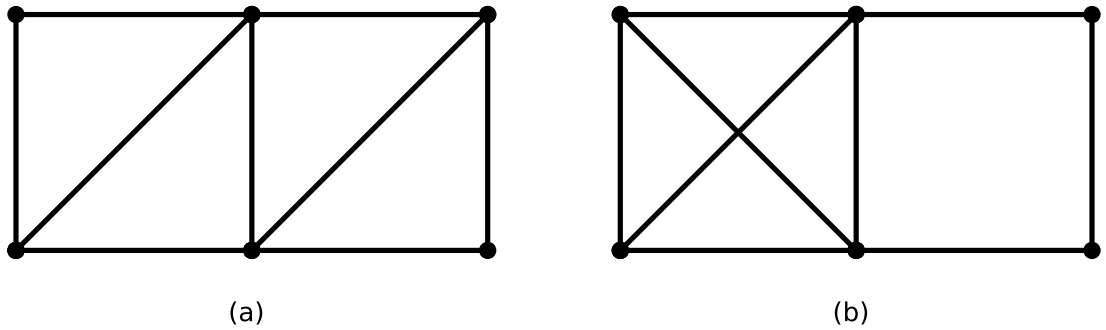

Figure 1.3: Two Graphs with 6 Nodes and 9 Edges which According to Maxwell Count $2 \times 6 - 9 = 3$, Both Should Be Isostatic. While (a) is Isostatic, (B) is Not Since the Square on the Right Can Be Sheared and Has An Internal Floppy Mode. Therefore the Square on Left is Redundantly Rigid and the Right One is Floppy. This Shows the Importance of Edge Distribution in Rigidity of a Structure and Subtleties in Using Maxwell Count to Determine Whether a Structure is Rigid.

At the isostatic point, no redundant edges are present ($N_r = 0$) and the mean coordination number is given by:

$$\langle z \rangle_{\text{iso}} = 2d - \frac{2F}{N} \tag{1.42}$$

At this point, the number of floppy modes F is determined by the global symmetries of the system. In d dimensions and with free boundary conditions for example, there are d translations and $\frac{1}{2}d(d-1)$ rotations, therefore $F = d(d+1)/2$. However, periodic boundary conditions only admit d translations and therefore $F = d$ under periodic boundaries. In the limit of a large system, we have $F \ll N$ and the second term in Eq. (1.42) becomes negligible. So the critical coordination number z_{c} becomes:

$$z_{\text{c}} = 2d \tag{1.43}$$

This critical point defines the point of mechanical stability for a large system. However, a condition such as $\langle z \rangle \geq 2d$ does not guarantee the rigidity of a network. The distribution of edges is an important factor in determining the overall rigidity since regions of a network can be over- or underconstrained even though the mean coordination is greater than $2d$.

The count of floppy modes in Eq. (1.39) is referred to as *Maxwell count*. In 1864, Maxwell developed this simple rule [14] to determine the rigidity of a framework based on the constraints counting of force equilibrium equations developed by Lagrange [15]. However, as mentioned above, this count only provides a global criterion and it is possible to create networks that are partially floppy and partially stressed while the count is satisfied (see Figure 1.3 for an example). Therefore in addition to the global properties of a network, the local arrangement of its nodes and edges should also be investigated when we examine its rigidity.

In 1970, Laman proved that a generic planar graph with $2N-3$ edges is minimally rigid, if and only if, every subgraph with n nodes has at most $2n-3$ edges (compatible with Maxwell count for $d = 2$) [16][4]. This ensures that no subgraph is redundantly rigid while some other subgraph is floppy like the network of Figure 1.3-b. Based on this theorem, a pebble game algorithm [17] can be used to efficiently check the rigidity of subgraphs [18, 19]. This algorithm allows one to analyze the rigidity of graphs with millions of nodes. In addition, since the pebble game is an integer algorithm it can avoid the common issues with numerical precision.

1.4 Linear Response and Elastic Properties of Rigid Networks

The floppy modes of a system are deformations that do not cost energy. However, a deformation generally has a finite energy cost. The linearized equations of motion derived in the previous sections can be used to find the response of a system to an external force. This mechanical response can be further used to control the material's properties. If an external force $\mathbf{F}^{\text{ext}}$ is exerted on a ball−and−spring network, the

[4]The generic nature of the planar graph is important. The existence of additional symmetries such as parallel lines can introduce additional degrees of freedom.

resulting node displacements $\mathbf{v}$ would satisfy the following equation[5]:

$$\mathbf{F}^{\text{ext}} = \mathbf{H}\mathbf{v} \tag{1.44}$$

where $\mathbf{H}$ is the Hessian. Both $\mathbf{F}^{\text{ext}}$ and $\mathbf{v}$ are column matrices with dN elements. Since the Hessian matrix contains the floppy modes, it is not invertible. However, for a given network and external force, the solution can be found numerically using least-squares method which finds a vector $\mathbf{v}$ that minimizes the Euclidean norm $|\mathbf{F}^{\text{ext}} - \mathbf{H}\mathbf{v}|^2$. The least-squares method can be used for any network containing overconstrained, isostatic, and underconstrained regions. The computational complexity of this method is $\mathcal{O}(N^3)$.

Assuming that all springs initially have their rest lengths, the initial elastic energy is zero. But as a result of the external force and node displacements, an elastic energy E is stored in the system which can be calculated from:

$$E = \frac{1}{2}\mathbf{v}^T\mathbf{H}\mathbf{v} \tag{1.45}$$

in the harmonic approximation. For a given deformation or external force, the stored energy is used to characterize the elastic properties of the network. The system's elastic response, however, depends on the properties of the external force. For example, by applying a local force on two ends of an edge, the response of the system to a dipole force can be studied [20]. In the following we study the elastic properties of ball−and−spring networks due to bulk deformations, *i.e.* deformations that are applied to the entire network and the external forces on individual nodes are a result of such deformations.

For simplicity, here we only focus on 2D spring networks with periodic boundary conditions (PBCs). But the results obtained in this section can be generalized to any

[5]Here, we use letter $\mathbf{v}$ to distinguish the set of displacements that are caused by an external force from $\mathbf{u}$ which represented any generic displacement in previous sections.

dimensions. A periodic network in 2D is specified with a supercell containing N nodes and N_e edges and two repeat vectors[6]. The linear combination of the repeat vectors with integer coefficients are translation vectors that tile the plane. From Eq. (1.39) we know that the number of floppy modes for a two dimensional periodic network at the isostatic points is:

$$2N - N_e = 2, \tag{1.46}$$

since the network has 2 trivial translational degrees of freedom.

The bulk deformations of a network under PBCs are applied on a supercell, specifically on the repeat vectors. Assume that the coordinates of nodes and the repeat vectors of the network are expressed in a coordinate system spanned by two axes $\mathbf{a}$ and $\mathbf{b}$ which are not necessarily unit vectors or orthogonal. After applying a small deformation, the $\mathbf{a}$ and $\mathbf{b}$ axes transform into two new vectors $\mathbf{a}'$ and $\mathbf{b}'$ given by [21]:

$$\begin{pmatrix} \mathbf{a}' \\ \mathbf{b}' \end{pmatrix} = (\mathbf{I} + \boldsymbol{\epsilon}) \begin{pmatrix} \mathbf{a} \\ \mathbf{b} \end{pmatrix} = \begin{pmatrix} 1 + \epsilon_{xx} & \epsilon_{xy} \\ \epsilon_{yx} & 1 + \epsilon_{yy} \end{pmatrix} \begin{pmatrix} \mathbf{a} \\ \mathbf{b} \end{pmatrix} \tag{1.47}$$

here $\boldsymbol{\epsilon}$ is the matrix of relative fractional changes in the lengths of $\mathbf{a}$ and $\mathbf{b}$. Due to this transformation, the coordinates of nodes undergo a change which leads to strain in the edges. The strain components can be written up to the first order as:

$$e_{xx} = a' - a \approx a\epsilon_{xx} + \frac{\mathbf{a}.\mathbf{b}}{a}\epsilon_{xy} \tag{1.48}$$

$$e_{yy} = b' - b \approx b\epsilon_{yy} + \frac{\mathbf{a}.\mathbf{b}}{b}\epsilon_{yx} \tag{1.49}$$

$$e_{xy} = e_{yx} = \mathbf{a}'.\mathbf{b}' - \mathbf{a}.\mathbf{b} \approx a^2\epsilon_{yx} + b^2\epsilon_{xy} + (\epsilon_{xx} + \epsilon_{yy})\mathbf{a}.\mathbf{b} \tag{1.50}$$

Although $\mathbf{a}$ and $\mathbf{b}$ are not necessarily orthogonal, they can always be expressed in an orthonormal coordinates system. If $\mathbf{a} \cdot \mathbf{b} = 0$ and $|\mathbf{a}| = |\mathbf{b}| = 1$, the strain tensor $\boldsymbol{e}$

[6]In the literature, it is common to use orthogonal repeat vectors with the same magnitude (the network is contained in a square box). However, it is sometimes unavoidable to use non-orthogonal repeat vectors to represent a certain geometry at minimum energy.

can be written as:

$$\boldsymbol{e} = \begin{pmatrix} e_{xx} & e_{xy} \\ e_{xy} & e_{yy} \end{pmatrix} = \begin{pmatrix} \epsilon_{xx} & \epsilon_{xy} + \epsilon_{yx} \\ \epsilon_{xy} + \epsilon_{yx} & \epsilon_{yy} \end{pmatrix} \tag{1.51}$$

The matrix $\mathbf{e}$ can be decomposed into symmetric and antisymmetric parts. However, it only has three independent components since $e_{xy} = e_{yx}$ according to Eq. (1.50). If $\epsilon_{xy} + \epsilon_{yx} = 0$, then $\mathbf{a}' \cdot \mathbf{b}' = 0$ which corresponds to pure rotation of the coordinates system. To exclude the rotations, we can then assume that $\epsilon_{xy} = \epsilon_{yx}$ with no loss of generality. As a result of this strain, the supercell volume changes such that the fractional change in volume or the *dilation* is:

$$\frac{\Delta V}{V} = \sum_{i=1}^{d} e_{ii} = \text{Trace}\,(\boldsymbol{e}) \tag{1.52}$$

where V is the volume e of the supercell after deformation. In addition to strain in the axes, the edge lengths in the network will also change after this distortion which creates stress (force per unit area) in the system. This stress is characterized by the stress tensor which is defined as [22]:

$$\boldsymbol{\sigma} = \frac{1}{V} \sum_{\alpha} \mathbf{r}_\alpha \otimes \mathbf{F}_\alpha \tag{1.53}$$

where the sum is over all the edges and $\otimes$ shows the outer (tensor) product. The stress tensor is expressed as a $d \times d$ matrix whose elements represent the force direction and the plane to which the force is applied. For example, σ_{xy} is the force applied in the $x-$direction to the unit area of a plane whose normal lies in the $y-$direction. The hydrostatic pressure P is the average of the normal stresses, or the average of main diagonal elements:

$$P = -\frac{1}{d}\text{Trace}\,(\boldsymbol{\sigma}) \tag{1.54}$$

The negative sign is included to emphasize that the forces are compressive. According to Hooke's law, the stress is proportional to strain for small deformations. Therefore

the independent stress components can be written as a linear combination of the strain components:

$$\begin{pmatrix} \sigma_{xx} \\ \sigma_{yy} \\ \sigma_{xy} \end{pmatrix} = \begin{pmatrix} c_{11} & c_{12} & c_{13} \\ c_{21} & c_{22} & c_{23} \\ c_{31} & c_{32} & c_{33} \end{pmatrix} \begin{pmatrix} e_{xx} \\ e_{yy} \\ e_{xy} \end{pmatrix} \Rightarrow \boldsymbol{\sigma} = \mathbf{ce} \tag{1.55}$$

where c_{ij} elements are called the moduli of elasticity[7]. The stress in the network can do work, resulting in a total energy density E/V given by:

$$\frac{E}{V} = \frac{1}{2}\boldsymbol{\sigma}^T \mathbf{e} = \frac{1}{2}\sum_{ij} c_{ij} e_i e_j \tag{1.56}$$

The elastic moduli are the second derivative of this energy density and symmetric under permutation of partial derivatives, *i.e.* $c_{ij} = c_{ji}$. Hence the energy density can be explicitly written as:

$$\frac{E}{V} = \frac{1}{2}\left(c_{11}e_{xx}^2 + c_{22}e_{yy}^2 + c_{33}e_{xy}^2\right) + \left(c_{13}e_{xx} + c_{23}e_{yy}\right)e_{xy} + c_{12}e_{xx}e_{yy} \tag{1.57}$$

for small deformations in harmonic approximation. Computationally, the elastic moduli are calculated by imposing a strain on the repeat vectors. As a result, the edges that cross the boundary exert an external force on the system. The response of the system is calculated using the linear response in Eq. (1.44) and the associated energy stored in the network is equal to the above expression. The distortion applied on a supercell can be quite general. However, three types of deformations are in particular important in the study of elasticity theory. These deformations are shown in Figure 1.4 and correspond to the elastic response of the system to bulk or shear deformations.

[7]It is conventional to write the stress and strain components in a more compact form (Voigt notation):

$$xx \to 1, \quad yy \to 2, \quad xy \to 3$$

which is used here to write the elastic moduli matrix. For example, $c_{13} \equiv c_{xxxy}$.

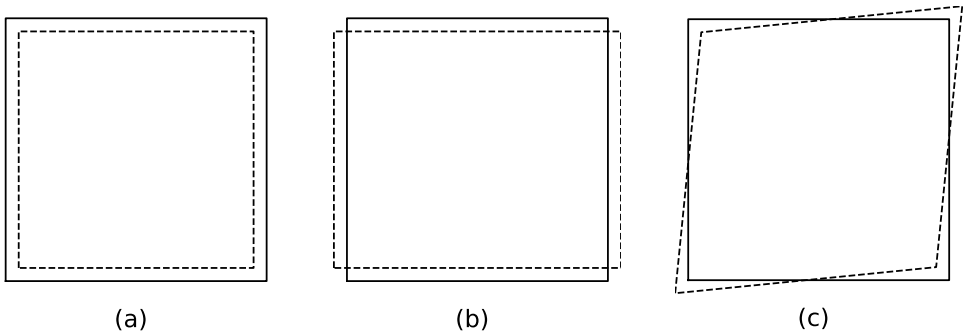

Figure 1.4: Elastic Deformation of a Square Supercell Under Bulk and Shear Distortions. The Deformed Supercell is Shown by the Dashed Lines. (a) The Uniform Bulk Compression of Supercell, (B) Shear$-xxyy$ Where the Cell is Compressed in the $y-$direction and Expanded in the $x-$direction, While the Area is Preserved, (C) Shear$-xy$ Where the Sides Facing Each Other are Sheared in the Opposite Directions Such that the Area is Preserved.

The first elastic moduli is the *bulk modulus* which is the response of a system to an infinitesimal hydrostatic pressure in which the supercell is compressed in both x and y directions (left panel in Figure 1.4). As a result, volume of the system is changed uniformly from V to $V - \Delta V$. The uniform compression corresponds to the following strain tensor ($\delta \ll 1$):

$$\boldsymbol{e} = \begin{pmatrix} -\delta & 0 \\ 0 & -\delta \end{pmatrix} \tag{1.58}$$

which corresponds to a dilation equal to -2δ. Hence, the stored energy after the bulk deformation is[8]:

$$\frac{E}{V} = \frac{1}{2}\left(c_{11} + c_{22} + 2c_{12}\right)\delta^2 = \frac{1}{2}K\left(\frac{\Delta V}{V}\right)^2 = \frac{2^2}{2}K\delta^2. \tag{1.59}$$

[8]Note that the elasticity definition of bulk modulus is compatible with the thermodynamic definition:

$$K = V\left(\frac{\partial^2 E}{\partial V^2}\right)_V,$$

since if the deformation is small, K can be assumed to be constant and:

$$\frac{E}{V} = \frac{1}{2}K\left(\frac{\Delta V}{V}\right)^2.$$

where E is found using the linear response theory and K is the bulk modulus of the network that can be calculated for a given δ.

The second elastic response corresponds to shearing the supercell such that in is contracted in the $y-$direction and expanded in the $x-$direction or vice versa (middle panel in Figure 1.4) and as a result, the volume of the supercell is unchanged. This is called the $xxyy-$shearing shown by G_{xxyy} and its corresponding strain matrix is expressed as:

$$\boldsymbol{e} = \begin{pmatrix} \delta & 0 \\ 0 & -\delta \end{pmatrix} \tag{1.60}$$

The change in the energy density for $xxyy-$shearing is:

$$\frac{E}{V} = \frac{1}{2}\left(c_{11} + c_{22} - 2c_{12}\right)\delta^2 = \frac{2^2}{2}G_{xxyy}\delta^2. \tag{1.61}$$

In this Dissertation, G_{xxyy} is simply reported as the shear modulus G. The third elastic moduli is another type of shear in which facing sides of the supercell are sheared in the opposite directions (right panel in Figure 1.4) with no volume change. This is called $xy-$shear, G_{xy} with the following strain matrix :

$$\boldsymbol{e} = \begin{pmatrix} 0 & \delta \\ \delta & 0 \end{pmatrix}. \tag{1.62}$$

The stored energy density due to the $xy-$shearing is:

$$\frac{E}{V} = \frac{1}{2}\left(c_{33}\right)\delta^2 = \frac{2^2}{2}G_{xy}\delta^2. \tag{1.63}$$

which can be used to calculate this specific type of shear modulus. In chapters four and five, we will frequently calculate the bulk and shear moduli of spring networks to design rigid networks with specific elastic properties. The numerical method involves multiplying the lattice vectors by the proper strain and measuring the energy density stored in the system due to this deformation. The bulk and shear moduli are then calculated using Eqs. (1.59) and (1.61)

1.5 Discussion

In this Dissertation, we will use both dynamical and constraint count approaches to study the rigidity of disordered networks. The rigidity of a structure is determined unequivocally by forming the dynamical matrix $\mathbf{D}$ and finding its eigenvalue spectra. Although, forming the dynamical matrix and diagonalizing it is computationally expensive for a large system. Using the language of degrees of freedom and constraints on the other hand, provides a framework to study rigidity in a more rigorous way.

In general, when we are interested in properties such as the number of floppy modes, stability, low frequency excitations, and force distributions in a rigid network, we use the dynamical approach. The zero eigenvalues of the dynamical matrix show the total number of floppy modes in the system. For example the dynamical matrix of a 2D periodic network must have only two zero eigenvalues, and all of its remaining eigenvalues must be positive for the network to be marginally stable. On the other hand, when we are concerned about rigid region decomposition of a network (*i.e.* knowing specifically which regions are stressed, isostatic, or floppy), or the marginality of the system, we will use the `Pebble Game`. Chapters two and three benefit from `Pebble Game` as their focus is mainly on the constraint count. Chapters four and five specifically discuss the elastic response of disordered networks. Therefore, those two chapters extensively use the ideas introduced here to design spring networks with desired elastic properties.

Chapter 2

REDUNDANCY IN PERCOLATING CLUSTERS

We introduce a novel method to study the effect of loops in connectivity percolation, borrowing the concepts of redundancy and stress from rigidity theory. In the context of rigidity theory, a redundant bond is a bond that is not necessary to maintain the network rigidity and leads to internal stress in the network. In the context of connectivity, loops are redundant since they do not add to the connectedness of a network. Therefore, any bond that closes a loop can be considered redundant while the bonds forming a loop correspond to the stressed bonds in rigidity. To illustrate the interplay between these two models, we study the effect and behavior of loops and redundant bonds in two types of randomly diluted systems including hierarchical and triangular networks. Finally, we show that the results obtained in this chapter can be used to understand the role of stress in rigidity percolation.

2.1 Introduction

Percolation theory is one of the simplest models in statistical physics that exhibits the characteristics of a geometrical phase transition and is widely used in the study of critical phenomena [23, 24]. The simple and powerful ideas of percolation theory have found their way into many fields including Physics, Geophysics, Material Sciences, and Sociological studies. Some of the most important applications of the theory include the study of fluid flow through porous media (for instance distribution of oil or gas inside porous rocks or oil reservoirs) [25, 26], the study of polymerization and gelation [27, 28], and electrical conductivity in a mixture of two or more media

[29, 30].

In almost every percolation type problem, we look for a connected pathway that spans the entire system at the transition point [19]. The formation of such macroscopic spanning cluster exhibits the characteristics of a sharp second order phase transition in the limit of infinite size. This makes percolation theory an interesting model for the study of phase transitions and critical phenomena. There are two main models used in percolation theory. The first one is site percolation model, where we start off with a set of N points distributed over the space. Each point (site) can be occupied with probability p and unoccupied with probability $q = 1 - p$. A group of occupied neighboring sites in space form a cluster. When $p = 0$, none of the sites are occupied and therefore there are no clusters in the system. If the sites are occupied in a randomly fashion such that the occupation of a site is independent from occupation of its neighbors, the value of p increases uniformly and small clusters of occupied sites start to form in the system. If two neighboring sites i and j are both occupied, we can connect them with a segment (bond) which creates a path from i to the j and vice versa. By connecting any occupied site to its nearest neighbors in a cluster, pathways are formed that can take us from one site in the cluster to any other. When p is small, the clusters are sparsely distributed over the space and there is not a connected pathway that spans the entire system. By increasing p, the size of occupied clusters increase and at some critical density $p = p_c$, a large enough cluster forms that connects the sites on one side of the systems to sites on the other side. This cluster is said to be percolating and the system represents a random site percolation model. Site percolation models have been explored thoroughly [23, 31, 32] and are useful in the study of forest fires, epidemics [33], and oil fields.

The second model used in the study of percolating systems is bond percolation. This model is employed when we are simulating the behavior of physical systems

such as molecular structures and polymers, and it will be extensively used in this Dissertation.

In bond percolation models, there is an array of sites distributed over the space in an ordered or disordered manner. All of the sites are assumed to be occupied, so here the density p is defined as the fraction of present connections or bonds to all the possible bonds in the system. This density also gives the probability of a bond being present. In other words, each bond in the system is present with probability p and missing with probability $q = 1 - p$. Adding a bond between two neighboring sites creates a path between them and a group of connected sites form a cluster (similar to the site percolation models). When there are no bonds present, the bond density p is zero. When p is small (but greater than zero), we only expect a few small isolated clusters to be present. But when p is near unity, we expect most of the nearest neighbor sites to be connected so that a large spanning cluster extends from one side of the system to the other. Because there is no spanning cluster for small p and there is a large spanning cluster for p near unity, there must be an intermediate value p_c at which a spanning cluster first exists. At this intermediate density, a drastic change in the correlation lengths of the system is observed. Note that in bond percolation models, instead of starting at $p = 0$ and adding bonds randomly, one can start at $p = 1$ and remove bonds randomly until the transition point $p = p_c$ is reached. In this case, p_c is the intermediate value of bond concentration where a spanning cluster last exists. For $p < p_c$, the clusters will shrink and break into pieces until there are no bonds left at $p = 0$. This method which will be widely used in this Dissertation is referred to as bond dilution. Bond dilution can be executed randomly or according to a specific set of rules. The transition point can vary based on the rules imposed on the dilution procedure.

The defining parameter of percolation is the connectedness, i.e., whether or not

there is a connected path between two points [34]. Since the connectedness shows a qualitative change at a well defined value of a continuous control parameter (p), we can see that the transition from a state with no spanning cluster to a state with one spanning cluster is a type of phase transition. The phase transition in percolation problems is of order to disorder (or vice versa) type. One of the extensively studied geometrical order parameters in bond percolation model is the number of bonds in the spanning cluster that is zero in the range $0 \leq p \leq p_c$ and a finite value for $p_c < p \leq 1$. But in principle, any quantity that changes from zero to a non-zero value at the transition point and remains finite for all values of the control parameter above critical value, can be considered an order parameter. In this chapter we will introduce a set of new order parameters which help us understand the effect and nature of loops in percolation transition in 2D networks. The static features of bond percolation transition in 2D networks have been extensively studied in the recent decades. For example the critical density p_c is known to be $\frac{1}{2}$ for the square lattice, $2\sin(\frac{\pi}{18})$ for the triangular lattice, and $1-2\sin(\frac{\pi}{18})$ for the hexagonal lattice [35, 36]. However all these features are only known for a specific order parameter that does not include any information about loops in the spanning cluster. In the following sections, we will look into the percolation transition of two types of networks. This includes hierarchical networks for which an exact solution exists and triangular networks that can only be studied numerically.

2.2 Bond Percolation in Hierarchical Networks

Hierarchical networks are one of the few models that have an exact solution in percolation theory and therefore are considered as a benchmark for numerical and computational studies [37, 38, 39, 40]. In order to construct a hierarchical network, we start with two sites A and B where the probably of a bond connecting them is

p: this simple mode with only two end points and one bond is considered generation $n = 0$ from which higher generations will evolve. To build $n = 1$ generation we simply replace the bond connecting two end points A and B with a rhombus shaped cell. The process of building a hierarchical network consists of repeating this simple step n times. At each step, a connected bond between two points is replaced with a rhombus cell, changing the number of bonds by a factor of 4. This is shown in Figure 2.1 for three generations. Repeating this n times results in a hierarchical network of generation n where the number of sites and bonds are given by:

$$\begin{cases} E_n = 4^n \\ V_n = \frac{1}{3}(4 + 2 \times 4^n) \end{cases} \tag{2.1}$$

The above equation gives the number of bonds only when $p = 1$ and all the bonds are present. At this point, there is a percolating path connecting A to B. If we start diluting bonds randomly from a network of generation n where $n \to \infty$, at some critical bond concentration $p = p_c$, the percolation will stop and there will be a phase transition. We can write an exact set of equations that relate the percolation probability and order parameters associated with generations n and $n - 1$. These equations can be solved for any bond concentration p by iteration.

To illustrate this, we calculate the probability p_n of having a percolating path from A to B in a network of generation n shown in the simple diagram of Figure 2.2. In this figure, both solid lines (black and blue) represent a percolating hierarchical network of generation $n - 1$ that is present with probability p_{n-1}, and the dashed lines show a disconnected path with probability $1 - p_{n-1}$.

So the probability of the two solid dots being connected in Figure 2.2 is calculated as:

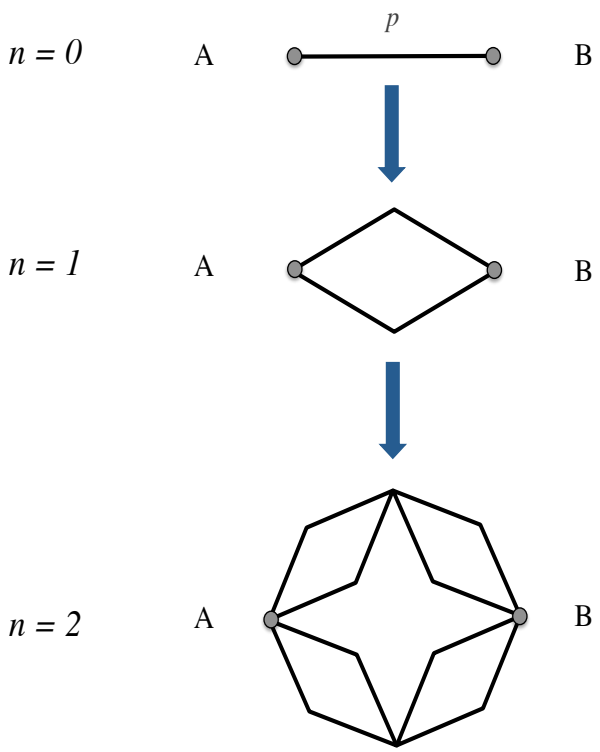

Figure 2.1: A Hierarchical Network Generated by Repeatedly Replacing Each Bond with a Rhombus Shaped Cell. Three Generations are Shown Here.

$$\begin{aligned} p_n(p) &= p_{n-1}^4 + 4p_{n-1}^3(1-p_{n-1}) + 2p_{n-1}^2(1-p_{n-1})^2 \\ &= -p_{n-1}^4 + 2p_{n-1}^2 \end{aligned} \tag{2.2}$$

with $p_0 = p$. Eq. (2.2) gives the probability of percolation in a hierarchical network of generation n by adding the probabilities in all three possible forms of connectivity in Figure 2.2. It is always useful to find the fixed points of a recursive relation such as Eq. (2.2). For any function $f(x)$, if there is a point $x = c$ that maps the function onto itself $f(c) = c$, it is said to be a fixed point. For a recursive function such as p_n defined above, a fixed point p^* would be a point where $p_n = p_{n-1} = p^*$. Solving this equation for p^* gives:

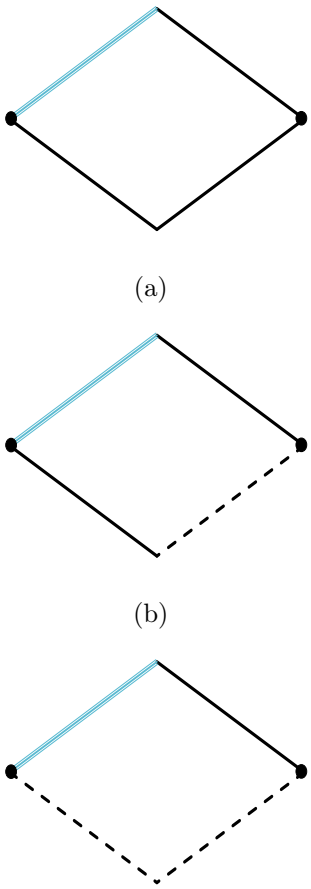

(a)

(b)

(c)

Figure 2.2: A Hierarchical Network of Generation n where n is a Large Number. The Blue Line in Each Panel Represents a Connected Network of Generation $n-1$. The Solid Black Line Shows a Percolating Cluster in Generation $n-1$ Connected with Probability p_n-1, and the Dashed Line is a Non-Percolating Cluster with Probability $1-P_n-1$. a) There is a Percolating Path on All Four Sides of the Network. B) One of the Sides is Not Percolating. C) Two of the Sides are Not Percolating. Note that We Cannot Have a Percolating Path From Left to Right if Three out of Four Sides are Non-Percolating.

$$p^* = 0$$

$$p^* = 1$$

$$p^* = \frac{\sqrt{5}-1}{2} = 0.618 \tag{2.3}$$

The first two points in Eq. (2.3) are the trivial stable fixed points meaning that if

we perturb Eq. (2.2) at points $p = 0$ and $p = 1$ and iterate it n times, the value of p_n will always go back to $p_n = 0$ and $p_n = 1$, respectively. The only unstable fixed point is $p^* = \frac{\sqrt{5}-1}{2} = 0.618 = p_c$ which is the critical concentration where the transition happens at large n.

To quantify the percolation transition at p_c, we should define an order parameter in the system. Since we are interested in the study of loops in bond percolation, a proper set of order parameters includes the fraction of bonds in the percolating cluster, the fraction of bonds in percolating cluster that are in a loop, and finally the fraction of redundant bonds in the percolating cluster. These order parameters are denoted by $P'(p)$, $S'(p)$, and $R'(p)$ respectively. The prime here refers to any quantity that belongs to the percolating cluster. Figure 2.3 demonstrates these order parameters. In Figure 2.3-a, a hierarchical network at $p = 1$ and $n = 3$ is shown. Figure 2.3-b, displays the same network at $p = 0.625$ after diluting about 1/3 of the bonds. All the bonds that are part of a loop are colored in black, while those that are not in any loops are shown in red. Part (c) of the figure shows the percolating cluster in magenta which is located in the lower half of the network since there are no paths connecting A to B in the upper half. As can be seen from part (c), there are 20 bonds in the percolating cluster, 8 of which belong to the two rhombus shaped loops near A and B, and 2 that are redundant. The number of redundant bonds equals the number of loops here. Dividing these counts by the total number of possible bonds ($N = 4^3 = 64$ according to Eq. (2.1)), gives $P'(p)$, $S'(p)$, and $R'(p)$.

Another interesting set of order parameters involves the quantities introduced above but in the current carrying (conducting) cluster [41]. The current carrying cluster is a sub-graph of the percolating cluster that will carry a non-zero current if there is a voltage difference V applied between the two ends of the network. It is obvious from Figure 2.3-c that many of the dangling ends in the percolating clus-

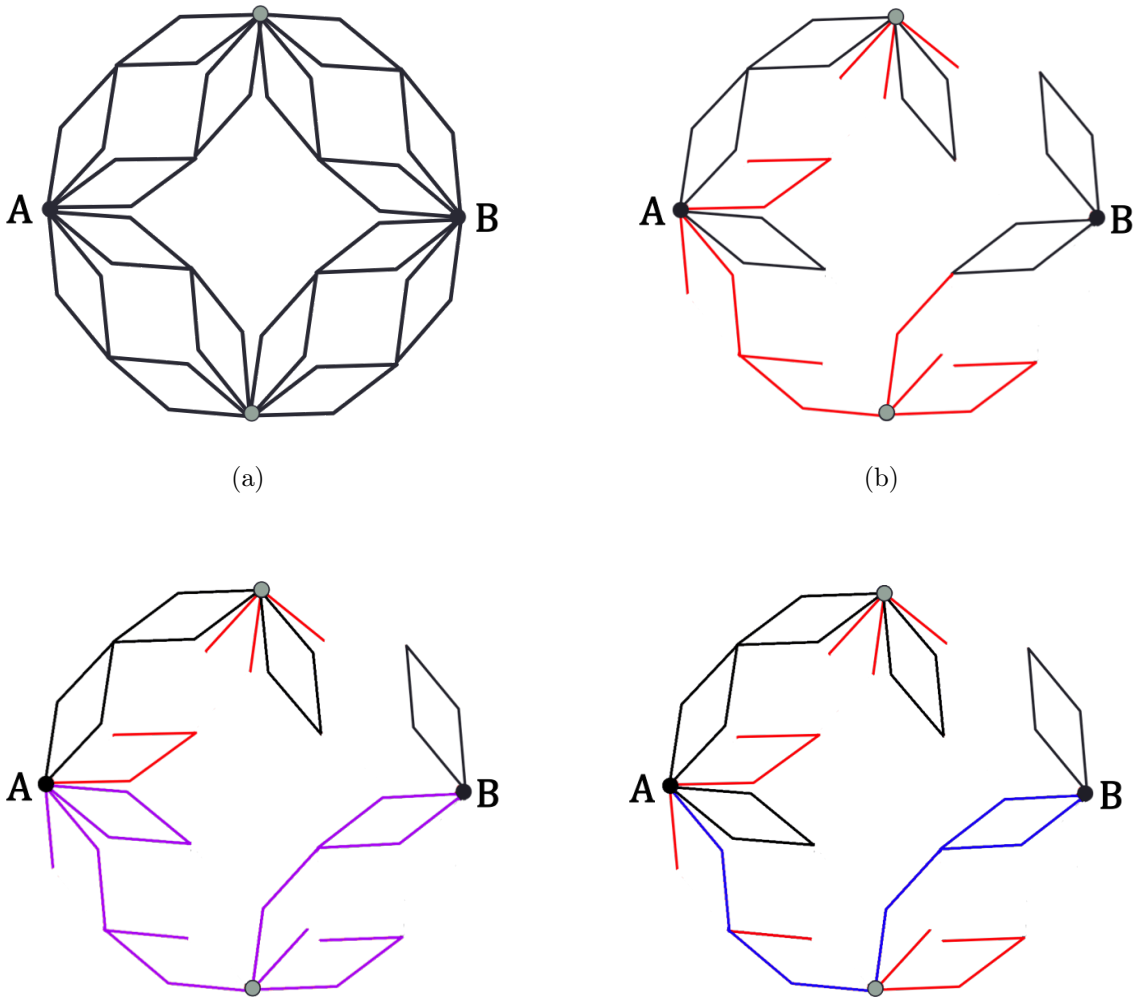

(a) (b)

(c) (d)

Figure 2.3: A) A Hierarchical Network of Generation $n = 3$ at $p = 1$. B) The Same Network at $p = 0.625$. Bonds that are Part of a Loop are Colored Black, While the Bonds that do Not Belong to Any Loops are Shown in Red. C) The Percolating Cluster is in Magenta and Includes Many Dangling Ends. D) The Conducting Part of the Percolating Cluster is Shown in Blue. This Conducting Sub-Graph Consists of Any Bonds that Will Carry the Current if There is a Voltage Difference Between Points A and B.

ter cannot carry any current. Therefore, the conducting cluster only consists of the blue backbone shown in Figure 2.3-d. The current carrying cluster in connectivity percolation is similar to the force carrying cluster in rigidity percolation where the rigidity of the spanning cluster is also under consideration. In both cases, the relevant order parameters describe the response of the network to an external load. In connectivity, they describe the response to an external potential whereas in the case of rigidity percolation, it is the response to an external force. So they both describe the transport properties of the networks. The set of order parameters we are interested in include the fraction of bonds in current carrying backbone, the fraction of bonds in current carrying backbone that are also in a loop, and the fraction of redundant bonds in current carrying backbone. These parameters are denoted by $P''(p)$, $S''(p)$, and $R''(p)$ respectively. In Figure 2.3-d, there are 10 bonds in the conducting cluster, 4 of which belong to the loop attached to B, and since there is only one loop in the backbone, there is also 1 redundant bond. Dividing these numbers by the total number of possible bonds ($N = 4^3$) gives $P''(p)$, $S''(p)$, and $R''(p)$ for this network.

In the following, we use the diagrams of Figure 2.2 to obtain generalized relations for all the order parameters introduced above. In each panel of this figure, the blue line represents a connected network of generation $n-1$, where for example the fraction of bonds in the percolating cluster is P'_{n-1}. The solid black line shows a percolating cluster of generation $n-1$ which is connected with probability p_{n-1}, and the dashed line is a non-percolating cluster with probability $1-p_{n-1}$. Using these definitions and the weights shown in Figure 2.2 for all the possible configurations, the fraction of bonds in the percolating cluster of the network is found:

$$P'_n(p) = \frac{1}{4}\left[4P'_{n-1}(p)p^3_{n-1} + 12P'_{n-1}(p)p^2_{n-1}(1-p_{n-1}) + 4P'_{n-1}(p)p_{n-1}(1-p_{n-1})^2\right]$$
$$= (p_{n-1} + p^2_{n-1} - p^3_{n-1})P'_{n-1}(p) \tag{2.4}$$

where $(P'_0(p) = p)$. To find the fraction of bonds in the current carrying backbone, we note that in diagram 2.2-b, there is a dangling cluster in the lower half of the network that will not conduct any current if a voltage difference is applied between the two solid end points. Therefore in counting the possible current carrying scenarios, we do not add that section to the number of conducting bonds:

$$P''_n(p) = \frac{1}{4}\left[4P''_{n-1}(p)p^3_{n-1} + 8P''_{n-1}(p)p^2_{n-1}(1-p_{n-1}) + 4P''_{n-1}(p)p_{n-1}(1-p_{n-1})^2\right]$$
$$= p_{n-1}P''_{n-1}(p) \tag{2.5}$$

with $P''_0(p) = p$. The procedure for calculating the fraction of bonds inside a loop, both in percolating and current carrying clusters, is very similar to this. There is only one subtlety regarding diagram 2.2-a which has an external loop since all four sides of the network are percolating. In that case, all the bonds that are in the current carrying backbone of the blue line but are not in any smaller loops will become part of the large external loop. Therefore we need to add the second term given below to the expressions of $S'(p)$ and $S''(p)$:

$$S'_n(p) = (p_{n-1} + p^2_{n-1} - p^3_{n-1})S'_{n-1}(p) + \left[P''_{n-1}(p) - S''_{n-1}(p)\right]p^3_{n-1} \tag{2.6}$$
$$S''_n(p) = p_{n-1}S''_{n-1}(p) + \left[P''_{n-1}(p) - S''_{n-1}(p)\right]p^3_{n-1} \tag{2.7}$$

With initial values $S'_0(p) = 0$ and $S''_0(p) = 0$. To calculate the fraction of redundant bonds in percolating and current carrying clusters, we note that again in diagram 2.2-

a, the larger external loop adds one more redundant bond to the network, therefore we have:

$$R'_n(p) = (p_{n-1} + p_{n-1}^2 - p_{n-1}^3)R'_{n-1}(p) + \frac{1}{4}(p_{n-1}^4) \tag{2.8}$$

$$R''_n(p) = p_{n-1}R''_{n-1}(p) + \frac{1}{4}(p_{n-1}^4) \tag{2.9}$$

With initial values $R'_0(p) = 0$ and $R''_0(p) = 0$. Table 2.1 shows a summary of all six order parameters with their initial values. It also includes two equations for the total fractions of looped and redundant bonds in the network ($S_n(p)$ and $R_n(p)$) which can be obtained by multiplying the numbers in generation $n-1$ by 4 and adding the appropriate terms for the external loop. These two quantities are not order parameters of the system but could provide some insight about the total effect of loops and redundancy in bond dilution models.

Quantities	**Initial Conditions**
$p_n(p) = -p_{n-1}^4 + 2p_{n-1}^2$	$p_0 = p$
$P'_n(p) = (p_{n-1} + p_{n-1}^2 - p_{n-1}^3)P'_{n-1}(p)$	$P'_0 = p$
$P''_n(p) = p_{n-1}P''_{n-1}(p)$	$P''_0 = p$
$S_n(p) = S_{n-1}(p) + \left[P''_{n-1}(p) - S''_{n-1}(p)\right] p_{n-1}^3$	$S_0 = 0, S''_0 = 0$
$S'_n(p) = (p_{n-1} + p_{n-1}^2 - p_{n-1}^3)S'_{n-1}(p) + \left[P''_{n-1}(p) - S''_{n-1}(p)\right] p_{n-1}^3$	$S'_0 = 0, S''_0 = 0$
$S''_n(p) = p_{n-1}S''_{n-1}(p) + \left[P''_{n-1}(p) - S''_{n-1}(p)\right] p_{n-1}^3$	$S''_0 = 0$
$R_n(p) = R_{n-1}(p) + \frac{1}{4}(p_{n-1}^4)$	$R_0 = 0$
$R'_n(p) = (p_{n-1} + p_{n-1}^2 - p_{n-1}^3)R'_{n-1}(p) + \frac{1}{4}(p_{n-1}^4)$	$R'_0 = 0$
$R''_n(p) = p_{n-1}R''_{n-1}(p) + \frac{1}{4}(p_{n-1}^4)$	$R''_0 = 0$

Table 2.1: Table of Calculated Order Parameters Plus Their Initial Values for Hierarchical Networks.

Since all the quantities given in Table 2.1 depend on the percolation probability p_{n-1}, we can expand them in terms of the bond density p. Although this would be a mathematically cumbersome task for a general n, but the expansions are possible for smaller values of n as is shown in Figure 2.4.

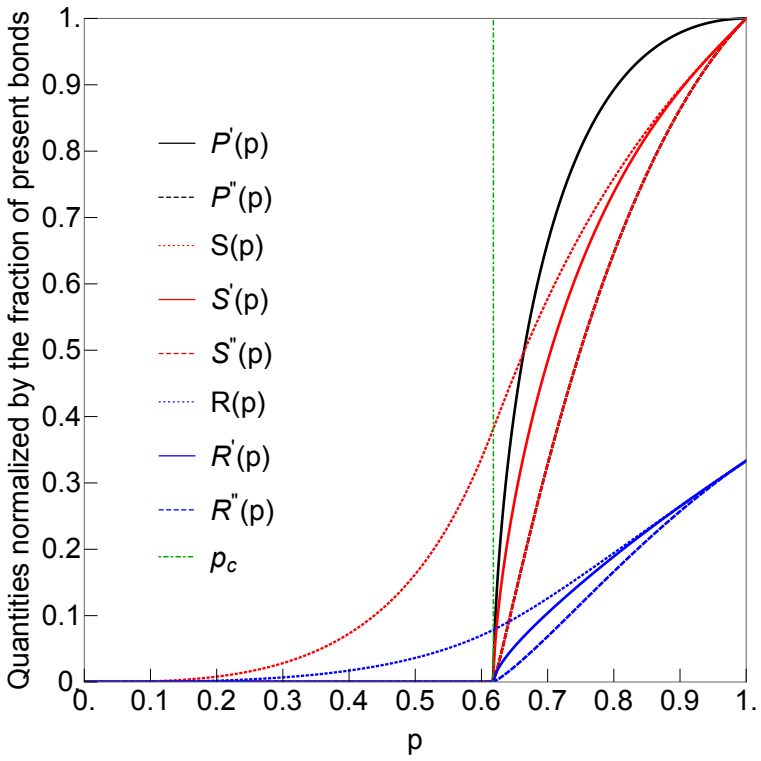

Figure 2.4: Plots of the Order Parameters (and Two Quantities $S(P)$ and $R(P)$) Versus Bond Concentration p in a Hierarchical Network of Generation $n = 20$.

In Figure 2.4, the two dotted curves in red and blue represent the total fractions of bonds in the network that belong to a loop $S(p)$ or are redundant $R(p)$, respectively. As can be seen from the figure, these two quantities are not order parameters as they vanish only when $p \to 0$ and there is not a significant change in their values at the critical point $p = p_c$ which is marked with the green vertical line. All the solid curves represent primed quantities which belong to the percolating cluster. All the dashed curves represent quantities in the current carrying cluster. The curve representing

$P''(p)$ is hidden underneath $S''(p)$. This means that for all values of p from $p = 1$ to $p = p_c$, every bond in the conducting cluster belongs to a loop that can be a small local loop or the large external loop. This is because for large n, there is usually more than one sequence of back to back bonds that go from point A to point B and vice versa. In other words, it is statistically unlikely to have only one single path connecting one side of the network to the other. Hence all the bonds that carry the current are part of at least one large loop that goes from point A to point B and back along different paths. At $p = 1$, all the bonds are present and the fractions of bonds in the percolating cluster and conducting cluster are both equal to unity. Also since there are no broken loops, all the bonds belong to at least one loop. So the fraction of looped bonds is also equal to unity. At this point, only one fourth of the bonds are redundant. Therefore, the fraction of redundant bonds in percolating and conducting clusters (as well as the entire network) is $\frac{1}{4}$ when $p = 1$. When bonds are selected and removed randomly, all the order parameters decrease continuously until at the critical point $p = p_c$ they all vanish and remain zero for $p < p_c$. This is the characteristic of a second order phase transition.

As can be seen from Figure 2.4, the critical transitions of order parameters exhibit scaling properties, which means they all depend upon probability p in a power-law fashion, with a critical exponent in the following form [23, 34]:

$$O(p) = A(p - p_c)^{\beta} \tag{2.10}$$

where $O(p)$ is a generic order parameter, A is the scaling factor, and β is the critical exponent. A system approaching the critical point can be described using a variety of quantities. However, it has been shown that most of the critical exponents describing these measurables are related to one another through scaling relations. To describe

the behavior of the system, we only need two independent critical exponents [42]. So it is usually a matter of taste to choose the fundamental exponents for a system. Since we are interested in exponents that define the order parameters seen in Eq. (2.10), we will use the set $\{\beta, \nu\}$ where ν describes the divergence of the correlation length ξ at the percolation transition, $\xi \sim |p - p_c|^{-\nu}$, and refers to the asymptotic expansion of the the largest finite cluster near critical point. The correlation length is not really a meaningful quantity to measure for hierarchical networks. However, we need to calculate its critical exponent ν since we will need it later to calculate β.

If two order parameters describing widely different quantities in different systems exhibit identical scaling behavior as they approach the critical point (i.e. if they both share the same set of critical exponents), they are said to belong to the same universality class and can be shown to have the same dynamical properties. In general, the critical exponents of a system do not depend on details such as its geometrical structure or the nature of interactions between the particles. Instead, they depend on very general properties such as the spatial dimension d, the coupling range, and the symmetries of the order parameters in the system.

To understand the behavior of hierarchical networks near criticality, we calculate the critical exponents associated with each order parameter introduced above. For any system that obeys Eq. (2.10) near p_c, the critical exponent β can be calculated by using the eigenvalues of linearized scaling relations for $p_n(p)$ and $O(p)$. The following steps should be repeated for for all the order parameters, but the details are shown for one parameter only assuming that $P'(p) \propto (p - p_c)^{\beta'}$. First, Eq. (2.2) is Taylor expanded near p_c as $p_n - p_c = \lambda_p(p_{n-1} - p_c\ )$ to find the eigenvalue of $p_n(p)$. This gives:

$$\lambda_p = \frac{dp_n}{dp_{n-1}}|_{p_c} = 4p_c - 4p_c^3 = 1.527 \tag{2.11}$$

Next, we expand Eq. (2.4) as $P'_n(p) = P'_n(p_c) + \frac{dP'_n}{dP'_{n-1}}|_{p_c}(P'_{n-1}(p) - P'_{n-1}(p_c)) = \lambda_{P'} P'_{n-1}(p)$ to obtain the eigenvalue of $P'(p)$ which yields:

$$\lambda_{P'} = \frac{dP'_n}{dP'_{n-1}}|_{p_c} = p_c + p_c^2 - p_c^3 = 0.764 \tag{2.12}$$

since $P'_n(p_c) = P'_{n-1}(p_c) = 0$ for large n. Both these eigenvalues are related to the critical exponents β' and ν in the following form:

$$\begin{aligned} \lambda_p &= b^{\frac{1}{\nu}} \\ \lambda_{P'} &= b^{-\frac{\beta'}{\nu}} \end{aligned} \tag{2.13}$$

where b is the dilation factor between successive generations of the network. Eq. (2.13) is a result of the scaling of the system as it changes from generation $n-1$ to generation n. According to the scaling theory [23], the effective percolation threshold scales with the system size as $p - p_c \propto L^{-\frac{1}{\nu}}$. For hierarchical networks, it is assumed that the system size is generation n is related to the system size in generation $n-1$ through dilation factor $L_n = b\, L_{n-1}$. This means the scaling relations for p_n and $P'_n(p)$ are in the form:

$$\begin{aligned} p_n - p_c &\propto (b\, L_{n-1})^{-\frac{1}{\nu}} \propto b^{-\frac{1}{\nu}} (p_{n-1} - p_c) \\ P'_n(p) &\propto (p_n - p_c)^{\beta'} \propto b^{-\frac{\beta'}{\nu}} P_{n-1}(p) \end{aligned} \tag{2.14}$$

which leads to relations in Eq. (2.13). Since b is ambiguous for hierarchical networks, we can eliminate it from the set of equations in (2.13) to obtain the following relation for the critical exponent β':

$$\beta' = -\frac{\log \lambda_{P'}}{\log \lambda_p} = 0.635 \tag{2.15}$$

Eq. (2.15) can be used to calculate the critical exponents for the set of all six order parameters $\{P', S', R', P'', S'', R''\}$. The results are shown in Table 2.2.

Order Parameters	**Critical Exponents**	**Critical Point**
P', S', R'	$\beta' = \frac{\log 2}{2\log(\sqrt{5}-1)} - 1 = 0.635..$	$p_c = \frac{\sqrt{5}-1}{2} = 0.618..$
P'', S'', R''	$\beta'' = \frac{\log 2}{2\log(\sqrt{5}-1)} - \frac{1}{2} = 1.135..$	$p_c = \frac{\sqrt{5}-1}{2} = 0.618..$

Table 2.2: Table of Critical Exponents and Fixed Points for the Order Parameters in Hierarchical Networks. All the Calculated Values are Exact.

It is surprising that all the order parameters in the percolating cluster share the same critical exponent and all those that are in the conducting cluster have the same exponent. This means that in hierarchical networks, the loops and redundant bonds in a cluster follow the behavior of bonds in that cluster near the transition point. According to the results in Table 2.2, there is also a simple relation between the critical exponents β' and β'', as $\beta'' - \beta' = 1/2$. This is quite unexpected since these order parameters describe very different quantities. However, based on these results it is obvious that in order to describe the percolating and conducting clusters in a hierarchical network near criticality, one only needs the set of two critical exponents $\{\beta', \nu\}$. The information provided by Table 2.2 also suggests that the ratios of all the quantities belonging to the same cluster must be finite near p_c. This ratio is basically the ratio of scaling factors in Eq. (2.10) and it has been calculated for several values of n as shown in Table 2.3.

n	$\frac{S'}{P'}$	$\frac{R'}{P'}$	$\frac{S''}{P''}$	$\frac{R''}{P''}$
8	0.61562	0.114819	0.978714	0.160243
9	0.616827	0.114829	0.986844	0.160311
10	0.61743	0.114833	0.991869	0.160339

Table 2.3: Amplitude Ratios of Different Quantities for Hierarchical Networks. The Values of the Amplitudes are Consistent as n Becomes Larger. So the Numbers Given in This Table Must Be a Proper Approximation for the Actual Values.

One might ask if the results obtained for hierarchical networks are universal and work for any system. In the following section, we will study the same set of order parameters and their critical exponents in triangular networks that are not exactly soluble. The definitions remain the same, but there are many more subtleties involved due to the computation nature of the problem.

2.3 Bond Percolation in Triangular Networks

The second model we study is the bond percolation in 2D triangular networks. The networks studied here are regular lattices, but the methods are applicable to any types of disordered networks as well. A triangular lattice is an arrangement of points where the nearest neighbors form an equilateral triangle and every site has a coordination number $z = 6$. When all the bonds are present $\langle z \rangle = 6$ and the lattice is extremely overconstrained and far from criticality. This provides the freedom to try a variety of interesting dilution protocols that could lead to very different types of networks with different physical and mechanical properties at the critical point. This is the main advantage in using triangular lattices and disordered triangulations instead of other types of lattices such as square lattice with $z = 4$ and hexagonal lattice with $z = 3$, which are either close to the critical point or underconstrained. In addition, the triangular lattice is very simple and its marginal bond density and critical exponents

for the fraction of bonds in the percolating cluster are well known [43, 44]. This provides a point of reference against which our results in the study of loops and redundancy can be assessed.

As we saw in previous section, hierarchical networks possess special topological advantages that allow the exact calculation of p_c and critical exponents β and ν. However, in most systems like 2D triangular lattices, even though the exact values of p_c can be calculated [35], the values of critical exponents can only be estimated numerically.

The definitions of the percolating cluster and order parameters associated with it are only meaningful in the thermodynamic limit $N \to \infty$. In addition, the larger the system size, the more accurate the measurements of critical parameters. Therefore, it is always desirable to push the size of the simulated systems to a larger limit. However, there are computational difficulties in generating and studying very large systems (e.g. with sizes in order of Avogadro's number), and in practice we can only generate systems with a finite size. One good way to overcome this limit is to use the proper boundary conditions. For example, by using periodic boundary conditions one might minimize the finite size effect and achieve a better approximation for large scale systems. Another way to reduce the finite size effect and improve the accuracy of the results is to ensemble average every measurement over many independently prepared samples. We will use both these strategies in this chapter. Although the boundary conditions employed in our simulations are cylindrical. This means the 2D networks are repeated infinitely in one direction while staying finite in the other direction. This choice is made for the sake of studying the current carrying cluster so that we can attach electrodes to the two finite sides. If the systems are periodic in both directions, the study of input and output currents becomes meaningless.

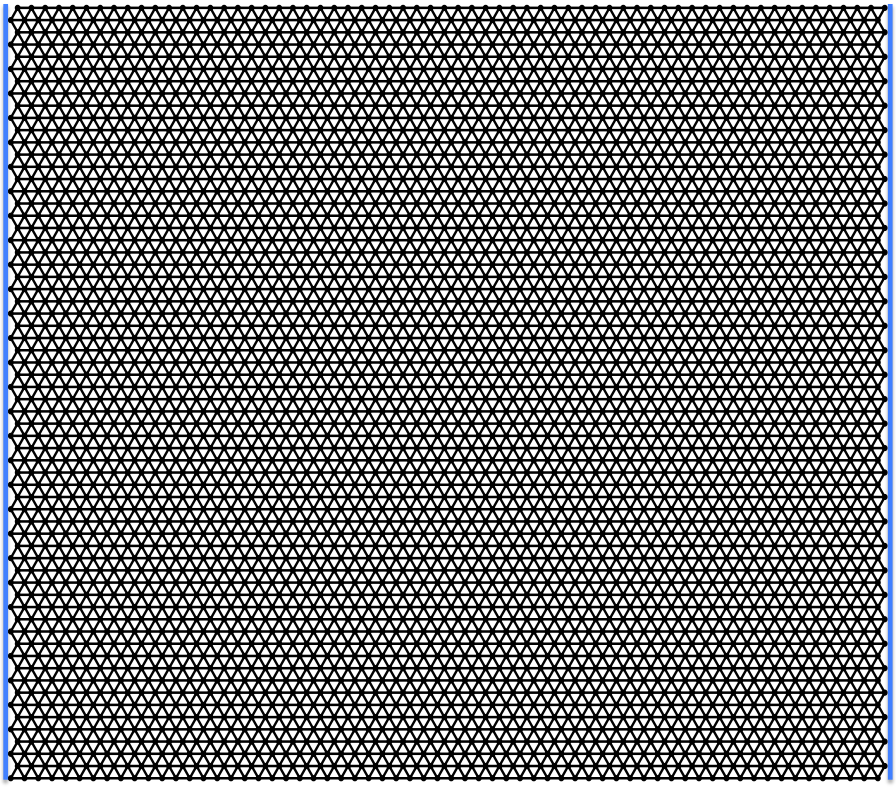

Figure 2.5: A Triangular Lattice with $L = 64$, $N = 64 \times 64 = 4096$ Sites, and $N_e = 12160$ Bonds at $p = 1$ where All the Bonds are Present and Belong to Internal Loops. The Lattice is Finite in the Horizontal Direction and Infinitely Repeated in the Vertical Direction. The Blue Lines Represent Two Electrodes at the Two Finite Sides of the Lattice.

Figure 2.5 shows a full triangular lattice with $L = 64$ and cylindrical boundary conditions. In this chapter, L will be used to denote the number of sites on each side of a triangular network. $L = 64$ means there are $N = 64 \times 64 = 4096$ sites in the entire lattice. If the lattice was periodic (infinite in both directions) the number of bonds would be $3 \times N = 12288$. But since it is finite in one direction, the actual number of bonds is $N_e = 12160$ which is smaller than the total number of bonds in a periodic lattice. The shown lattice is infinite in the vertical direction and finite in the horizontal direction. To make the lattice infinite, we add copies of the central

supercell at the top and bottom and connect the sites on the top edge to the sites on the bottom edge such that the network repeats itself in that direction. This is why the boundaries are named cylindrical. The blue lines on the left and right represent two electrodes that are held at a potential difference V.

By removing bonds randomly from network of Figure 2.5, we can observe the changes in values of the order parameters $\{P', S', R', P'', S'', R''\}$ as p approaches p_c. The analytically known value of threshold probability for triangular lattices in 2D is $p_c = 2\sin(\pi/18) \approx 0.347$. This means in order to reach the percolation transition, we must remove almost two thirds of the bonds from the network.

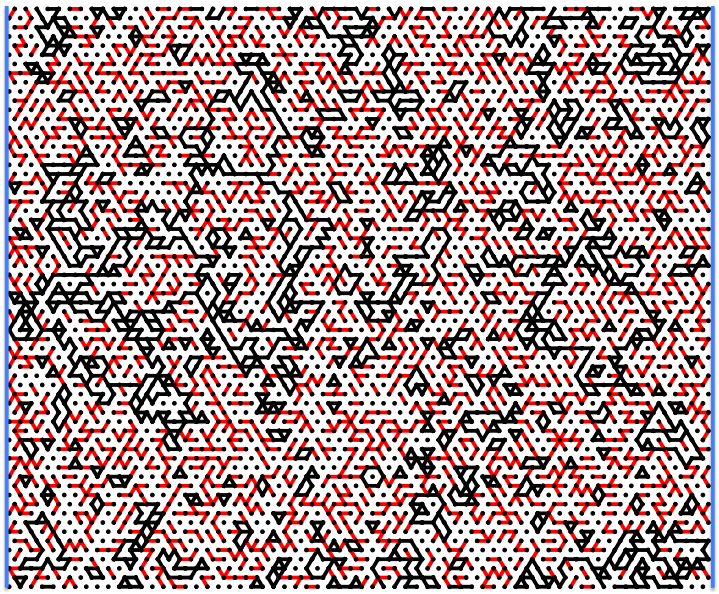

Figure 2.6: The triangular lattice in Figure 2.5 randomly diluted up to $p = 0.349$. The black bonds are the ones that belong to a loop (either internal or external) and the red ones are those that are not part of any loops.

Figure 2.6 shows the $L = 64$ lattice at $p = 0.349$ which is slightly above the transition point. The black color represents bonds that are part of a loop. The color red is used to show bonds that do not belong to any loops in the network. At this density, there is a percolating cluster that spans the network, but there are also many

isolated smaller clusters. Figure 2.7 displays this percolating cluster after all the smaller clusters are removed.

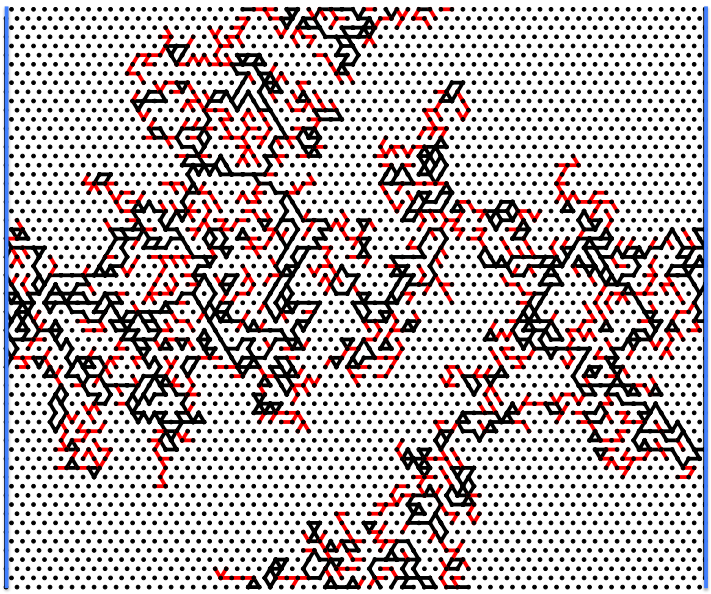

Figure 2.7: The Percolating Cluster in the Randomly Diluted Triangular Network After Removing All the Isolated Clusters From the Network. As Can Be Seen, This Cluster Spans the Network in Both Horizontal and Vertical Directions.

In the percolating cluster of Figure 2.7, there are many bonds that have branched out of the backbone in the form of dangling ends. These bonds do not carry the current when there is a potential difference between the two blue electrodes. Therefore the conducting cluster is a sub-graph of the percolating cluster that connects the right electrode to the left one as can be seen in Figure 2.8. The few red bonds in the conducting cluster of Figure 2.8-b are those that will break the percolating cluster into two smaller clusters if removed. However, the number of those red bonds is very small compared to to size of the conducting cluster. When the system size increases, the chances of having one single path from left to right or top to bottom decrease significantly. Therefore most of the bonds in the conducting cluster are also part of either a small loop or a larger loop that connects the two electrodes.

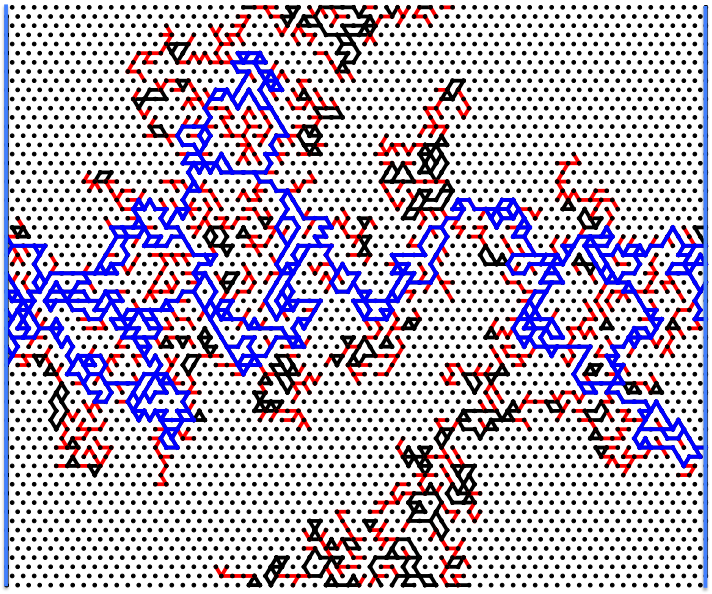

(a)

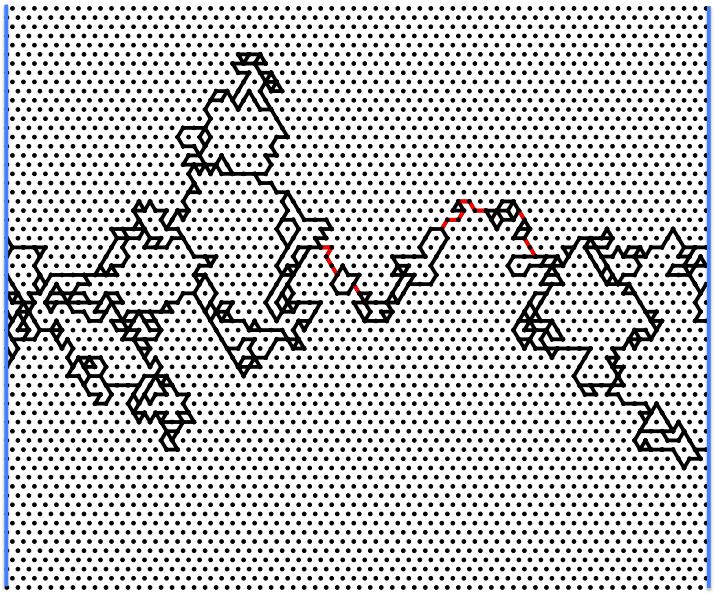

(b)

Figure 2.8: A) An Overlay of the Percolating and Current Carrying Clusters in the Network of Figure 2.6. The Conducting Part of the Percolating Cluster is Shown in Blue. B) Only the Conducting Cluster in the Network of Figure 2.6 Is Shown. This is the Cluster that Would Carry the Current if There is a Potential Difference Applied Between the Two Blue Electrodes.

In the following section, we will review the computational tools and techniques that have been used to measure the set of order parameters in triangular networks.

2.3.1 Computational Methods

In this section, we discuss the details of computational methods used to identify the percolating and conducting clusters and measure the fractions of looped and redundant bonds in them. Similar to the case of hierarchical networks, we will show all the quantities that belong to the percolating cluster with a prime sign and all the quantities that belong to the current carrying or conducting cluster with a double prime sign. The percolating cluster is the largest cluster that spans the network either from left to right or top to bottom or in both directions. If the largest cluster is percolating from left to right and from top to bottom, we will weight all the measured quantities P', S', and R' with 1. However, if it is percolating from left to right only, the quantities will be weighted by $\frac{1}{2}$. When the largest cluster does not percolate in any directions or percolates only from top to bottom, the quantities will be all weighted by 0.

The current carrying cluster is a cluster that spans from left electrode to the right electrode in Figure 2.8. If is spans in both directions, we weight all the quantities P'', S'', and R'' by 1. If it only spans from left to right, the double primed quantities are weighted by $\frac{1}{2}$. Finally, if there is not a connected cluster that percolates from left to right, then the weight would be 0.

To spot the largest cluster in the network, we use pebble game [45, 46] which is an integer algorithm to find the rigid region decomposition of networks. The pebble game identifies the largest rigid cluster while we are only concerned with the connectivity of bonds and not their rigidity. Therefore, we should find a mapping from the largest rigid cluster into the largest percolating cluster. One useful way to create such a

mapping is by adding an auxiliary ghost site and connecting it to all the sites in the network. An illustration of this is shown in Figure 2.9. The network in Figure 2.9-a is a simple loop that percolates from left to right and top to bottom. From a rigidity point of view, the network is not rigid. Because according to Eq.(1.39):

$$F = 2N - N_e + N_r = 8 - 4 + 0 = 4$$

There are 4 degrees of freedom one of which is an internal floppy mode. This mode is extended over the entire network, making all the sites hinges. Here the largest rigid cluster is each of the single bonds. This means if we run the network of Figure 2.9-a through pebble game, no spanning rigid clusters will be found. However, if we add a single auxiliary site as shown in blue in Figure 2.9-b, and connect it to all the sites in the network, the new structure becomes overconstrained and rigid. In the construction of 2.9-b there are:

$$F = 2N - N_e + N_r = 10 - 8 + 1 = 3$$

floppy modes that correspond to the three trivial motions (two translations and one rotation) for a 2D system. There is also one redundant bond that adds a state of self stress to the system, causing all the bonds to be stressed. Therefore there is a rigid (and overconstrained) cluster that percolates from left to right and top to bottom.

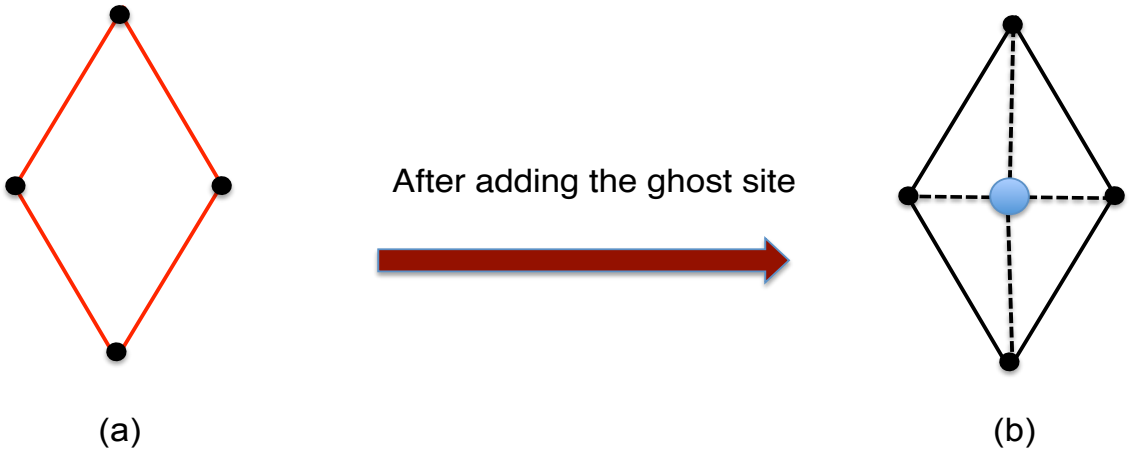

Figure 2.9: The Pebble Game Can Be Used to Identify the Percolating Cluster and Bonds within a Loop Using a Ghost Site. In the Presence of the Ghost Site, All the Bonds that are Part of a Loop Will Be Recognized as Stressed by the Pebble Game.

This illustrates the mapping between rigidity percolation and connectivity percolation that allows one to use the pebble game to study loops and redundancy in random percolation. By adding a ghost site to any network, the percolating cluster becomes a rigidly percolating cluster due to triangulations created by the ghost site. If there is an isolated site, connecting it to the ghost site will create a dangling bond that is not part of the largest rigid cluster. On the other hand, all those bonds that belong to a loop, become stressed due to the redundancy caused by connections to the ghost site. This means after adding the ghost site and running the network through pebble game, the largest rigid cluster is equivalent to the largest connected cluster in the original network. Also, all the stressed bonds identified by the pebble game correspond to the looped bonds in the original cluster. Once the largest cluster is found using this method, we can check if there are any sites on the left and right edges that both belong to that cluster. If they do, it means there is a connected path from left to right. Similarly, we can check the percolation from top to bottom and determine the weights of the order parameters in the percolating cluster.

Te calculate the number of redundant bonds, we use the adapted version of

Eq. (1.39) for connectivity percolation. In this case, a single floppy mode is associated with an isolated cluster and the left-hand side of Eq. (1.39) represents the total number of isolated clusters. Each floppy mode or degree of freedom, corresponds to a motion along the orthogonal line to the plane of the network. Therefore, each site has 1 degree of freedom and each bond counts as 1 constraint. So the modified version of Eq. (1.39) for connectivity percolation in 2D is:

$$F - N_r = N - N_e \tag{2.16}$$

where N is the number of sites, N_e is the number of bonds (or edges), and N_r is the number of redundant bonds. Since we are only interested in the number of redundant bonds in the spanning cluster (and not the entire network), we can apply Eq. (2.16) to the percolating cluster only and neglect all the other smaller isolated clusters in the network. In this case, $F = 1$ and N_r can simply be calculated by counting the number of sites and bonds in the percolating cluster:

$$N_r = N_e - N + 1 \tag{2.17}$$

Note that all these counts are performed after removing the ghost site and the bonds that are connected to it.

To identify the current carrying cluster, we simply apply a voltage difference V between the two blue electrodes one the left and right edges of Figure 2.8-b and solve the Kirchhoff's current balance equations for each site [47]:

$$\sum_{j=1}^{n} I_{ij} = \sum_{j=1}^{n} V_i - V_j = 0 \tag{2.18}$$

By writing Eq. (2.18) for every site i in the network, we obtain a set of equations that relate the known voltages to the unknown voltages. By moving all the known voltages (voltages of those sites that are on the electrodes) to the right-hand side of the equations, and doing a little bit of algebra, we reach to a simple set of linear equations in the form:

$$L_{ij}X_v = V \tag{2.19}$$

where L_{ij} is the Laplacian matrix, X_v is the set of unknown voltages, and V is the set of known voltages. The Laplacian is a symmetric matrix that has the following form:

$$L_{ij} = \begin{cases} z_i & \text{if } i = j \\ -1 & \text{if } i \neq j \text{ and } i \text{ and } j \text{ are in contact} \\ 0 & \text{otherwise} \end{cases} \tag{2.20}$$

where z_i is the coordination number (i.e. degree) of site i. By solving the $L_{ij}X_v = V$ equations, we find the voltages on all of the sites. If the voltage difference between two adjacent sites is greater than zero, it means there is a current flow in the bond connecting them. This method is used to find all the current carrying bonds in the network. Once the current carrying cluster P'' is identified, pebble game plus the ghost site are used to measure the fraction of bonds that are inside a loop S''. Finally, a similar argument to that of Eq. (2.17) can be used to obtain the faction of redundant bonds in the conducting cluster R''. Figure 2.10 displays the transition of all these quantities as the bond concentration p approaches its critical value p_c. All the values have been normalized by the total number of bonds present.

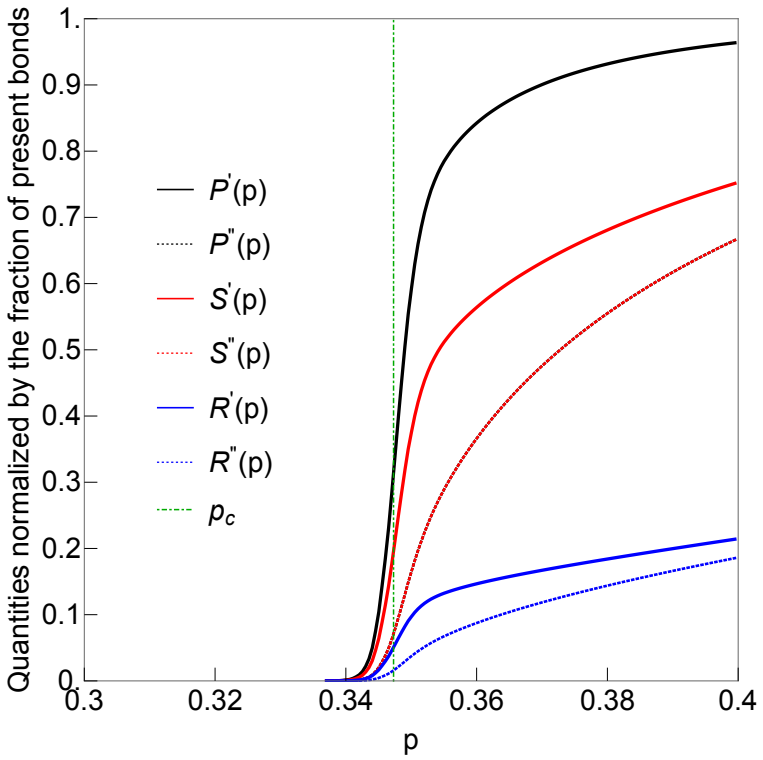

Figure 2.10: Plots of All the Order Parameters Versus Bond Concentration p for a Randomly Diluted Triangular Network with $L = 600$ and $N = 600 \times 600$ Sites.

As can be seen from Figure 2.10, all the bonds in the current carrying cluster are also looped, therefore the plot of P'' is overlaid by that of S''. As discussed in the case of hierarchical networks, this is due to the fact that for large networks, it is highly unlikely to have only one single current carrying path in the network. Multiplicity of possible paths that carry the current from left electrode to the right one is the main reason most bonds in the conducting cluster are inside a loop. This effect can easily be seen from Figure 2.8-b: the fraction of non-looped bonds in the current carrying cluster is negligible even for a small network of size $L = 64$. This fraction approaches zero as the network size increases. In the following section, we will look into the procedures that are used to extract p_c and critical exponents β and ν from the plots of order parameters.

2.3.2 Results

Figure 2.10 shows that there is a second order phase transition near $p = 0.34$. However the transition is not very sharp and the point at which the order parameters become zero does not match the analytically known critical point which is at $p_c = 2\sin(\pi/18)$ (marked with the green dashed line). Instead, the order parameters have a small tail that leads to zero slowly rather than going to zero at the expected p_c. Also, even though all the order parameters of one size become zero at the same time, the critical point p_c varies based on the system size. This is called the finite size effect which appears in the form of a size dependent difference between the predicted value and the measured value of a quantity. This difference decreases as the system size grows larger. The main reason for this kind of difference is that the predicted value is only valid for truly large systems in thermodynamic limit. But in practice, the systems we study computationally are far from this limit. To see the finite size effect more clearly, all the measurements have been executed over 6 different system sizes $L = 100$, 200, 300, 400, 500, and 600, each ensemble averaged over 500 independent realizations with the results shown in Figure 2.11. First, the networks are randomly diluted up to the point $p = 0.4$ and then the measurements are done in the range $0.3 < p < 0.4$. As can be seen from the figure, the tails shrink by increasing the system size. This means in the limit $L \to \infty$, all these order parameters would obey equation 2.10 and will go to zero exactly at the expected critical point. Since in reality we cannot produce systems of infinite size, we will use finite size scaling techniques to obtain an approximation for the critical quantities such as p_c, β', β'', and ν. The main idea of finite size scaling is to simulate the critical behavior of infinite systems by scaling a set of finite systems [48]. For example, if $P'(p, L)$ is a quantity that depends on two variables, p being an independent control parameter and L being the

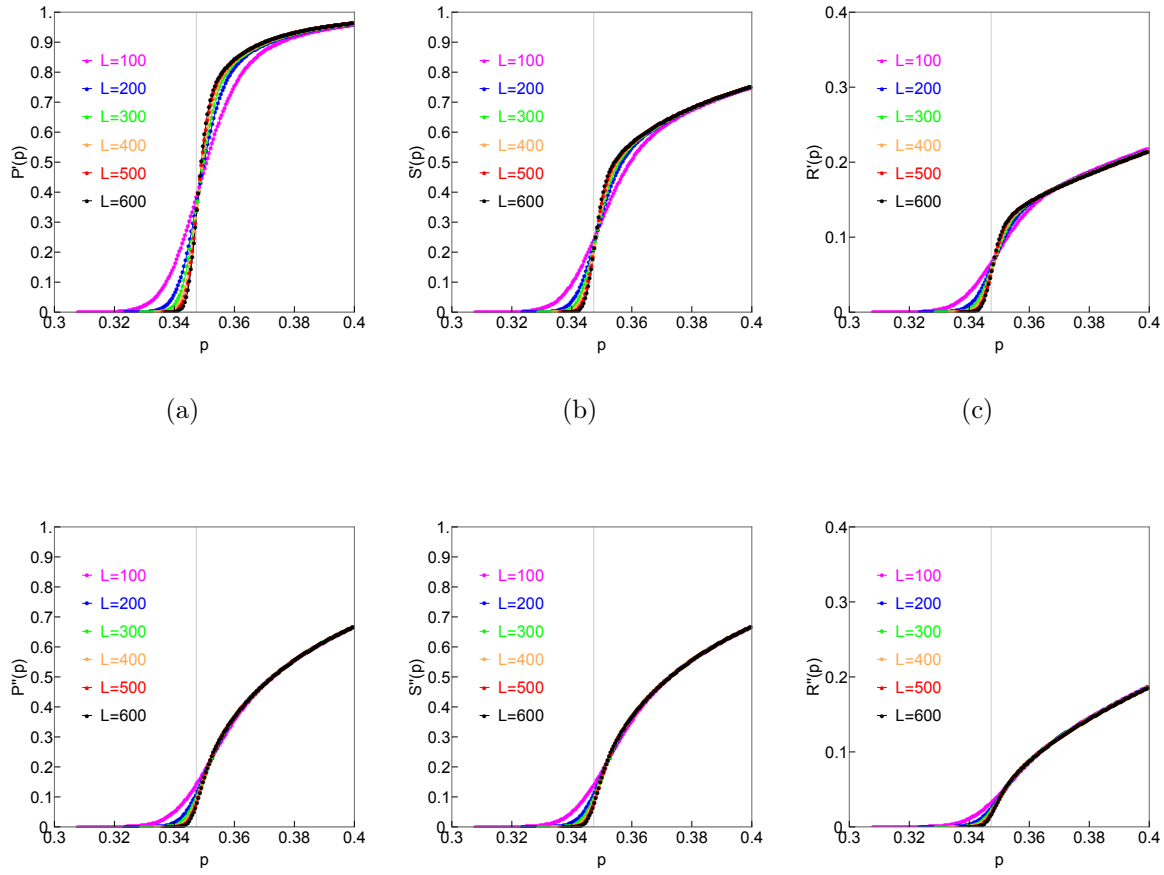

Figure 2.11: Plots of the Order Parameters in Randomly Diluted Triangular Networks. The Network Sizes Include $L = 100$, 200, 300, 400, 500, and 600. Each Size is Ensemble Averaged Over 500 Independent Realizations and the Order Parameters are Shown in the Region Close to the Critical Point Only. a) Fraction of Bonds in the Percolating Cluster, $P'(P)$. B) Fraction of Bonds in the Percolating Cluster that Belong to a Loop, $S'(P)$. C) Fraction of Redundant Bonds in the Percolating Cluster, $R'(P)$. D) Fraction of Bonds in the Current Carrying Backbone, $P''(P)$. E) Fraction of Bonds in the Current Carrying Backbone that Belong to a Loop, $S''(P)$. F) Fraction of Redundant Bonds in the Current Carrying Backbone, $R''(P)$.

system size, it will scale according to the following relation:

$$P'(p,\infty) = L^{-\frac{\beta'}{\nu}}\,\Phi\,[(p-p_c)L^{\frac{1}{\nu}}] \tag{2.21}$$

where β' is the order parameter exponent, ν describes the divergence of a typical length scale as one approaches p_c, and Φ is the scaling function. For Eq. (2.21) to reduce to $P'(p,\infty) \propto (p-p_c)^{\beta'}$, the scaling function must have the form $\Phi(x) \sim x^{\beta'}$ for all $x > 0$. This means the plots of $P'(p,L)$ for different values of p and L would collapse into one curve if $P'(p,L)L^{\beta'/\nu}$ is plotted against the combined quantity $x = (p-p_c)^{\beta'}L^{1/\nu}$, and β' and ν are chosen properly. By applying the scaling assumption introduced above, one can estimate the numerical values of the critical exponents by plotting Eq. (2.21) while adjusting the values of these critical parameters until a satisfactory data collapse is achieved. There are ways to estimate the critical point p_c if its value is not known a priori [49, 50]. For the bond percolation models, the exact value of p_c is known for the percolation transition of largest spanning cluster. Since all quantities in percolating and current carrying clusters are weighted similarly, we know that the transition point for all of them must happen at $p_c = 2\sin(\pi/18)$ for an infinitely large system. To be able to estimate the value of β' using Eq. (2.21), one also needs to determine ν properly. As mentioned before, ν describes the scaling of the correlation length which is proportional to the system size L and its value depends upon the spatial dimension of the system. The best known value for 2D systems of infinite size is $\nu = 4/3 \simeq 1.33$ [44] and this is the value we will use to find β' and β''. However, to confirm that 4/3 is a good approximation for ν, we are going to calculate its numerical value for the systems we have here. The best method to find the estimated value of exponent ν is through the scaling of critical points, as for finite size systems p_c varies from one realization to another. As can be

seen from Figure 2.11, the critical points for systems of different sizes, approach the exact value of $p_c = 2\sin(\pi/18)$ (shown with the gray vertical line in each plot) as the system size grows. The variance of p_c is determined by $\sigma_L^2 = \langle (p_c - \langle p_c \rangle)^2 \rangle$ where $\langle\rangle$ denotes ensemble averaging over all realizations of size L. This variance decreases proportional to $L^{-\frac{1}{\nu}}$ and goes to zero when $L \to \infty$. Thus ν can be determined by studying the plot of p_c against $L^{-\frac{1}{\nu}}$ as shown in Figure 2.12.

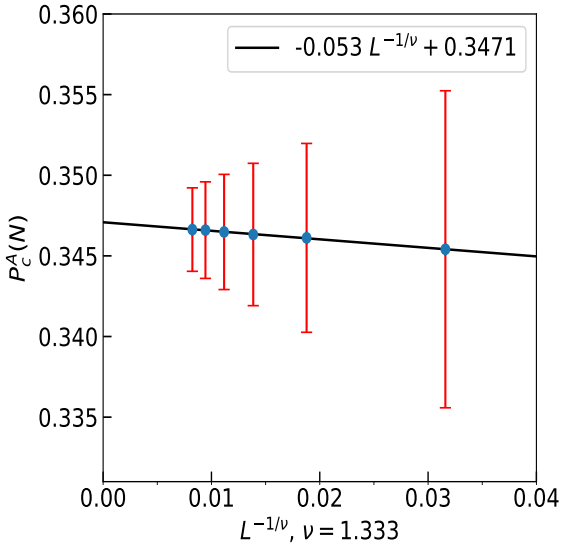

Figure 2.12: Plot of the Critical Points for Systems of Different Sizes Against $L^{-\frac{1}{\nu}}$. The Blue Points Show the p_cs, the Red Lines are the Error Bars (One Standard Deviation) for the Ensemble Averaged p_cs, and the Black Line is a Weighted Linear Regression Fit that Intercepts the Vertical Axis at $p_c = 0.3471 \pm 0.0001$. The Intercept Shows the Value of p_c when $L \to \infty$ which is Achieved when $\nu = 1.333$. It is Very Close to the Exact Value of the Critical Point which is $p_c = 0.3472$. This Means $4/3 \simeq 1.333$ is a Reasonable Approximation for the Value of Exponent ν.

The rightmost point in the plot of Figure 2.12 is the average p_c for realizations of size $L = 100$ and the leftmost point displays the average p_c for realizations of size $L = 600$. As the system size L grows, the points approach the vertical axis. By applying a weighted linear regression, which is shown by the black line in the figure, one can find the intercept that corresponds to the p_c of an infinitely large system.

When $\nu = 1.333$ is used in the plot, the linear fit intercepts the vertical axis at $p_c = 0.3471 \pm 0.0001$ which is close to the predicted value of $p_c = 0.3472$. This means $\nu = 4/3$ is a good approximation for the value of this critical exponent and therefore we will use it when estimating the values of β' and β''.

The next step is to plot $P'(p, L)L^{\beta'/\nu}$ versus $(p-p_c)^{\beta'}L^{1/\nu}$ where the known values $2\sin(\pi/18)$ and $4/3$ will be used for p_c and ν, respectively. If β' is estimated properly, all the curves in Figure 2.11-a will collapse into one curve. Slight changes in the value of β' will affect the collapsing of the data, but these variations are not necessarily visible to the eye. So to find the best value of β', we use the following algorithm:

I First, we make a rough guess for β' and use that guess to collapse the data.

II Then we fit a polynomial of degree n (here $n = 20$) to each of the data curves that somewhat lie on top of each other.

III Using theses fitted polynomials, we evaluate each curve in 100 distinct points in the range $[-0.5, 0.5]$ which is the most convenient range for $x = (p - p_c)^{\beta'}L^{1/\nu}$. If all six curves in Figure 2.11-a are perfectly collapsed, they should be exactly the same at each given x.

IV To quantify the collapse quality, we calculate the standard deviation of the evaluated fitted curves at each x and then find the average of all 100 standard deviations for the chosen β'.

V By changing the β' infinitesimally (step size of 10^{-4} here) and repeating steps 1-4, we collect an array of mean standard deviations versus β'.

VI The minimum of the mean standard deviation is found by scanning the range of β' values. This minimum is the point where the best collapse happens.

Figure 2.13 shows an example of this process where β' is found by collapsing the $P'(p)$ curves. As can be seen from the figure, the minimum value of the mean standard deviation occurs when $\beta' = 0.1385 \pm 0.0001$. This is very close to $\beta = 5/36 = 0.1388$ which is known as the critical exponent describing $P'(p)$ in bond percolation models [43].

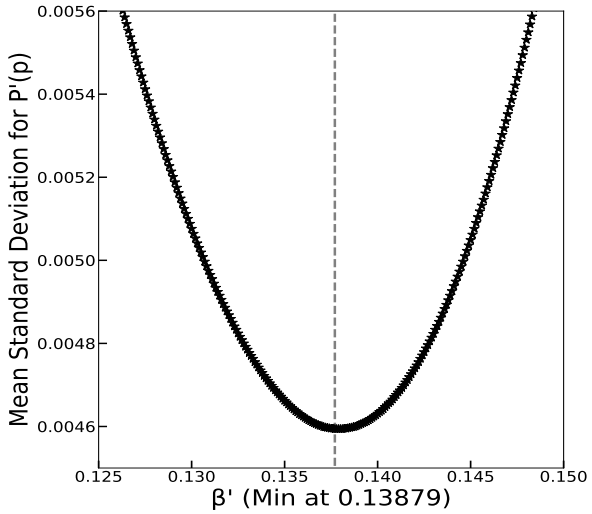

Figure 2.13: The Mean Standard Deviations for Various Values of β', Calculated by Collapsing $P'(P)$ Curves for Sizes L = 100, 200, 300, 400, 500, and 600. The Minimum Value of the Standard Deviation Occurs when $\beta' = 0.1385$. The Gray Dashed Line Marks the Minimum Point.

Critical Quantities	**Known Value**	**Calculated Value**
p_c	$2\sin(\pi/18) = 0.3472$	0.3471 ± 0.0001
ν	$4/3 = 1.333$	1.333
β'	$5/36 = 0.1388$	0.1385 ± 0.0001

Table 2.4: Table of Comparison Between the Known and Calculated Values of a Few Critical Quantities Used in the Study of Connectivity Percolation on Randomly Diluted Triangular Networks. The Found Values for p_c (Exact) and ν are Very Close to Their Expected Values. Using the Known Values of These Two Quantities, We Can Calculate the Critical Exponent β' which is Also Accurate and Close to Its Known Value.

Comparing the calculated and known values of critical quantities p_c, ν, and β', confirms that the procedure used for estimating β' is accurate for this purpose. Table 2.4 shows a summary of these values. This procedure can then be applied to all the order parameters in Figure 2.11 separately. Table 2.5 displays the values of the critical exponents for the set of order parameters studied here. All the shown exponents are calculated using the algorithm introduced above.

Order Parameters	**Critical Exponents**
$P'(p)$	$\beta' = 0.1385$
$S'(p)$	$\beta' = 0.1638$
$R'(p)$	$\beta' = 0.1962$
$P''(p)'$	$\beta'' = 0.5002$
$S''(p)$	$\beta'' = 0.4999$
$R''(p)$	$\beta'' = 0.5368$

Table 2.5: Table of Critical Exponents for Connectivity Percolation on the Randomly Diluted Triangular Networks. All the Values are Calculated Numerically Using the Method Shown in Figure 2.13.

Once the values of proper critical exponents are calculated, we can use them in the scaling relation 2.21 to collapse all data into one curve. Figure 2.14 shows the finite size scaling achieved by using the critical exponents of Table 2.5 for each order parameter.

2.4 Discussion

Unlike the case of hierarchical networks (Table 2.2), where we only needed two distinct exponents to describe the critical behavior of all primed and double primed order parameters, the entries of Table 2.5 are all different except for the exponents

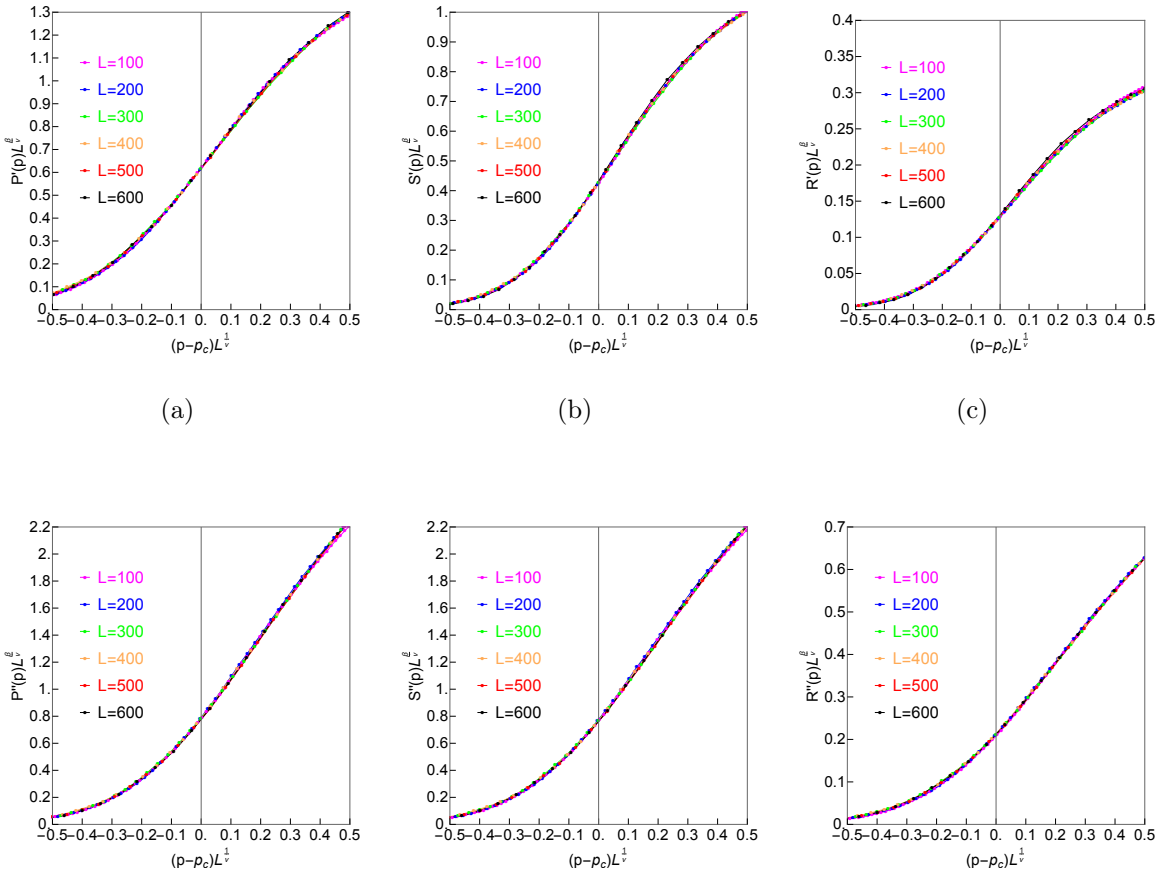

Figure 2.14: The Plots of Scaled Order Parameters After Choosing the Critical Exponent that Leads to the Smallest Errors in the Collapsed Curves. a) Scaled $P'(P)$, B) Scaled $S'(P)$, C) Scaled $R'(P)$, D) Scaled $P''(P)$, E) Scaled $S''(P)$, F) Scaled $R''(P)$.

describing $P''(p)$ and $S''(p)$ which are numerically very close with a difference of $O(10^{-4})$. This makes sense as the two quantities were shown to follow the same curve in plots of Figure 2.10. This means in the case of random bond dilution in triangular networks, we need more than two exponents to study the behavior and impact of loops in percolating and current carrying clusters near the transition point. Despite the differences seen among the values of β' and β'' in Table 2.5, it is obvious that there are two distinct ranges to which β' and β'' belong. For example, all the values of β' are in the range $(0.1385 - 0.1962)$, while β''s are closer to one half and are in

the range $(0.4999 - 0.5368)$ with no intermediate values between the two ranges. So the overall picture obtained from Table 2.5 is similar to what we observed for the hierarchical networks. The differences between the values of β' and β'' could be due to numerical errors or lack of good statistics. Or it could be that the hierarchical networks are distinctive.

In this chapter we study the percolation transition of connecting and conducting clusters in two different types of systems: hierarchical and triangular networks. In particular, we are interested in the effect of loops in bond percolation. To this end, we define a new set of order parameters that account for the total number of loops and the fraction of bonds that are involved in loops in a cluster. In the case of hierarchical networks, our calculation reveal that the critical behavior of loops in a cluster (which are a sub-group of the entire cluster) matches the critical behavior of the cluster as a whole. This shows that there is a high degree of fractal behavior associated with these types of networks. In triangular networks on the other had, the behavior of loops in a cluster is slightly different from the behavior of the cluster as a whole. In these networks, the sub-groups go to zero slightly faster than the system itself at the transition point. This is revealed by larger values of the critical exponents describing the looped and redundant bonds as is shown in Table 2.5.

Loops in a connectivity percolation model are similar to stressed regions in a rigidity percolation model. Rigidity percolation is a type of percolation model where the rigidity of the spanning cluster is of interest. When we are concerned with the mechanical rigidity of a spring network, some of the typical questions we ask are:

- How many degrees of freedom does the system have?
- Is there a single macroscopic cluster of sites in which they are rigidly connected?

And if we apply ideas from percolation theory, we can also ask:

- Does this rigid cluster span the system?

A percolating rigid cluster can be made of stressed regions that contain redundant bonds. According to the definition presented in the previous chapter, a redundant bond in a rigid cluster is a bond that is not necessary to maintain the rigidity of the cluster. In that sense, loops are unnecessary to maintain the connectedness of a percolating cluster or conductivity of a current carrying cluster. Hence, those bonds that close a loop in a percolating path can be considered redundant. The concept of redundancy is the key component in understanding the interplay between connectivity percolation and rigidity percolation. Thus the study of redundant bonds and loops in a percolation model can shed light on the effect of stress in rigidity percolation which is a problem with a higher degree of complexity [51]. Table 2.6 shows the mapping between the quantities that were studied in this chapter for connectivity and conductivity percolation and their corresponding quantities in rigidity percolation.

Bond Percolation Theory	**Rigidity Percolation Theory**
Percolating cluster	Rigidly percolating cluster
Current carrying cluster	Force carrying cluster
Bonds in a loop	Stressed bonds
Bonds that close a loop	Bonds that are redundant for the rigidity

Table 2.6: The Mapping Between Quantities in Connectivity Percolation and Quantities in Rigidity Percolation.

All the ideas introduced in this chapter, can be used to study the effect of redundant bonds and stress in rigidity transition.

Chapter 3

RIGIDITY LOSS IN DISORDERED SYSTEMS: THREE SCENARIOS

This chapter is a reprint of the following journal article:

Ellenbroek, Wouter G., Varda F. Hagh, Avishek Kumar, M. F. Thorpe, and Martin Van Hecke. "Rigidity loss in disordered systems: Three scenarios." Physical review letters 114, no. 13 (2015): 135501.

My contribution to this work includes developing computer codes to generate all the network samples studied here, performing the measurements in Figure 3.3 and generating Figures 3.1-3.3.

We reveal significant qualitative differences in the rigidity transition of three types of disordered network materials: randomly diluted spring networks, jammed sphere packings, and *stress-relieved* networks that are diluted using a protocol that avoids the appearance of floppy regions. The marginal state of jammed and stress-relieved networks are globally isostatic, while marginal randomly diluted networks show both overconstrained and underconstrained regions. When a single bond is added to or removed from these isostatic systems, jammed networks become globally overconstrained or floppy, whereas the effect on stress-relieved networks is more local and limited. These differences are also reflected in the linear elastic properties and point to the highly effective and unusual role of global self-organization in jammed sphere packings.

3.1 Introduction

Disordered elastic networks and sphere packings represent a large class of amorphous athermal materials, ranging from (bio)polymer networks to granular media and foams [52, 53, 54]. Random networks of springs lose their rigidity when enough springs are cut; this random bond dilution process is known as rigidity percolation (RP) [55, 56, 57, 18, 19]. Packings of soft spheres do the same when their confining pressure is lowered towards zero: this is called (un)jamming [4, 58, 59, 60, 61]. These rigidity loss scenarios have been studied extensively, in particular for the simplest cases of networks of harmonic springs [18, 19] or soft frictionless harmonic spheres [58, 59, 60, 61]. In that case, the linear elastic properties of packings can be mapped to that of a spring network, where each contact is replaced by the appropriate spring [62, 63, 1]. Lowering the pressure, the number of bonds in the equivalent network decreases.

Given this close correspondence, it is surprising that the nature of the RP and unjamming transitions, and of their respective marginally rigid states, are significantly different. For packings of a large number (N) of soft spheres, extensive studies have shown that *(i)* the connectivity, i.e., the average number of contacts z per particle, goes to $z_c = 2D + \mathcal{O}(1/N)$ at the marginal point, where D is the space dimension [4, 58, 59, 60, 61, 54, 64, 65, 66, 67], *(ii)* the system remains homogeneously jammed up to the point of unjamming (with the exception of individual loose particles called rattlers or very rare small particle clusters) [58], and *(iii)* the shear modulus, G vanishes as $\Delta z := z - z_c$ whereas the bulk modulus K remains finite when $\Delta z \to 0$ [4, 58, 59, 60, 61, 62]. In contrast, in rigidity percolation of generic networks, extensive studies have revealed that for large systems *(i)* the connectivity z, which gives the average number of springs per node, approaches $z_c = 3.9612\cdots < 2D$

for the bond diluted triangular network [18, 19], *(ii)* the largest rigid cluster takes on a heterogeneous, fractal shape, and *(iii)* both the shear modulus, G, and bulk modulus, K smoothly vanish at the critical point in a way typical for a second order phase transition [18, 19].

To understand these differences, we note that the small difference in z_c points to a huge, qualitative difference between jammed and random networks. Based on extensions of the ideas of Maxwell [14]), a simple mean field argument locates the marginal point where the number of degrees of freedom (DN coordinates) is balanced by the number of constraints ($zN/2$ bonds) at $z = 2D$. This argument is exact if all the constraints are independent and there is a single rigid cluster. If there are redundant bonds, z_c can deviate from $2D$, although proper counting of *actual* degrees of freedom and *independent* constraints would remove this apparent violation of Maxwell's criterion [68]. Indeed, the rigid network in RP contains both redundant constraints (bonds) and flexible hinges (sites) at the marginal point so that $z_c \neq 2D$. In contrast, we will show that sphere packings at the jamming transition are isostatic everywhere: nothing can move (except a few rattlers) and *every bond is essential* for the rigidity of the network. Jammed systems show a high degree of organization, leading to highly non-generic networks [1].

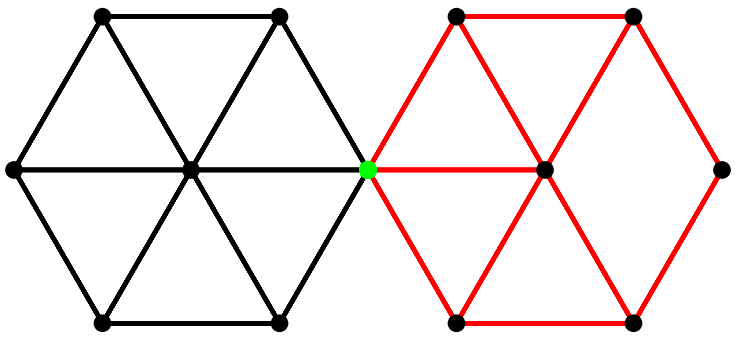

Figure 3.1: (Color Online) Rigid Region Decomposition, where There are Two Rigid Regions, One (Black Bonds) Overconstrained and the Other Isostatic (Red Bonds), Separated by a Hinge (Light Green Site). The Sites which are Not Hinges are Colored Black.

Several open questions thus arise: What is different in the topology and geometry of the underlying networks of random springs and jammed packings? Can we conceive other families of networks with different rigidity loss transitions? Here we address these questions, by determining the overconstrained and underconstrained regions using the pebble game [18, 19]. This is an integer algorithm that analyzes the topology of generic spring networks, by a very effective decomposition of such networks into rigid regions, with both unstressed (isostatic) and stressed (overconstrained or superfluous [69]) rigid regions, and the hinges that separate rigid regions.

Figure 3.1 illustrates such an analysis for a small network. The 12 black bonds (Figure 3.1 left) might carry finite forces whilst maintaining force balance: such bonds are redundant, as any one of these bonds could be removed and the remainder would still be rigid, and are called *stressed*. We emphasize that a stressed bond typically, but not necessarily, carries a finite force: the concept of stressed/redundant bonds should not be confused with, e.g., the prestress [70, 1]. The 11 red bonds (Figure 3.1 right) show a rigid cluster that is exactly isostatic, and removal of any of these bonds would break the cluster. Such bonds are called unstressed, and necessarily carry zero force. Finally, the green node in the center of this network is a hinge (defined as a site that belongs to at least two rigid clusters). For more complex networks, the pebble game is an effective algorithm to unambiguously determine the rigid clusters [18, 19].

3.2 Pebble Game Analysis

We will now characterize three families of network topologies by the pebble game. Unless otherwise stated RP will refer to the *bond diluted triangular network* in this letter, which is the best studied system. For all networks, we use periodic (wrap-around) boundary conditions.

Figure 3.2 shows dramatic differences in the nature of the marginal states depend-

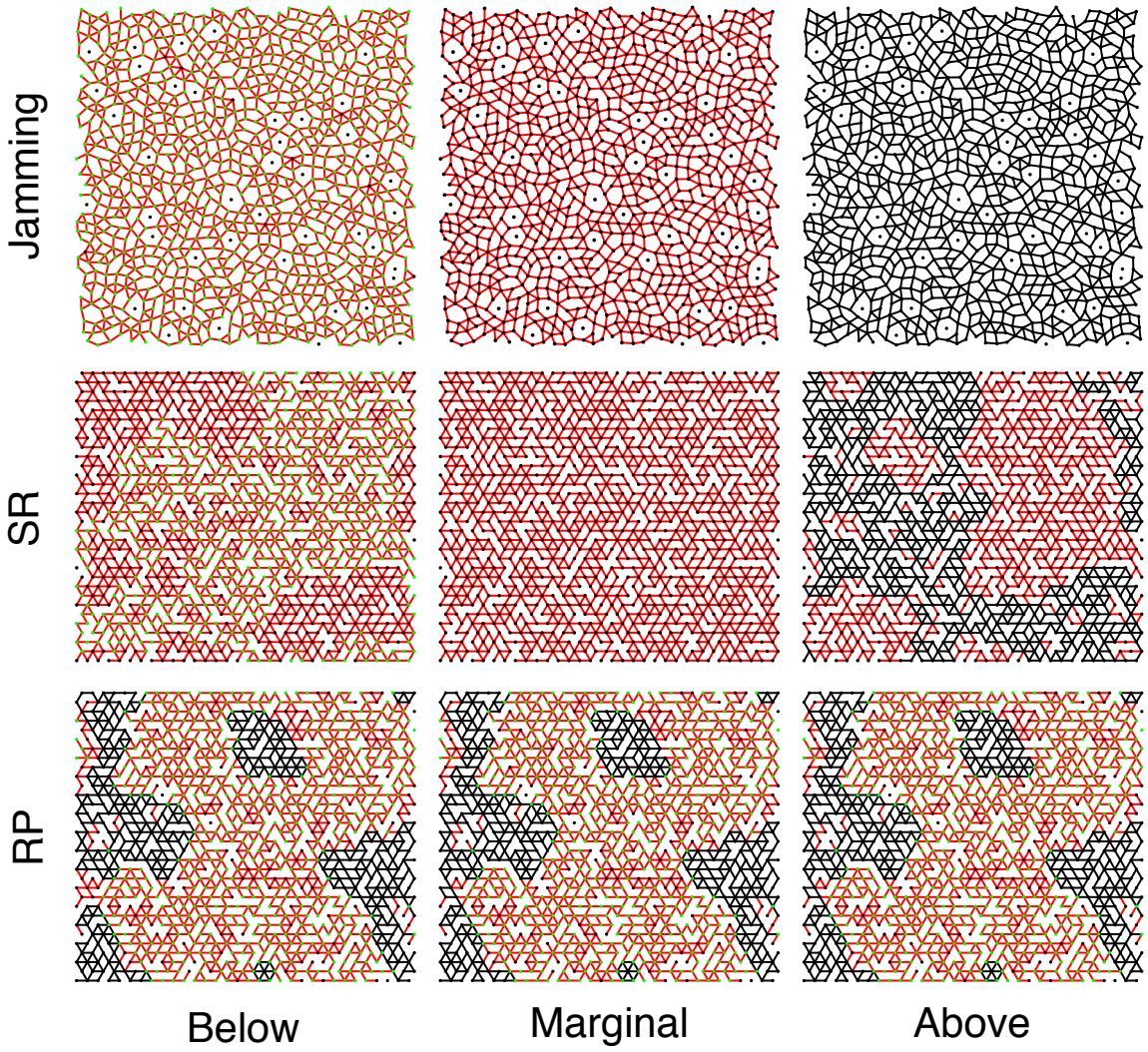

Figure 3.2: (Color Online) Pebble Game Results for a Jammed Packing (Top Row), a Stress-Relieved Triangular Network (Middle Row) and Rigidity Percolation (Bottom Row). The Center Panel is the Marginal Case in All Three Panels, with the Left Panel Having a Single Bond Removed and the Right Panel a Single Bond Restored. The Marginal States of Both Jammed Systems as Well as the SR Network is Fully Isostatic (Red), Whereas the Marginal State for RP Features Floppy Modes (Involving the Green Hinge Sites) and Has 34% of All Bonds Stressed (Black).

ing on the physical process that generates these networks. The top row shows the jammed-packing-derived networks one contact above the marginal state (right) and with one/two contacts randomly removed (center/left). Strikingly, in the marginal state of the jammed network, all bonds are isostatic (red), just above it, the whole

system is overconstrained (black), and when a single bond is removed, almost every site becomes a hinge (green). In terms of the network topology, this is a massively first order transition. In the bottom row of Figure 3.2, the gentle evolution through the marginal state in RP is shown. The marginal state contains both isostatic and redundant pieces in the percolating rigid backbone, as well as significant numbers of green hinges — adding or removing a single bond hardly changes the configuration, typical of a second order transition.

We now introduce a third family of networks that becomes isostatic everywhere at their marginal point — as in jamming — by cutting bonds randomly, but only if they are stressed. This stress-relieving (SR) cutting algorithm leads, by construction, to the percolating marginally rigid cluster being *precisely and exactly isostatic* everywhere, without any overconstrained or underconstrained regions. This also means that in both jamming and SR (but not RP) the transition happens at the mean field Maxwell point, so that the mean coordination is $2D$ with zero redundant constraints anywhere.

In the middle row of Figure 3.2 we show the pebble game analysis for SR cutting, starting from a triangular network. An isostatic state with a single cluster is produced at the marginal point, reminiscent of the jammed state. However, this marginal state is very different in character: both adding or removing a bond has a less dramatic effect than in jamming. Hence, isostaticity everywhere is not the only nontrivial feature of the jammed state: its organization is such that its globally isostatic state is changed *everywhere* by the addition or subtraction of a *single constraint*, in stark contrast to SR networks.

Both stressed and random bond removal can be performed on any initial configuration, including jamming-derived networks at given connectivity z_j. Doing so yields *two* two-parameter families of networks, each characterized by z *and* z_j. Starting

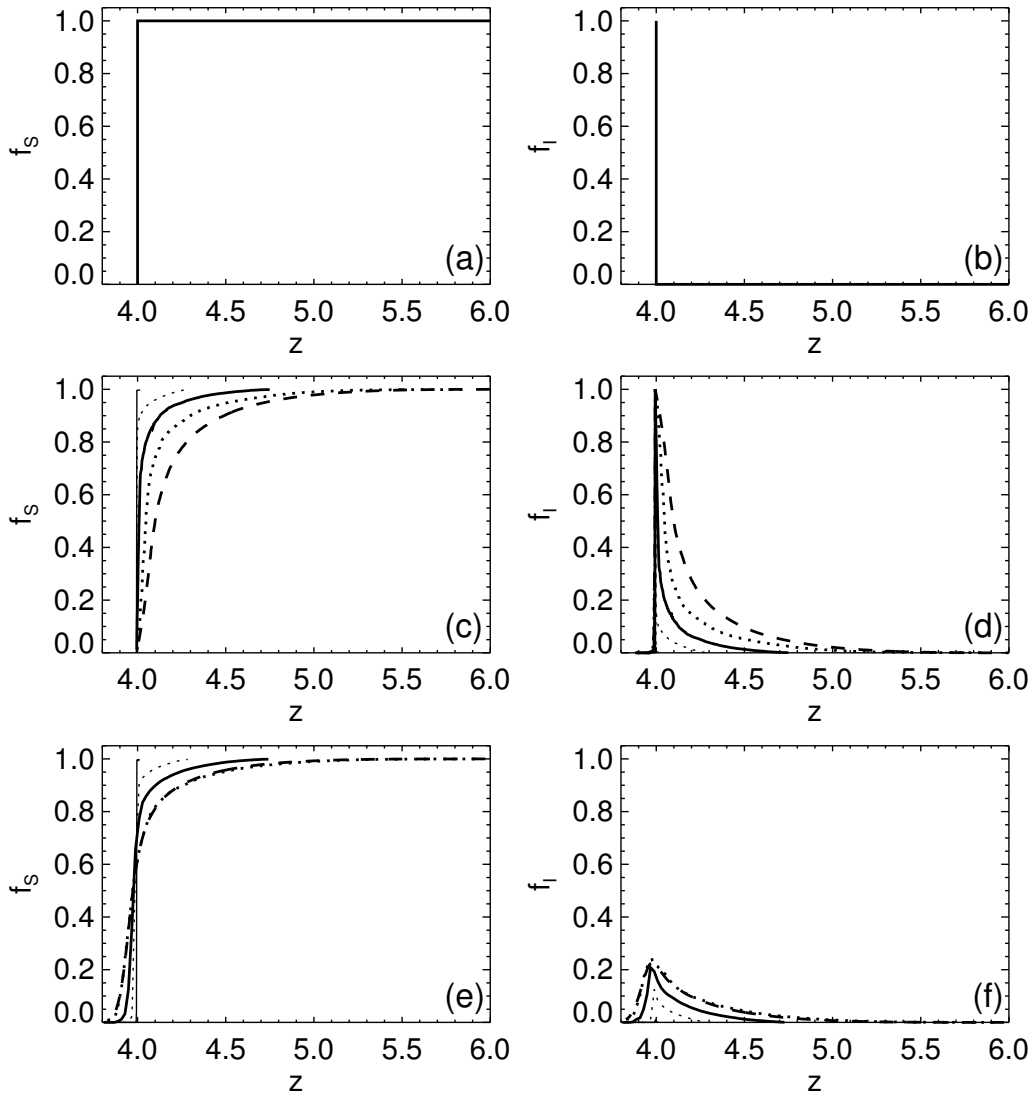

Figure 3.3: Fraction of Stressed (Left) and Isostatic (Right) Bonds in the Rigid Backbone for Jamming (Top), Stressed Bond Dilution (Middle) and Random Bond Dilution (Bottom). In C-F, Line Styles Indicate Starting Point for Bond Removal: Jammed Networks at $z_j = 4.01$ (Solid, Thin), $z_j = 4.3$ (Dotted, Thin), $z_j = 4.7$ (Solid, Thick), $z_j = 5.98$ (Dotted, Thick) and Triangular (Dashed, Thick). Data is Averaged Over 300 Triangular Nets Or 25-50 Jamming-Derived Networks.

with z_j close to $2D$, we can for example probe how, and how quickly, the network topology crosses over from jammed to generic or SR-like.

In Figure 3.3 we compare the fractions of stressed and isostatic bonds for jamming (top row), SR (middle row) and RP (bottom row), where the latter two have initial

configurations corresponding to jammed networks at four different values of z or a triangular net. For jamming, the fraction of stressed bonds, f_s, discontinuously jumps from one to zero, and the fraction of isostatic bonds, f_i, jumps from zero to one when z is lowered, consistent with the picture shown in Figure 3.2. This happens because in jammed sphere packings only contacts that carry a positive force can be detected and therefore all bonds in the network must be stressed. For *random* bond dilution, $f_s(z)$ and $f_i(z)$ remain continuous irrespective of z_j, and for large z_j, these functions smoothly approach those of the triangular net.

In the middle row of Figure 3.3 we show $f_s(z)$ and $f_i(z)$ for the same five families of networks for *stressed* bond dilution. The data shown here appears to have a discontinuity around $z = 4$; it is an open question whether this discontinuity persists in the thermodynamic limit. For $z_j = 5.98$, the apparent jump is small, and the curves are closer to those of the triangular net. However, we still see deviations from the triangular case which is surprising given that here we have to cut almost $1/3$ of the bonds to reach the critical point. For smaller z_j, the apparent jumps in f_s and f_i grow, approaching the step functions of jamming — this is easy to understand, as for $z_j \to 4$ an increasingly small fraction of bonds gets removed before reaching $z = 4$.

3.3 Discontinuous Response to Bond Addition and Removal

The response to addition or removal of bonds is a measure for the degree of organization in the network, and to quantify the discontinuous response at the marginal point more precisely, we introduce two new indices. The first is h, the ease-of-breakup index which is defined by removing one bond randomly from the marginal state, counting the number of new green hinges, averaging over every bond in the network, and dividing by the number of sites so that $0 < h < 1$. The second is s, the ease of stressing index, defined by adding one bond randomly, counting the number of new

stressed bonds, average over all bonds and divide by the number of bonds so that $0 < s < 1$. High values of h and s imply strong self-organization of the network.

We find that in networks representing packings near unjamming the index $h \approx 0.97$ and $s \approx 0.98$ (cf. top row of Figure 3.2), while for RP networks, both indices are very small ($h \approx 0.0003$ and $s \approx 0.001$) as expected for a second order transition (see Figure 3.2). Intermediate values of h and s are found for SR ($h \approx 0.28 \pm 0.04$ and $s \approx 0.47 \pm 0.05$) where the spread is specific to our system sizes and is expected to go down for larger systems. We have made an additional isostatic marginal state by adding bonds to an empty triangular net, avoiding adding stressed bonds, which also produces a marginal isostatic state, but with even lower index values: $h \approx 0.21$ and $s \approx 0.40$. The large values of both h and s for the jammed state show how remarkably self-organized it is.

To understand the large h index for jamming, we start from the globally isostatic jammed network at the critical point: according to Laman's theorem [16], the number of bonds equals $2N - 3$ and the number of bonds b in subgraphs of n nodes satisfies $b \leq 2n - 3$. After we remove a bond, only subgraphs that have precisely $2n - 3$ bonds are isostatic. Examples of these are $n = 3$ triangles or $n = 4$ double triangles (Figure 3.2). Here all nodes are at the cluster's edge and are hinges — "black dots" can only arise in the interior of isostatic clusters. The large value of h thus implies that $n > 4$ isostatic clusters are very unlikely to occur in jamming.

We now suggest that large n isostatic clusters are suppressed due to the homogeneity of jammed systems, using a variation on a well-known bond cutting argument [59, 60, 71, 72]. Consider a large (hypothetical) isostatic cluster C with n nodes and $2n-3$ *internal* connections, and n_e nodes at the edge of C. All $\mathcal{O}(n_e)$ connections that cross the boundary of C (for SR and RP there may be fewer) do not contribute to internal connections, so that the mean contact number of C is of order $2n + n_e$ —

as $n_e \sim \sqrt{n}$, this is significantly above the global mean contact number $2n$, even for relatively large clusters (for a $n = 100$ circular cluster we estimate $z \approx 4.3$). Whereas RP and SR systems below the marginal point clearly have such subgraphs, these become extremely unlikely for jammed systems. Thus, the h-index in jamming is much larger than in SR or RP because spatial fluctuations in local contact numbers are smaller [73]. How precisely this homogeneity arises remains an open problem.

To understand the large s index for jamming, we note that for jammed networks all bonds carry a positive force and are stressed, as jammed systems are at finite pressure. For SR and RP networks there is no positivity condition on the contact forces, and both isostatic zero force regions and stressed regions where positive and negative forces precisely balance can occur. This difference is clearly illustrated in SR and RP networks above the marginal point, where stressed regions can have convex edges where forces of opposite sign balance — this is ruled out in jamming. We believe that such differences also underlie the inequality of the s index for jamming and SR.

3.4 Elastic Moduli

We calculate the elastic moduli of the networks in linear response from the dynamical matrix [74, 75, 76]. In Figure 3.4 we show shear (G) and bulk (K) moduli as a function of z for the same four values of z_j as in Figure 3.3 and for the generic triangular net, both for random bond dilution and for stressed-bond-only dilution. Clearly, a very simple scenario unfolds: *(1)* For $z_j \approx 6$, the functions $G(z)$ and $K(z)$ are virtually identical to those for bond dilution of triangular nets. *(2)* $G(z)$ is essentially independent of z_j, consistent with our earlier observations [1]. *(3)* The behavior of K is richer. For jammed networks with $z = z_j$, K weakly depends on z but remains finite ($K_j(z = 4) > 0$). However, for all z_j that we have investigated, we find that

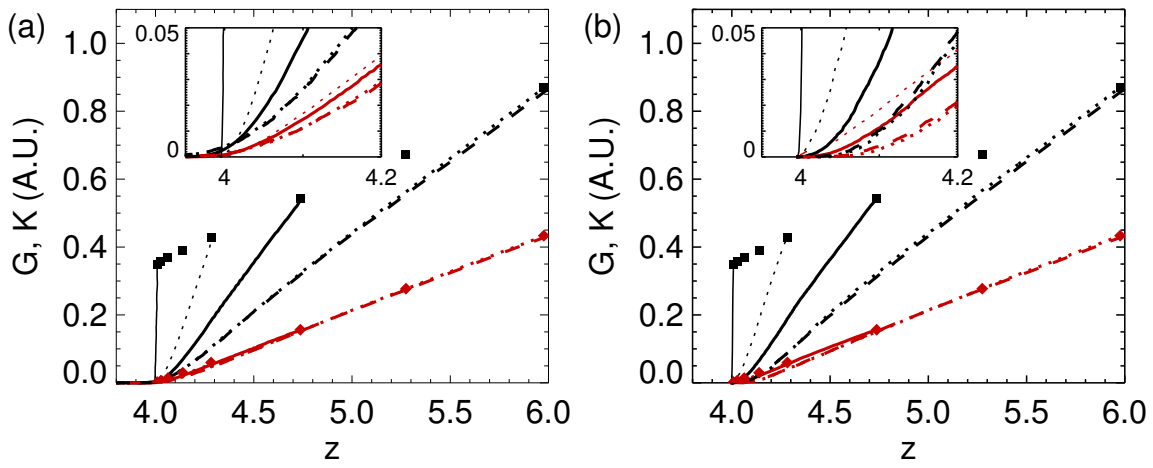

Figure 3.4: (Color Online) Shear Modulus G (Red) and Bulk Modulus K (Black) for (a) Random Bond Dilution and (B) Stressed Bond Dilution. As in Figure 3.3, The Initial Condition is the Network of a Jammed Packing at $z_j = 4.01$ (Solid, Thin), $z_j = 4.3$ (Dotted, Thin), $z_j = 4.7$ (Solid, Thick), $z_j = 5.98$ (Dotted, Thick) and Triangular Networks (Dashed, Thick). as the Initial Condition. Insets Show Zoom-Ins Around the Transition. Solid Squares and Diamonds Denote the Moduli of the Jammed Packings as Published Earlier in Ref. [1].

upon bond dilution K vanishes as

$$K(z, z_j) = K_j(z_j)\,[(z_j - z)/(z_j - z_c)]^{\alpha} \quad , \tag{3.1}$$

where α is close to unity. Our systems are too small to precisely determine α, although the smoothing near $z = 4$ is consistent with $\alpha \approx 1.4$ as found for 2D triangular nets.

Is this difference in moduli related to h and s? Strictly speaking, no: it is the network's geometry, not topology, which determines the elastic response (even small geometric perturbations of networks, be they quasicrystals [77] or jammed [78], can strongly perturb K). However, both the the large value of s and the finite value of K, are intimately connected to the repulsive nature of contacts in jamming [62, 1, 77]. Clearly the network reorganizations of jammed systems when they are decompressed (such geometric reorganizations are absent in SR and RP), leads to networks where finite positive contact forces can balance, and h and s tend to one.

3.5 Discussion

It was known that jammed networks had to satisfy the Maxwell condition globally and had to satisfy the Hilbert criterion locally [53], but neither of those imply the self-organization in terms of rigid cluster analysis that we uncover. From a design perspective, our two-parameter families of networks are attractive because they allow to independently set the ratio G/K of elastic moduli and the connectivity z (Figure 3.4). Fully random networks are non-optimal in propagating rigidity, as unhelpful stressed regions remain in the backbone. SR networks are better, but still become soft against compression at their marginal point. Jamming can be seen as a strategy to find special, perhaps optimal geometries of spring networks in terms of propagating rigidity and resistance to compression, although jammed networks are not the only ones that have finite K at the marginal point [77]. We have not been able to come up with algorithms that generate networks with the same intricate network topologies as jamming, and suggest that whether this is possible remains an important open problem [79, 80].

Finally, many other marginal networks have been studied recently [81, 82, 83]. Square and kagome lattices with randomly added braces, which are even more homogeneous than jammed networks, were shown to also have a very sharp rigidity transition [84] with (in our terminology) h and s close to one, consistent with our findings. One alternative protocol to create networks that are isostatic everywhere was introduced by Lopez *et al.* [80]. For small N, these networks become macroscopically floppy upon removal of a single bond, but this effect disappears as N increases, and we expect that their networks are similar to our SR networks, with $K \to 0$. Another recent conditional cutting protocol allows for the independent tuning of the ratio of bulk and shear moduli [85]. We hope that our work will inspire work to an-

alyze such network topologies, leading to better understanding which other families of networks can be constructed, with distinct properties of the stressed and isostatic bonds, hinges, h and s indices, and elastic moduli.

Acknowledgments

We acknowledge discussion with N. Upadhyaya and V. Vitelli, who did early calculations on the bulk modulus in a two-parameter family of networks. WGE acknowledges support from NWO/VENI. MvH acknowledges support from NWO/VICI. The work at Arizona Sate University was supported by the National Science Foundation under grant DMR 0703973NSF. AK would like to acknowledge funding from GAANN P200A090123 and the ARCS Foundation.

Chapter 4

JAMMING IN PERSPECTIVE

This chapter is a reprint of the following submitted article:

Hagh, Varda F., Eric I. Corwin, Kenneth Stephenson, and M. F. Thorpe; “Jamming in Perspective"; arXiv:1803.03869 (2018).

My contribution to this work includes developing computer codes to generate the network samples, conducting all the measurements, writing the manuscript, and generating all of the figures in this chapter.

Jamming occurs when objects like grains are packed tightly together (e.g. grain silos). It is highly cooperative and can lead to phenomena like earthquakes, traffic jams, etc. In this Letter we point out the paramount importance of the underlying contact network for jammed systems; the network must have one contact in excess of isostaticity *and* a finite bulk modulus. Isostatic means that the number of degrees of freedom are exactly balanced by the number of constraints. This defines a large class of networks that can be constructed without the necessity of packing particles together compressively (either in the lab or computationally). One such construction, which we explore here, involves setting up the Delaunay triangulation of a Poisson disk sampling and then removing edges to maximize the bulk modulus, until the isostatic plus one point is reached. This construction works in any dimensions and here we give results in 2D where we also show how such networks can be transformed into a disk pack.

4.1 Introduction

Disordered packings of athermal frictionless particles are a standard model for studying the jamming transition in amorphous materials such as granular media [86], foams [87], colloidal suspensions [88], and glasses [89]. Every jammed system can be represented by a disordered spring network. To create this network, the center of mass of each particle is replaced with a vertex with an edge between two vertexes if their equivalent particles are in contact. The network embedding of a jammed system is isostatic *plus one*, meaning that the number of degrees of freedom (dN where d is the dimension and N is the number of vertexes) and constraints (N_e that is the number of edges) are balanced in a way that there is exactly one state of self stress in the system. This extra *plus one* is necessary for mechanical stability and a finite bulk modulus [13, 90]. This then becomes a combinatoric rather than a geometry problem as only the network topology is involved; assuming the network is generic (no symmetry) which is the case in disordered networks, glasses etc. The Maxwell count for an isostatic system, which has a *periodic super cell*, is such that the number of floppy modes, F, are exactly zero, so

$$F = dN - N_e - d = 0 \tag{4.1}$$

with the dimension $d = 2$ in this Letter. The last term is to make sure that the d macroscopic translations are properly accounted for.

We use the pebble game [45, 46] (a numerical algorithm based on Laman's theorem [91]) in 2D to determine the rigid region decomposition of the network. For jammed systems at the isostatic point, the system is isostatic everywhere, with no stressed edges. We refer to this as *locally isostatic* [92]. This is a stricter requirement than just applying Eq. (4.1) once globally, as it requires that all subgraphs are also

isostatic. Clearly just applying (4.1) globally could give locally stressed regions balanced by other regions containing floppy modes and hinges, as happens in rigidity percolation [7].

4.2 A New Approach to Jamming

Traditional computational methods available to create jammed packings, usually with disks or spheres, include some mixture of molecular dynamics, event driven dynamics, and energy minimization schemes [93, 94, 95, 96, 97, 98]. The new method introduced here, produces a jammed network with precisely one state of self stress and expands the set of what was previously accepted as jammed. To be precise, we define a jammed network as being *isostatic plus one excess contact* and having a *finite bulk modulus*. By finite we mean $O(1)$ and not $O(1/N)$ which will go to zero as the number of vertexes N tends to infinity. Such a network has the consequence that when one edge is removed, the network is locally isostatic. With this definition, we are now free to adopt any construction method that will achieve this. There is the traditional method which packs particles together by compression and a new method described here. Other definitions of jammed systems are available (see Theorem 1 in [99]) but we have found the above to be the most useful in practice.

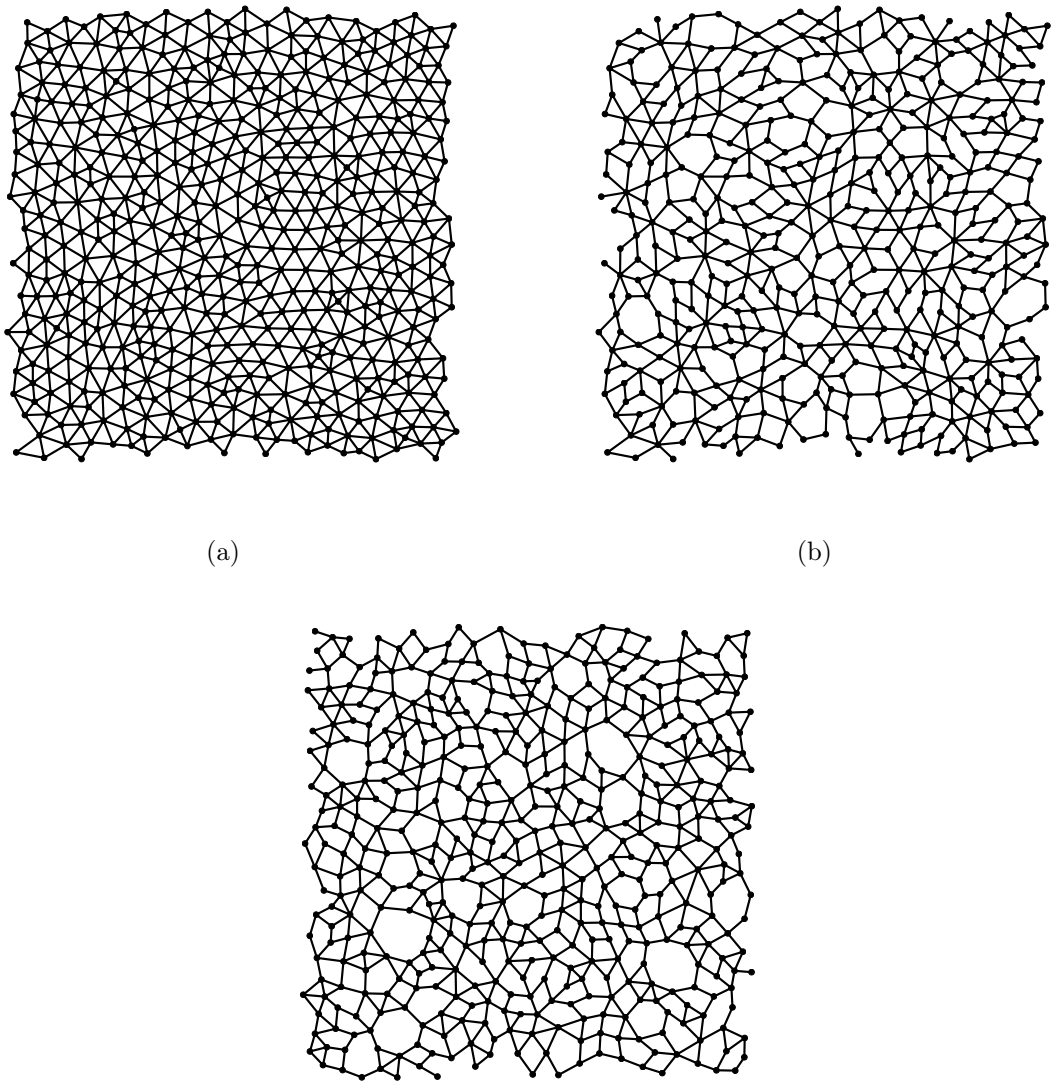

(a) (b)

(c)

Figure 4.1: A) Delaunay Triangulation of a Poisson Disk Sampling with 512 Points. B) The Same Network at the Isostatic Plus One, After Pruning Edges that Minimally Reduce the Bulk Modulus and Removing the Rattlers. C) The Network Representation of a Polydisperse Jammed Pack, Formed by Compressing Disks, with Approximately Same Number of Vertexes as in Part (B).

The new approach uses an algorithm that allows for precise control over the number of contacts in excess of isostaticity [100, 101, 102]. We focus on the network as being fundamental to the jammed state and show that in two dimensions, the network

can always be replaced by a disk pack, as well as vice-versa. Often it is useful to add a single additional edge (or contact) to create a single state of self stress and we will refer to this as *isostatic plus one*. We note that this is often referred to confusingly as isostatic in the literature and we strongly discourage this usage. These systems are delicately balanced and a single edge present at isostaic plus one does make a global difference at the isostatic point; no matter how large the system.

For a non-crystalline system to be jammed it is necessary but not sufficient for it to be isostatic plus one. An additional degree of cooperativity needs to be introduced by demanding that the bulk modulus drops from finite to zero as a single edge is removed in going from isostatic plus one to the isostatic state. A locally isostatic network can be easily achieved by randomly removing stressed edges from a highly overconstrained network, but the resulting network will not necessarily have a finite bulk modulus at isostatic plus one [7]. Therefore the finiteness of bulk modulus does *not* follow from the system being locally isostatic when an edge is removed. A convenient way to characterize the extreme cooperativity of jammed networks is through two indexes s and h, where s measures the fraction of stressed edges, when any one additional edge is added to an isostatic network, and h measures the fraction of hinged vertexes when any one edge is removed. This comes entirely from the static properties, using the pebble game, and is a very convenient way to establish the marginality of jammed networks without getting into the details of low frequency dynamics [71, 103] which is discussed in detail in the Supplemental Material. If rattlers are removed, both locally isostatic and jammed networks can have $s = 1$ and $h = 1$ [7], so this cannot be used to distinguish between them[1]. Hence we need to include in the definition of jammed states that the bulk modulus is finite at isostatic plus one.

[1]When pruning a spring network, if we do not remove the rattlers that appear in the form of vertexes with coordination number $z = 2$, the s and h indexes will be slightly smaller than 1.

The new method to generate polydisperse jammed packs at zero temperature does not require exploring the entire energy landscape to bring the system into zero internal energy and isostaticity. Instead, it builds the system within a single local energy minimum. We try to keep cavities to a minimum so all packing fractions are within the range $0.77 < \phi < 0.82$ after removing the rattlers.

4.3 Computational Methods

This new method is based on a pruning algorithm that is used to manipulate and control the elastic properties of disordered harmonic spring networks [85]. These disordered networks are usually created by minimizing the energy of N repulsive frictionless particles in a periodic box and stopping at a coordination that is slightly above jamming transition point. Therefore they already have encoded in them the properties of jamming and should not be thought of as generic networks. By contrast, in this work we generate the initial networks *de novo and far from jamming*, using computational geometry only. The disordered jamming-like networks are then created by performing a simple set of steps. A summary of the procedure is presented below:

- We start by generating N points in a box with periodic boundary conditions that are distributed by Poisson disk sampling [104, 105]. The Poisson sampling is used for aesthetic purposes only and is not necessary for the process. We have confirmed that the same results are obtained when a uniform distribution of points is used.

- We then find the Delaunay triangulation of these points [106]. To make the triangles look more regular, we move each vertex to the centroid of the polygon formed by its nearest neighbors, iteratively, until every vertex is at the centroid of its neighbors. An example of such generated samples is shown in Figure 4.1-a.

This geometrically generated network is highly over-constrained and far from isostatic (with a mean coordination of $\langle z| =\rangle 2N_e/N = 6$), therefore we need to remove N_r redundant edges to push it down to the isostatic plus one point as desired.

- There are $\binom{N_e}{N_r}$ ways to prune these N_r redundant edges from the network. It is well known [107, 108] that the contribution of a removed edge to the bulk modulus is largely independent of its contribution to the shear modulus, although these moduli cannot increase by removing an edge ([109], pp. 110-111). Since jammed packs maintain a finite bulk modulus while the ratio of shear (G) and bulk (K) moduli vanishes at jamming point [110], at each step we find and remove the edge that maximizes the bulk modulus of the remaining network. Maximizing the bulk modulus is not strictly necessary as similar results can be obtained if we remove an edge randomly from the top 20% of edges that have minimal contribution to the changes in bulk modulus.

- We repeat the process, until we arrive at isostatic plus one where $\langle z\rangle \simeq 4$. The resulting network has a finite bulk modulus and is shown in Figure 4.1-b. Figure 4.2 shows how the bulk and shear elastic moduli of the network change as the edges are pruned. The behavior of the shear modulus is reminiscent of random rigidity percolation models [7] as well as jamming.

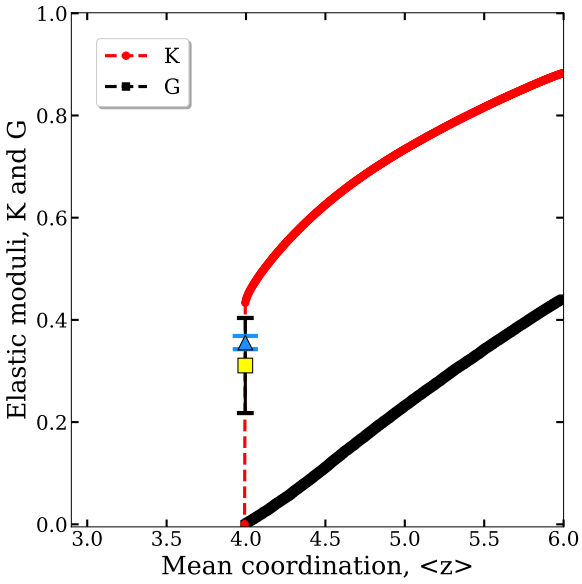

Figure 4.2: (Color Online). The Ensemble Averaged Bulk K (Red) and Shear G (Black) Elastic Moduli of 100 Samples with 512 Vertexes as the Edges are Removed From Mean Coordination$\langle z\rangle = 6$ Down to $\langle z\rangle \simeq 4$. The Yellow Square, with a Wide Spread, Shows the Average of Bulk Moduli for 100 Samples Generated by `CirclePack`. The Blue Triangle, with a Tighter Spread, Shows the Average of Bulk Moduli at Isostatic Plus One for 100 Samples Generated by Conventional Jamming Algorithms. The Jammed Systems Have the Same Disk Size Distribution as Circle Packs.

4.4 Results

At this point we have a spring network that is identical to the network representation of a jammed pack (an example is shown in Figure 4.1-c) in all the following aspects (none of which holds for a percolating rigid network at the marginal point):

1. The network has one excess contact past mathematical isostaticity (isostatic plus one),

2. The bulk modulus of the network is finite and $O(1)$,

3. The ratio of shear and bulk elastic moduli (G/K) scales as $\Delta z = \langle z\rangle - z_J$ where z_J is the mean coordination at the marginal point,

4. It is marginal, as both its s and h indexes are equal to 1 and its density of states for low excitation frequencies is akin to that of a jammed system as is shown in the Supplemental Material,

5. It is stable as revealed by the study of its dynamical matrix. All of the eigenvalues are positive (except for the two trivial translational eigenvectors whose eigenvalues are zero).

6. 100% of the forces along the edges in the network are positive definite and their distribution exhibits a scaling behavior similar to jamming[2]. This is very different from percolating networks at the critical point where the fraction of compressive forces is about 50%.

This network can now be mapped into a disk packing [111]. We locate disks for a given periodic network using methods of circle packing, a topic introduced by William Thurston, [112, 113]; the standard reference is [114], see in particular Chapter 9. A *circle packing* (or disk packing) is a configuration of circles satisfying a prescribed pattern of tangencies. In our setting, prescribed tangencies are those of the given network, which is treated as a graph on a topological torus. Computations are carried out in the software `CirclePack`, [115]. They require a triangulation, so a single auxiliary vertex is temporarily added to each complementary cell of the network. For the resulting triangulation, circle packing theory (see [116] and [114][Prop 9.1]) guarantees the existence of a geometric torus and an associated circle packing on that torus. `CirclePack` computes disk radii and lays the disks out as a periodic circle packing in the plane. While the result of `CirclePack` is unique up to scaling and rigid motions, there are many such packings that could satisfy the constraints of the

[2]See the Supplemental Material Section.

original network. Discarding the disks for the auxiliary vertexes leaves a circle packing with locations and radii for the vertexes of the original network, as in Figure 4.3-a.

`CirclePack` changes the geometrical configuration of vertexes. However, the connectivity of the system does not change and the bulk modulus remains finite after this transformation with a standard deviation of $s = 0.09$ for the samples studied here, as can be seen in Figure 4.2.

The generated circle packing holds all but one of the properties of the pruned networks discussed above. It is at isostatic plus one, has a finite bulk modulus of $O(1)$ and a vanishingly small shear modulus of $O(1/N)$. It is also marginal with $s = h = 1$, and stable which means it would not change for a small enough compress-decompress protocol. The difference is that not all the forces in the system (although a majority of 72% to 99% of them in the samples studied here) are necessarily positive definite (item 6 above). This comes as a result of our non-unique mapping from the network to the disk packing.

Every circle packing has a distribution of radii that can be assigned to particles in a standard molecular dynamics simulation to generate a polydisperse 2D disk packing that can be compared to the packing generated by the newly introduced algorithm. In this approach, we first scale the radii of particles to achieve a starting packing fraction well above the jamming transition; typically packing fraction $\phi_J \simeq 0.85$ for disks. Particles interact through a standard contact harmonic potential. The system is minimized to its inherent structure at this initial density using a quad-precision GPU implementation of the FIRE algorithm [117, 102]. Configurations at a desired excess number of contacts can be achieved by exploiting the scaling of total energy $U \propto (\phi - \phi_J)^2$, where ϕ_J is the isostatic jamming density. The system is successively brought to lower energies and thus lower numbers of excess contacts by rescaling the radii and re-minimizing. The re-scalings are chosen to achieve approximately 10 steps

per decade of $\phi - \phi_J$. This process continues until the number of excess contacts is reduced to the desired value. At each density the number of excess contacts is calculated on the rigid core of the system by first removing *rattler* particles lacking at least $d + 1$ non-cohemispheric contacts. The blue triangle in Figure 4.2 shows the average bulk modulus of 100 samples generated by this method. The standard deviation is in order of $s = 0.01$, which is smaller than the standard deviation obtained from results of `CirclePack`.

There are measurables that are not universal - like the density, pair distribution function, etc. These vary widely for conventional jammed packs as well as in the jammed systems here, depending largely upon the number of rattlers, the size of convex cavities that are present, and the protocol that is being used to generate the jammed packs. For instance, the average packing fraction of 100 test samples generated by `CirclePack` is $\phi \simeq 0.77$ which is lower than that of samples generated by our standard algorithm where $\phi \simeq 0.82$ after removing the rattlers. We emphasize again that the circle packing construction used here is not unique and does not create packings with all positive definite forces. This then explains the lower density as it is well known that attractive interactions (or indeed frictional interactions) allow one to create critically jammed packings at significantly lower densities. The precise ways the disks of various radii are located is also not a crucial issue and can vary from well mixed to some clustering. Figure 4.3 shows the comparison of two samples with 512 particles.

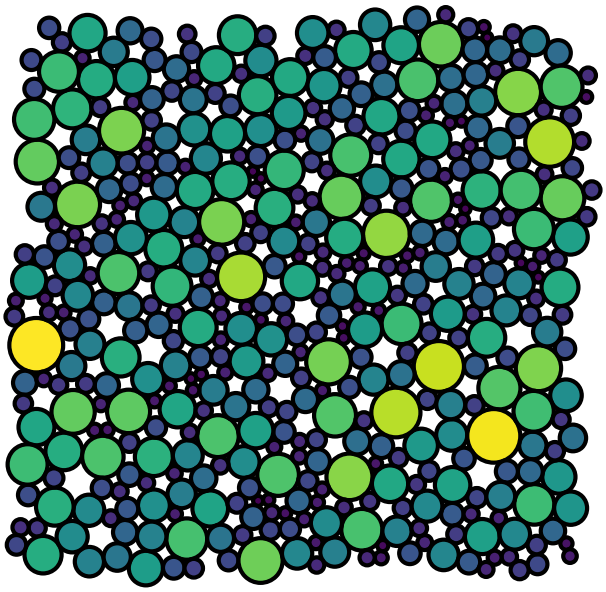

(a)

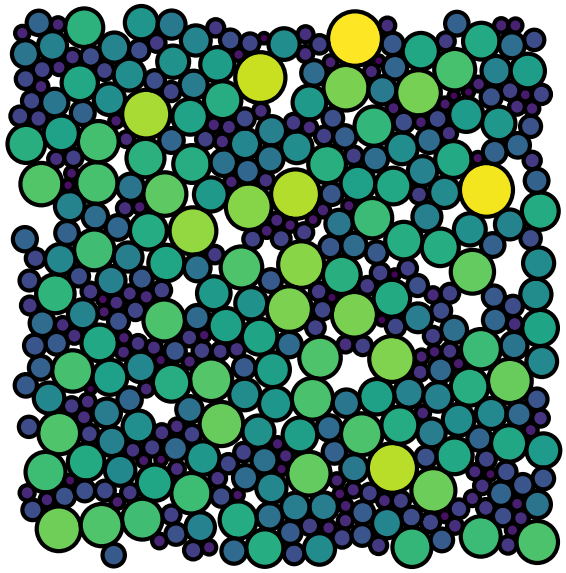

(b)

Figure 4.3: (Color Online) a) Packing Generated by Pruning Algorithm and `CirclePack` B) Rattler Free Packing Generated by Standard Algorithms.

4.5 Discussion

In this Letter, we have shown that the essence of the jamming transition is the underlying network involved at the isostatic plus one point. But another ingredient is required - that the bulk modulus goes from a finite value to zero as one constraint is removed to take the network from isostatic plus one to isostatic. This not only clarifies the nature of the jamming transition, but shows that conventionally jammed networks (formed by compacting particles together) are part of a larger group of networks controlled by topology with the added cooperative geometric ingredient that the bulk modulus remains finite. Such cooperativity is essential to make the network jammed, and much more restrictive than merely being isostatic. We have also demonstrated that all of the interesting macroscopic properties of jammed matter derive from the marginality of the system and its bulk mechanical properties. As such, both our generated networks and their equivalent circle packings behave as properly jammed systems for all bulk interrogations. However, the microscopic properties of jamming are only satisfied by the pruned networks and not the circle packs. This is because the force distributions in pruned networks and jamming follow similar scaling laws, whereas the circle packings fail to do so since forces are not positive everywhere. We note finally that in all the networks discussed in this Letter, the shear modulus goes from $O(1/N)$ at isostatic plus one, to zero at isostatic. The ideas in this Letter generalize easily to any dimensions, but the final step of going from a network to a hypersphere pack is only possible in 2D.

4.6 Supplemental Material

4.6.1 Vibrational Modes

Here we look into the density of states (DOS) in the pruned network constructions and their equivalent circle packs and compare the results to physically jammed systems. First, we study the evolution of DOS in the disordered networks as they are pruned from $\langle z \rangle = 6$ to $\langle z \rangle \approx 4$. For a 2D spring network of area A, the number of allowed wave modes between wave numbers 0 and q is [21]:

$$n(q) = \frac{A}{(2\pi)^2}\,\pi q^2 \tag{4.2}$$

We assume the vibrational frequencies are low enough for the dispersion relation to be almost linear for both longitudinal (L) and transverse (T) acoustic modes:

$$q = \frac{\omega}{v_\alpha} \tag{4.3}$$

where $\alpha = T, L$. This means the number of vibrational modes $n(\omega)$ is quadratic in frequency which leads to the following form for density of states:

$$\mathcal{D}(\omega) = \frac{dn(\omega)}{d\omega} = \frac{A}{2\pi v_\alpha^2}\,\omega \tag{4.4}$$

On the other hand, the longitudinal and transverse sound velocities are related to the bulk (K) and shear (G) moduli of a 2D spring network in the following form:

$$\begin{aligned} v_L &= \sqrt{\frac{G+K}{\rho}} \\ v_T &= \sqrt{\frac{G}{\rho}} \end{aligned} \tag{4.5}$$

where $\rho = N/A$ is the mass density. Here the mass density is equal to the number density of the system since all vertexes have unit mass. By inserting Eq. (4.5) into

Eq. (4.4) and using the normalization $g_{\mathcal{D}}(\omega) = \mathcal{D}(\omega)/N$ so that $\int g_{\mathcal{D}}(\omega)\, d\omega = 1$, we can write the probability distribution function of the vibrational modes in terms of the elastic moduli of the system [118]:

$$g_{\mathcal{D}}(\omega) = \frac{\omega}{2\pi}\left(\frac{1}{G} + \frac{1}{G+K}\right) \tag{4.6}$$

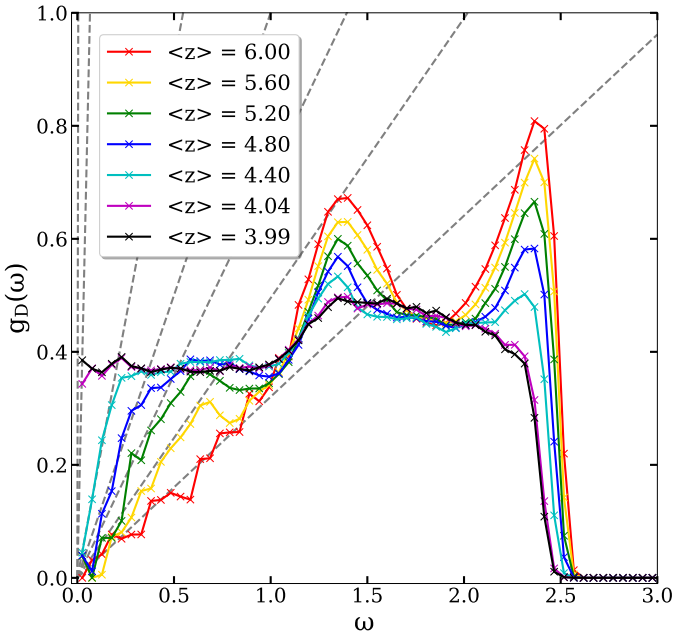

Figure 4.4: (Color Online) The Evolution of Probability Density Function for Acoustic Modes in Disordered Spring Networks as the Bonds are Pruned From $\langle z \rangle = 6$ Down to $\langle z \rangle \approx 4$ (Isostatic Plus One) While Keeping the Bulk Modulus Finite. The Dashed Lines Display Eq. (4.6) For the Average Elastic Moduli Associated with Each Value of $\langle z \rangle$ Shown on the Colored Curves. The Results are Ensemble Averaged Over 100 Samples, Each with 512 Vertexes.

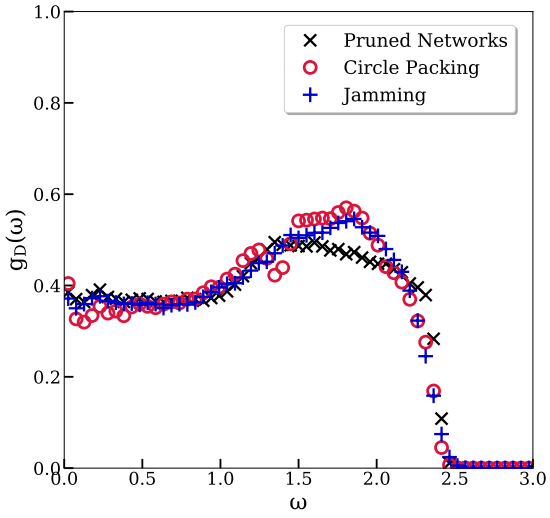

(a)

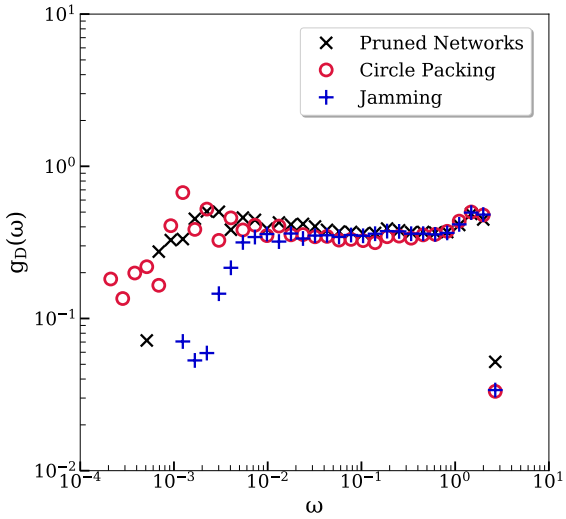

(b)

Figure 4.5: (Color Online) a) The Probability Density Function for Vibrational Modes in 2D Pruned Networks (Blue), Their Equivalent Circle Packs (Red) and Jammed Systems (Black) in Linear Scale. B) The Plot of Part (a) in Logarithmic Scale.

The linearity of $g_{\mathcal{D}}(\omega)$ versus ω is the Debye-like low frequency behavior that is

expected to be seen in any material with non-zero values of sound velocities. This is observed for networks far from marginality in the lower left corner of Figure 4.4. When the edges with smallest contribution to the bulk modulus are removed from a fully triangulated disordered spring network, the shear modulus approaches zero almost linearly, while the bulk modulus remains finite. Therefore the first term on the RHS of Eq. (4.6) diverges and the density of states becomes flat near the transition point which is a characteristic of the vibrational modes in disordered systems at their marginal transition point [86, 119, 118].

Figure 4.5 shows the plots of $g_{\mathcal{D}}(\omega)$ for three types of systems studied in the Letter: the pruned networks at isostatic plus one, their equivalent circle packings, and the jammed systems generated by using the size distribution of circle packs both in linear and logarithmic scale. The marginality of all these systems is evident by their flat density of states at low frequencies.

4.6.2 Distribution of Forces

Figure 4.6 shows the probability distribution of forces at isostatic plus one for the pruned networks and the jammed systems. While they look quite similar on this scale, a plot of the cumulative distribution of forces (Figure 4.7) reveals an intriguing distinction. The physically jammed packing has a low force scaling exponent for all forces that is consistent with the mean field full-replica symmetry breaking results [102], as is expected for a jamming transition that happens deep within the marginal glass phase. However, the pruned network has an exponent in the CDF consistent with 1, which matches well with the single-replica symmetry breaking result for stable glasses[120].

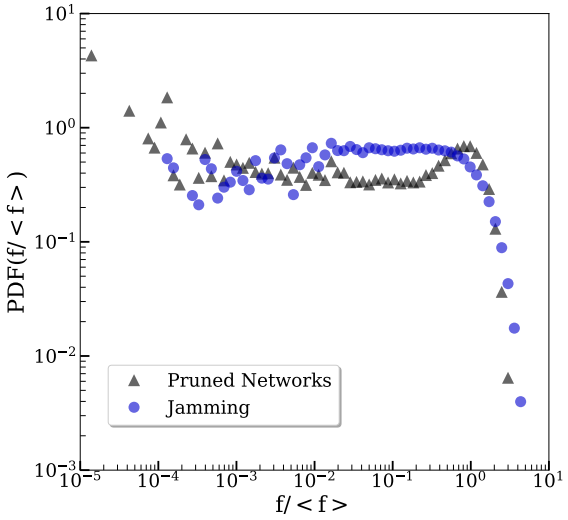

Figure 4.6: (Color Online) The Probability Distribution Function of Forces for Pruned Networks (Gray Triangles) and Jammed Systems (Blue Circles) at Isostatic Plus One. Both Exhibit a Nearly Constant Distribution of Forces for Small Forces.

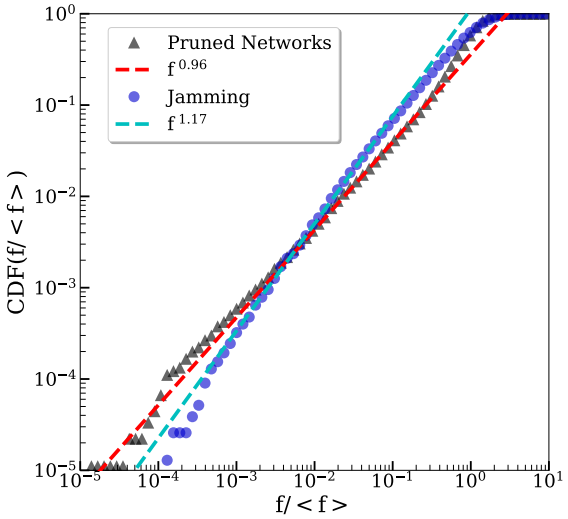

Figure 4.7: (Color Online) The Cumulative Distribution Function of Forces for Pruned Networks (Gray Triangles) and Jammed Systems (Blue Circles) at Isostatic Plus One. Best Fit Power Laws are Over Plotted in Red for the Pruned Networks and Teal for the Jammed Systems.

Acknowledgements

We acknowledge discussions with Wouter Ellenbroek and Louis Theran on the properties of isostatic disordered networks. The work at Arizona State University is

supported by the National Science Foundation under grant DMS 1564468. EIC is supported by the NSF under Career Grant No. DMR-1255370 and a grant from the Simons Foundation No. 454939. This work used the Extreme Science and Engineering Discovery Environment (XSEDE), which is supported by National Science Foundation grant number ACI-1548562. Specifically, it used the Bridges system, which is supported by NSF award number ACI-1445606, at the Pittsburgh Supercomputing Center (PSC). This work also used the University of Oregon high performance computer, Talapas. We gratefully acknowledge the support of NVIDIA Corporation with the donation of a Titan X Pascal GPU used in part for this research.

Chapter 5

DISORDERED AUXETIC NETWORKS WITH NO RE-ENTRANT POLYGONS

This chapter is a reprint of the following submitted article:

Hagh, Varda F., and M. F. Thorpe. "Disordered auxetic networks with no reentrant polygons." Physical Review B 98, no. 10 (2018): 100101.

My contribution to this work includes developing computer codes to generate the network samples, conducting the measurements, writing the manuscript, and generating all of the figures in this chapter.

It is widely assumed that disordered auxetic structures (i.e. structures with a negative Poisson's ratio) must contain re-entrant polygons in 2D and re-entrant polyhedra in 3D. Here we show how to design disordered networks in 2D with *only* convex polygons. The design principles used allow for any Poisson ratio $-1 < \nu < 1/3$ to be obtained with a prescriptive algorithm. By starting from a Delaunay triangulation with a mean coordination $\langle z \rangle \simeq 6$ and $\nu \simeq 0.33$ and removing those edges that decrease the shear modulus the least, without creating any re-entrant polygons, the system evolves monotonically towards the isostatic point with $\langle z \rangle \simeq 4$ and $\nu \simeq -1$.

5.1 Introduction

Consider a homogeneous extension of a rod whose sides are free. If we apply a uniform force at the two ends of the rod in opposite directions, it will undergo a transverse expansion when compressed and a transverse compression when stretched

along the applied forces. This is the familiar behavior of most materials. This deformation can be quantified by Poisson's ratio, which is defined as the negative ratio of transverse contraction strain to longitudinal expansion strain. In d dimensions, the Poisson's ratio of any bulk material is related to its bulk (K) and shear (G) elastic moduli by [121]:

$$\nu = \frac{dK - 2G}{d(d-1)K + 2G} \tag{5.1}$$

which reduces to $\nu = (K - G)/(K + G)$ in 2D. Since for any material $K, G \geq 0$ for stability, we must have:

$$(K = 0) \quad -1 \leq \nu \leq \frac{1}{d-1} \quad (G = 0) \tag{5.2}$$

where $\nu = (d-1)^{-1}$ corresponds to an incompressible fluid or rubber with a vanishingly small shear modulus compared to its bulk modulus. Note that $\nu = 0$ corresponds to $K - 2G/d = \lambda = 0$ where λ is the Lame' constant [122], as occurs in cork for example [123]. Thus a negative ν corresponds to negative Lame' constant which is not forbidden by thermodynamics but is unusual. *Normal* materials have a positive Poisson's ratio. From a continuum elasticity point of view, this is because most materials have a larger resistance to changes in their volume (described by the bulk modulus K) compared to resistance to changes in their shape (defined by their shear modulus G) [124].

Eq. (5.1) suggests that by designing a structure where $K < 2G/d$ or simply $K < G$ in 2D, one can fabricate materials with a negative Poisson's ratio. These types of materials and structures are called auxetic. The concept of a negative Poisson's ratio goes back to Saint-Venant in 1848 [125] for anisotropic materials. In the modern era, this concept was extensively described by Love in 1944 [126], and later

was investigated by Gibson in 1982 [127]. In 1987, Lakes re-fabricated conventional polymer foams with a positive Poisson's ratio by heating under pressure to create re-entrant structures on the sub-millimeter scale which then led to foams with a negative Poisson's ratio that were isotropic [128]. These investigations suggested that auxetic behavior is the result of a mechanism that involves the geometrical structure of the material and its deformation under compressive load. A variety of of these materials were designed and fabricated at the end of 80's and the beginning of 90's [129, 130, 131, 132, 133]. Since then, many similar efforts (theoretically, computationally and experimentally) have led to auxetic materials [134]. These include auxetic cellular foams [135, 136, 137, 138, 139, 140, 5, 141], auxetic regular and disordered networks [142, 143, 144, 145, 146, 147, 148, 149, 150], microporous polymers [130, 151, 152, 153], and laminated fiber composites [154, 155]. In this paper, we will focus on disordered auxetic networks [150] with only convex and no re-entrant polygons.

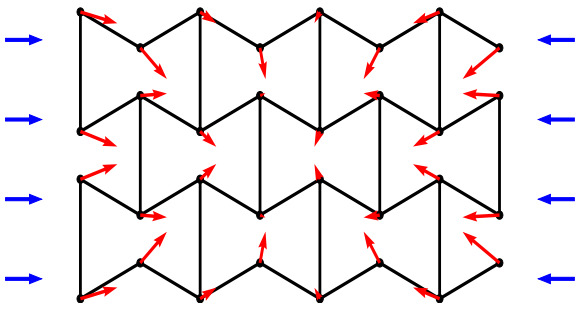

Figure 5.1: (Color Online) A Hexagonal Re-Entrant Honeycomb with Bow Tie Shaped Polygons. This Type of Re-Entrance is Common in Engineered Materials with Negative Poisson's Ratio. The Horizontal Blue Arrows on the Sides Represent the External Load that is Applied to the System. The Red Arrows, Attached to the Nodes, Show the Movements of All the Nodes in Response to the External Load. The Magnitudes of Arrows Have Been Multiplied by 10^3 to Make Them Visible to the Eye.

It is important to note that theoretical studies of auxetic materials fall into *two*

distinct classes. In the *first* category, of interest here, the material is over-constrained with all the elastic moduli being non-zero and proportional to the spring constant(s) in the system where for simplicity, we assume the same spring constant for all edges present. In the *second* category of auxetic structures, the structure is under-constrained and a single internal *mechanism* or *floppy mode* is involved in which the associated eigenvector shows auxetic behavior but there is no restoring force and all the elastic moduli are zero (for a recent treatment with references see [156, 157, 158]). All the edges retain their original lengths when the system undergoes a deformation. In this case, Eq. (5.1) cannot be used for the Poisson ratio as $K = G = 0$, and instead the ratio of traverse to longitudinal strain is used. Note that for almost any material with a few floppy modes (few meaning between say 2 and 5), a negative Poisson's ratio can usually be achieved by using a well-chosen linear combination of floppy mode eigenstates. Thus we regard the *first* category as being more challenging and focus on that here as it is of the most interest for experimental fabrication.

Most presently known auxetics with non-zero elastic constants and nearest neighbor central forces are networks with a re-entrant node structure [159]. A re-entrant or pointed node in a network is a node where two adjacent edges make an angle greater than 180°. A classic example of this can be seen in Figure 5.1. The mechanism of deformation for these types of networks is very well understood and involves the collapse of all the bow tie units as they are pushed from any direction.

In this paper, we demonstrate a computational method to build two dimensional disordered networks with Poisson's ratios in the range $-1 < \nu < 1/3$ and *convex polygons only*. We have been unable to find any examples of *disordered* networks in the literature with controllable Poisson's ratios and nearest neighbor central forces that did not contain re-entrant polygons. The known auxetic structures such as chiral honeycombs [142] that do not possess any re-entrance, have unit cells with a

specific type of symmetry (e.g. rotational, chiral, mirror, etc.). When there is such a symmetry in the system, a single mechanism like unrolling can drive the system auxetic. Our interest on the other hand, is in linear elasticity where the edges of a disordered network are springs and the network is over-constrained. Such a network has no symmetry (other than the repetitive structure associated with the supercell) and when all the polygons are convex, its structure resembles that of glassy and jammed networks that are widely studied in rigidity theory [2, 7].

5.2 Computational Methods

In the recent years, topological optimization methods have been widely used to design networks with specific elastic and mechanical properties [85, 150, 8]. In this paper, we use tuning by pruning method to generate networks that have a finite shear modulus of order 1 and an infinitesimal bulk modulus of order $O(1/N)$, so that $K \ll G$. Here, N denotes the number of nodes in the network. In the limit $N \to \infty$, the bulk modulus of these systems becomes zero and therefore the Poisson's ratio, as defined by Eq. (5.1), becomes exactly $\nu = -1$. The networks are generated by starting from a fully triangulated spring network with mean coordination $\langle z \rangle = 6$ and periodic boundary conditions. The starting network is a Delaunay triangulation [106] of a set of points generated by Poisson disk sampling in 2D [104, 105]. An example can be seen in Figure 5.2-a.

The contribution of different edges to the elastic moduli of a harmonic spring network can span over several orders of magnitude [108]; affecting the bulk and shear moduli in very different ways in some cases [85, 107]. This means removing some of the edges can cause a significant drop in either the value of bulk or shear modulus (or both), while the removal of some other edges does not change the moduli by a significant amount. The wide distribution of edge response in these networks allows us

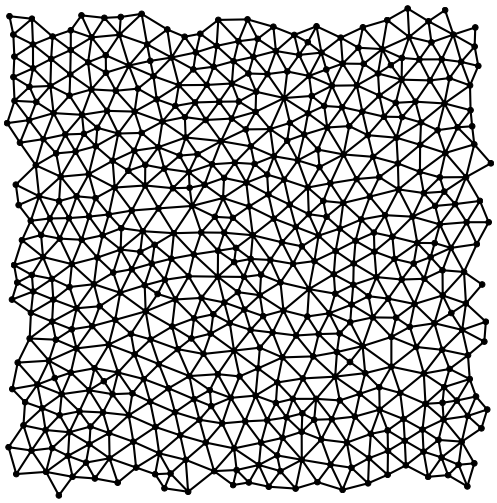

(a)

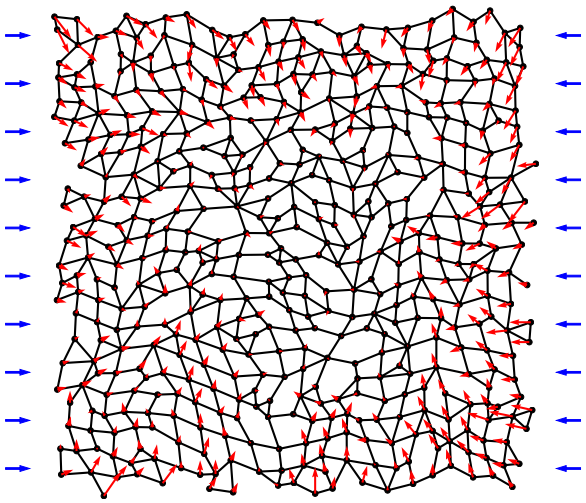

(b)

Figure 5.2: (Color Online) a) A Disordered Triangular Network with Mean Coordination $\langle z \rangle = 6$ Before Removing Any Edges. B) The Same Network After Removing One Third of the Edges While the Convexity of All the Polygons is Conserved. The Mean Coordination Number is $\langle z \rangle \simeq 4$ And the Network Has a Negative Poisson's Ratio of $\nu = -0.9998$. The Horizontal Blue Arrows on the Sides Represent the External Load that is Applied to the System. The Red Arrows, Attached to the Nodes, Show the Movements of All the Nodes u_i in Response to the External Load. The Magnitudes of Arrows Have Been Multiplied by 10^3 to Make Them Visible to the Eye.

to identify and remove those edges that have the minimum contribution to the changes in bulk or shear modulus. For example, removing edges that have the minimum contribution to the bulk modulus can be used to build networks with a finite bulk modulus that resemble a jammed system [8].

Here, we remove those edges that have a smaller contribution to the shear modulus of the system. The shear modulus is measured by compressing the network in the horizontal direction, while stretching it in the vertical direction. This deformation causes a change in the lengths of the springs which all are assumed to have a unit spring constant, $k = 1$ (N/m). These springs have no physical width and there is no energy associated with bending them. Therefore the effective spring constant is only based on stretching or compressing the edges. The energy stored in the system (E) is then measured and the shear modulus is calculated using the following equation [160]:

$$G = \frac{1}{2}\frac{E}{A\delta^2} \tag{5.3}$$

where A denotes the total area of the network and δ is the strain applied to the system. Note that the shear modulus G is independent of δ in the linear regime ($\delta \ll 1$). If we iteratively remove the edges with the smallest contribution to G from a mean coordination $\langle z \rangle = 6$ down to $\langle z \rangle \simeq 4$, the Poisson's ratio will monotonically go from $\nu \simeq 1/3$ to $\nu \simeq -1$ and the resulting network will have a larger resistance to shearing than to hydrostatic compression. This method of pruning naturally introduces re-entrance into the system. To avoid the emergence of re-entrant nodes and hence maintain the convexity of all the polygons in the network, one more crucial condition is added to the pruning protocol. This extra condition is Hilbert's mechanical stability [111], which is imposed on all nodes at each step of the pruning process. The Hilbert's condition guarantees that each node must have at least $d+1$ incident edges and the geometrical arrangement of edges is such that applied forces can cancel each

other out. This geometrical condition is useful for the global mechanical rigidity of the network. In 2D this means no angles between adjacent edges can be greater than 180°, and hence re-entrance is prevented.

As an aside, all the removed edges could be replaced with very weak springs (for example a thousand times weaker) to get back to the original Delaunay triangulation which would still be auxetic. The only polygons then are triangles which of course are convex. However, this illustrates that to be meaningful, the notion of convexity has to be tied in with springs of comparable magnitude. Any auxetic network with non-convex polygons, can also be modified by adding a single auxiliary node inside each re-entrant polygon and connecting that new node to the nodes of the polygon with very weak springs. This will form a local triangulation and will make the network entirely convex. But, again, it is not a meaningful way of circumventing the meaning of *convex*.

To be precise, we first generate disordered triangular networks with mean coordination $\langle z \rangle = 6$ that are Delaunay triangulation of a Poisson disk sampling with $N = 500$ points on a 2D plane. We then loop over all the edges and collect those that will not violate the Hilbert's stability condition if removed. This guarantees that the removal of an edge will not create any non-convex polygons in the network. The contribution of each removable edge to the shear modulus of the system is then measured and the edge list is sorted in an ascending order based on the value of their contribution. Finally, we select the first 10% of the edges with smallest contributions to G and remove one of these randomly. More than one third of the edges need to be removed to drive the original triangulated network to an auxetic network with $\nu \simeq -1$ and the mentioned process is repeated at each step. We could have selected the edges with smallest contribution, but chose one out of the smallest 10% to demonstrate that the result is robust, and the results are virtually identical.

Figure 5.2-b shows an auxetic network generated by this method. As can be seen from the figure, there are no re-entrant nodes introduced to the system, and yet the network has a negative Poisson's ratio $\nu = -0.9998$. The small deviation of the Poisson's ratio from -1 is a finite size effect and would vanish in the $N \to \infty$ limit. The red arrows show the displacements $\{u_i\}$ of all the nodes when we apply a small strain of order $\delta = 10^{-4}$ in the horizontal direction (shown by the blue arrows) and let the system relax. The center of mass has been fixed here which leads to $\sum_{i=1}^{N} u_i = 0$ and therefore there is not much motion happening at the central parts of the network. The scale of these motions are magnified 10^3 times to make them visible to the eye, since we are in the linear regime and the motions are infinitesimal. However this magnification is for visualization only as anharmonic effects are present at such large displacements for non-collinear networks of harmonic springs.

The mechanism behind the auxetic behavior of the networks built here is not trivial, and a simple explanation has eluded us, but lies within the method used to build them. The generating process is very cooperative, as in each step an edge is removed based on how its contribution to the shear modulus is compared to all the other edges in the network. This cooperative process adds to the complexity of the mechanism that involves the deformation of such systems, and is a particular example of a larger phenomena that involves pruning spring networks in special ways to obtain desired properties. Another example is to produce jammed networks [8], and yet another to produce allosteric effects of a similar kind to those seen in proteins [161]. To date these are all empirical algorithms and the underlying mathematics remains to be understood.

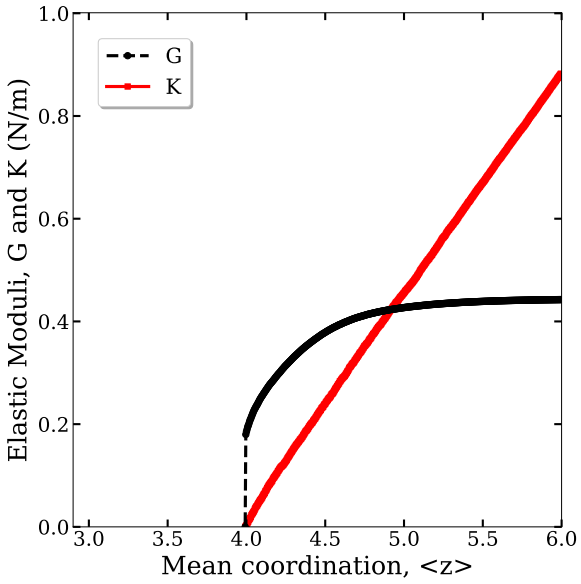

Figure 5.3: (Color Online) The Plots of the Shear (G) and Bulk (K) Moduli as the Edges that Minimally Affect G are Pruned From Mean Coordination $\langle z \rangle = 6$ Down to $\langle z \rangle \simeq 4$. The Results are Ensemble Averaged Over 50 Samples, Each with $N = 500$ Nodes.

We monitor both the shear and bulk moduli of these networks as they are pruned. The bulk modulus is measured in a similar way to the shear modulus by using Eq. (5.3). Figure 5.3 shows the behavior of both bulk and shear moduli against the mean coordination of the system. The mean coordination is defined as the average number of edges at each node. All data points are ensemble averaged over 50 samples with $N = 500$ nodes. Both these elastic moduli decrease monotonically as the edges are removed [109], as required by general principles.

At the starting point, the bulk modulus of a triangular network is greater than the value of its shear modulus; therefore the Poisson's ratio is a positive number, as can be seen from Eq. (5.1). It should be noted that if the nodes in a network are connected by central forces and if *every node* is a center of symmetry, then because of the Cauchy condition between elastic constants, $c_{12} = c_{44}$, the Poisson's ratio would be $\nu = (d+1)^{-1}$ which in 2D gives $\nu = 1/3$. This is the case for a 2D regular

triangular network [162] and is also closely true for a Delaunay triangulation of the kind shown in Figure 5.2-a. The algorithm used here to select the removed edges aims to keep the shear modulus of the system above zero. Since the changes in bulk modulus are only loosely correlated with changes in the shear modulus, driving the network to maximize the shear modulus does not force it to also maximize the bulk modulus. The bulk modulus decreases linearly as it would do with random dilution [7]. This makes the difference between bulk and shear become smaller and smaller until at about $\langle z \rangle \simeq 4.92$ they become equal. For any edges removed after this, the shear modulus is larger than the bulk modulus and therefore the Poisson's ratio becomes negative. As $\langle z \rangle = 4$ is approached, the bulk modulus goes to zero while the shear modulus remains non-zero; therefore the Poisson's ratio approaches -1. Note that the last edge that is removed, takes the system to the isostatic point plus one edge [8] where there is one state of self-stress in the system [158] and the shear modulus is of order 1, while the bulk modulus is $O(1/N)$. The removal of an additional edge is meaningless as this would take the system to the isostatic point where the total number of degrees of freedom and constraints are balanced such that the only remaining floppy modes are the macroscopic rigid motions. At the isostatic point, the network is still mechanically stable but both the bulk and shear moduli are exactly zero and therefore Poisson's ratio becomes undefined.

Figure 5.4 shows the behavior of the ensemble-averaged Poisson's ratio as the networks are pruned. The central line, shown as red, is the Poisson's ratio, while the blue vertical bars highlight the standard deviation of the measurements over 50 samples, each with $N = 500$ nodes. As can be seen from the plot, the Poisson's ratio of these systems spans over the range $(-1, 1/3)$. The small standard deviations mean that this method can be used to design and build any disordered convex structure with a desired Poisson's ratio by choosing the corresponding mean coordination that

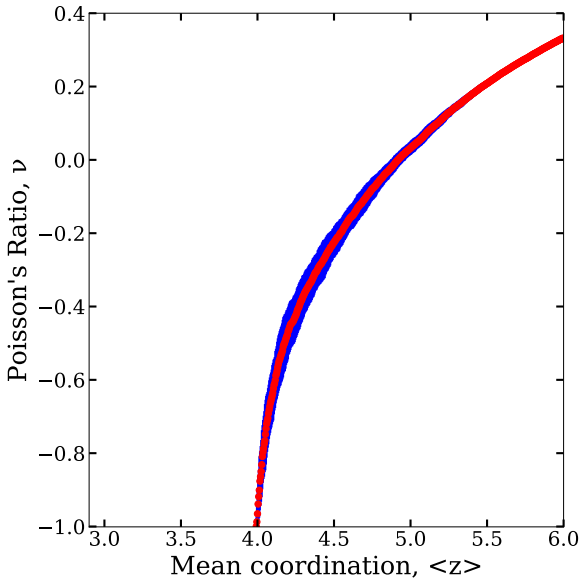

Figure 5.4: (Color Online) The Poisson's Ratio Versus the Mean Coordination $\langle z \rangle$ For the 50 Samples Used in Figure 5.3. The Red Dots Along the Central Line Show the Value of the Averaged Poisson's Ratio and the Blue Vertical Bars Show the Standard Deviation for Each Data Point.

can be read from Figure 5.4.

5.3 Discussion

In Summary, here we introduce a method to produce disordered auxetic networks with near neighbor forces without re-entrant polygons in 2D. The algorithm that we use produces networks with any desired value of the Poisson's ratio in the range $-1 < \nu < 1/3$ by tuning the mean coordination $\langle z \rangle$ down from 6 to 4 using a specific protocol. This protocol involves removing edges that minimally reduce the shear modulus while maintaining Hilbert's mechanical stability condition at each node. Any desired value of the Poisson ratio can be achieved by this method, all the way down to -1. Starting from a Delaunay triangulation, this leads to a disordered network where all the polygons remain convex at every stage. We chose all the spring constants to be the same, but they could differ by factors of 2 etc., and similar

results would be obtained. This result remains quite perplexing and we have no easy geometric explanation at this time Examination of Figure 5.2 shows that while many of the polygons are far from their maximum area, none are pathologically compressed - with width/length ratios for each polygon being typically in the range 1 to 2. We anticipate that similar results can be obtained in 3D.

Acknowledgements

We acknowledge useful discussions with Sidney Nagel, Andrea Liu, Louis Theran, and Mahdi Sadjadi. The work at Arizona State University is supported by the National Science Foundation under grant DMS 1564468. This work used the Extreme Science and Engineering Discovery Environment (XSEDE), which is supported by National Science Foundation grant number ACI-1548562.

Chapter 6

CONCLUSION

The rigidity of a material determines its mechanical properties and allows elaborate control over the conformational response to the external load; whether a structure should maintain its integrity or should move under load in a certain way depends on its rigidity. In this dissertation, the goal is to study the rigidity of disordered materials. Disordered or amorphous solids make up many of the materials we use on a daily basis, including glasses and plastics. The systems studied here are all 2D, but for most cases, the methods can be generalized to any spatial dimensions (except those that require rigid region decomposition of the pebble game).

Many of the physical and mechanical properties of materials can be understood by using ball−and−spring networks, where the nodes represent the building blocks (atoms or molecules) of the matter and the edges resemble the interactions between these building blocks. For the purpose of rigidity and linear response, it is useful to consider the interactions as harmonic potentials. Therefore the edges in the networks are modeled as harmonic springs.

In Chapter one, the concept of rigidity is explored from a mathematical point of view, where all the required tools and definitions are introduced. In a spring network, moving the nodes leads to changes in the lengths of the springs which subsequently results in a non-zero energy in the system. The changes in the lengths, either in the form of contraction or elongation, are described in terms of a rigidity matrix $\mathbf{R}$ that consists of edge vectors between the interconnected nodes in the network. When the system is allowed to relax, it tends to go back to its original structure where all the springs had their rest lengths and the energy stored in the system was zero. As

a result, the system starts to oscillate about the energy minimum with vibrational modes that are specified by the eigenstates of its dynamical matrix, $\mathbf{D} = \mathbf{R}^T\mathbf{R}$. The number of zero eigenvalues of the dynamical matrix indicates the number of floppy modes or degrees of freedom in the system. The eigenvectors of these zero eigenvalues determine the motions for which there is no energy cost. The number of floppy modes in a spring network is a good indicator of its rigidity since it reveals how the degrees of freedom and constraints are balanced out. When a spring network is fully rigid, meaning that its floppy modes are only limited to the trivial rigid motions, it will also have non-zero elastic moduli. These elastic moduli quantify the response of the entire system to external load. Two of the widely studied elastic moduli are the bulk and shear moduli that describe the response of the system to specific deformations. These moduli are proportional to the energy that is stored in the system due to deformation. Chapter one includes a section on the relation between the energy and elastic moduli where the derived equations are extensively used throughout this dissertation.

Chapter two introduces ideas from percolation theory by studying the effect of loops and redundancy in percolation transition of two distinct network models. The percolating cluster in a network is the connected pathway that spans the system. The fraction of edges that are in the percolating cluster is an appropriate order parameter that quantifies the critical behavior of the network near transition point. Any loops in the percolating path are redundant from a connectivity point of view since they do not add to the connectedness of the path. Therefore, for each loop in the system there is a corresponding edge that can be considered redundant. Using this definition for redundancy, we defined new order parameters to describe the fraction of edges inside the loops and the fraction of redundant edges. These two order parameters, along with the fractions of edges in the percolating and current carrying clusters, were measured in two types of system: hierarchical networks and triangular networks. Our studies

on the behavior of loops and redundancy in hierarchical networks revealed that loops and redundant edges in a cluster (either percolation or conducting) have a similar critical behavior to that of the cluster as a whole. This is due to the hierarchical nature of these networks where the sub-systems behave exactly like the system itself. However, in the case of triangular networks, this is not necessarily true as the results have shown that critical exponents describing the fractions of looped and redundant edges in a cluster (which are subsets of that cluster) are larger than that of the fraction of edges in that cluster. Hence in this case, there is a difference between the critical behavior of the system and the critical behavior of its subsystems.

These results give an insight into the effect of redundancy in rigidity transition. Redundancy is, in fact, the key concept that provides a direct mapping between ideas of percolation theory and rigidity in networks. In rigidity percolation, one is concerned not only with the connectedness of a spanning cluster, but also whether if that cluster is rigid. Comparing the problem of connectivity percolation to that of rigidity percolation has revealed that the looped edges in a percolating cluster are equivalent to the stressed edges in a rigid cluster. Although the concepts of stress and redundancy in rigidity theory have been known for a long time, their impact on the rigidity transition has not been explored adequately due to the complexity of the problem. In that regards, the methods introduced in Chapter two can be used to study the behavior of redundant and stressed edges in percolating rigid clusters. It is not trivial whether the results would be similar to the ones obtained here, but it is a problem worth exploring in future.

In Chapter three, the rigidity transition in three types of networks is discussed. These include randomly diluted networks, stress diluted networks, and jammed networks. Randomly diluted networks were obtained by starting from a 2D triangulation and removing edges randomly while the rigidity of the largest percolating cluster was

monitored. Measuring the fraction of edges in the largest rigid cluster and the fraction of stressed edges in that cluster showed that these quantities both go to zero in a fashion that is characteristic of a second order phase transition. The results achieved for the fraction of stressed edges in the largest rigid cluster were similar to the fraction of looped edges in the percolating cluster, studied in the previous chapter.

The second type of systems studied here are locally *isostatic* networks, which are networks with no redundant edges and no internal degrees of freedom. These networks were generated by starting from a fully triangulated spring network and removing edges from the stressed regions only. This process forces the stressed regions to shrink, until at the isostatic point, there is no stress left in the system. The isostatic point is the marginal point where a rigid percolating cluster last exists. This type of transition is identified as a second order phase transition as well. However, it is found to be different from the random dilution as there is a sharp transition point that can be calculated exactly using the constraint count method introduced in Chapter one.

The last group studied in this chapter includes jammed networks. A 2D jammed network is a mapping of conventional disk packing into network representation. By pushing a set of disks together, either in the lab or computationally, one can reach the jamming point where the system is rigid without any disks overlapping. At that point, replacing the center of each disk with a node and connecting two nodes if their equivalent particles are in contact, generates a jammed network. The networks built this way are locally isostatic and possess interesting self-organized bulk properties. For example, removing an edge from a locally isostatic jammed network, leads to collapse of the entire network. On the other hand, adding a single edge to a locally isostatic jammed network, makes all the edges undergo stress. Therefore the network is fully stressed up to isostatic plus one edge and removing edges when the network is overconstrained does not break the largest rigid cluster into smaller clusters. This also

means that the fraction of stressed edges in the largest percolating cluster remains 1 up to the isostatic plus one point and then suddenly drops to zero. This models the rigidity transition in these types of networks as a first order phase transition.

Another interesting property of jammed networks that was not observed in randomly diluted and stress diluted networks is the behavior of their bulk modulus. The results have shown that the bulk modulus of a jammed system remains finite ($O(1)$) until isostatic plus one and then drops to zero by removing an edge. In the other two systems studied in Chapter three, the bulk modulus went to zero as the edges were diluted in an almost linear fashion. These two unique properties invited us to think about the relationship between the rigid properties of jammed networks and their elastic response. This led to the key question "Is there a way to generate rigid networks with the exact same elastic properties of jammed networks that are indistinguishable from them?" Chapter four provides an answer to this question.

In Chapter four, a new definition for jamming is introduced based on the rigid properties and linear response of jammed networks. In this new definition, a network is considered to be jammed if it is at the isostatic plus one point, and has a non-zero bulk modulus of $O(1)$. We attempted a variety of computational methods to create such networks. The only successful attempt, which is reported in Chapter four, was based on a tuning by pruning algorithm that monitors the elastic moduli of a network and removes the edges based on their contribution to changes in these moduli. In a disordered triangular network, the contributions of different edges to the elastic moduli are distributed over a range. There are edges, removal of which, would decrease the values of bulk or shear modulus by a large amount. On the other hand, there are edges that would not change one of the moduli significantly. Identifying an edge with the smallest contribution to the bulk modulus and removing it from the network leaves a diluted network whose bulk modulus has been lowered

infinitesimally. This process can be repeated until the desired number of edges is reached. Such a network has a finite bulk modulus which drops to zero after removing the last redundant edge. These networks are similar to jammed networks in every possible way and can be mapped into two dimensional circle packs using the Circle Packing theorem. The resulting circle packs share all of the bulk properties of jammed disk packs. For example, they have a finite bulk modulus and every contact holds a finite stress. Therefore these systems can be considered jammed in terms of our new definition. However, there is one microscopic property that is different about these systems. When it comes to jammed networks, the study of forces along the edges, which can be found by calculating the zero eigenstate of the force matrix RR^T, indicates that all the forces in the network are positive or *compressive*. In the case of circle packs, the zero eigenvector of the force matrix turns out to have a fraction of *tensile* forces as well.

Previously, it was believed that the compressive forces in jammed systems are a result of the system having a finite bulk modulus. The circle packs generated in Chapter four however, have a finite bulk modulus without carrying %100 compressive forces. Since not all the forces in these circle packs are positive definite, one could argue that they are applicable to the jamming of attractive or sticky particles. This has relevance to many colloidal structures as well as potentially to some technologically relevant materials, such as the structures of magneto- or electro-rheological materials. With our expanded definition of jamming, completely new systems, like the recently discovered bilayers of vitreous silica now belong in this class as they satisfy all the criteria set here [163].

We expect more examples of jammed networks to be forthcoming in this less restricted definition of jamming and hope that the use of results obtained in Chapter four may allow us to explore a broader range of the glass and jamming phase diagrams

than just physically jammed systems would allow. On the other hand, the relation between compressive forces and the bulk properties of jammed networks, and the study of distribution of these forces can also be the subject of future exploration.

The idea of controlling the mechanical response of a spring network by removing those edges that have a minimal contribution to its bulk modulus, can be used to design new mechanical metamaterials with any desired elastic properties. This idea was extended to Chapter five, where we used the methods introduced in the previous chapter to produce spring networks with negative Poisson's ratios. These types of structures are referred to as *auxetic*. There have been many attempts in design and fabrication of auxetic structures since the 1940's. However, none of them have focused on disordered auxetic systems. In fact, there are very few known examples of the disordered auxetic materials [150], all of which contain non-convex polygons.

In Chapter five, we have designed auxetic disordered networks that contain convex polygons only. This is interesting in particular because the resulting networks resemble a jammed network, but instead of having a finite bulk modulus and a positive Poisson's ratio, they have a finite shear modulus and a Poisson's ratio of almost -1. To ensure the convexity of all the polygons, we had to add one extra condition to the pruning procedure. In this extra condition, Hilbert's stability criteria was imposed on all the nodes at each step. Hilbert's condition means that each node in a 2D network should have at least 3 incident edges and the angle between any two adjacent edges should not be greater than or equal to 180°. These types of disordered auxetics with no re-entrant polygons have not been reported before and their counter intuitive structure calls for further exploration. The deformation mechanism of these networks is also very complex and we do not have a geometrical explanation for their auxetic behavior. The experimental fabrication of the structures introduced in Chapter five is something that we would like to pursue in future, since it would allow us to un-

derstand their mechanism and would possibly open a new avenue for the fabrication of industrial non-crystalline materials with controllable response to the mechanics of the their environment.

Chapter 7

COMPUTATIONAL TOOLS

Numerical methods and techniques have been integrated into research in theoretical physics over the past few decades. In the course of my doctoral work, I have extensively used computational tools and have developed many softwares that can be used to reproduce the results reported in this dissertation. Most of the programs used in this dissertation are written in `Python` because of its flexibility and great collection of open source packages such as `Numpy` and `Scipy` which are nowadays fundamental for scientific computing with `Python`.

7.1 Rigidpy

Since this dissertation is written on the rigidity of disordered networks, many of the used programs share the same structure where a framework is built using the connectivity table and coordinates of the vertexes, and then the rigidity and dynamical matrices are calculated. To integrate all the small scripts together, my colleague Mahdi Sadjadi and I have developed a `Python` package named `Rigidpy` that provides a convenient application program interface to study the rigidity and linear response of networks with periodic boundary conditions. The program can be modified to apply to any kind of desired boundary conditions. It is written a generic spatial dimension d with $d = 2$ in the dissertation. The package uses many of the built-in functions in `Numpy`, `Scipy`, and `Networkx`. It is open source and available at `https://github.com/vfaghirh/rigidpy`. The main components of this package include:

1. **Framework rigidity**: A framework is the set of coordinates and connectivity table of a graph. A framework is created by `Rigidpy` using two input files that include the coordinates of N points in pairs $\{x, y\}$:

```
0.67534     0.08986
```

```
0.04657     0.00345
0.11090     0.86786
0.00398     0.03711
...
```

and list of contacts in pairs $\{p_1, p_2\}$ representing points (labeled from 0 to $N-1$) that are mutually in contact. The edge list has the form:

```
0 1
0 2
2 5
3 8
...
```

Once the framework is created, this submodule uses the two repeat vectors $\{a_1, a_2\}$ to calculate the rigidity matrix, the stress matrix, Hessian matrix, dynamical matrix, and the eigenvalues and eigenvectors of dynamical matrix.

2. **Geometrical optimization**: This submodule finds the closest local energy minimum for a given set of edge lengths by optimizing the graph geometry using a conjugate gradient algorithm.

3. **Modulus**: This submodule uses the built framework to calculate the bulk and shear moduli of the network. The inputs include the coordinates of the graph vertexes, the edge list, and the lattice repeat vectors. The lattice vectors are multiplied by appropriate strains and the changes in the lengths of the edges are calculated. Then the moduli are calculated using methods introduced in Chapter one.

[1] W. G. Ellenbroek, Z. Zeravcic, W. van Saarloos, and M. van Hecke. Non-affine response: Jammed packings vs. spring networks. *EPL*, 87(3):34004–, 2009. ISSN 0295-5075.

[2] Michael F Thorpe. Continuous deformations in random networks. *Journal of Non-Crystalline Solids*, 57(3):355–370, 1983.

[3] Chase P Broedersz and Fred C MacKintosh. Modeling semiflexible polymer networks. *Reviews of Modern Physics*, 86(3):995, 2014.

[4] Andrea J Liu and Sidney R Nagel. Nonlinear dynamics: Jamming is not just cool any more. *Nature*, 396:21–22, 1998.

[5] Kenneth E Evans and Andrew Alderson. Auxetic materials: functional materials and structures from lateral thinking! *Advanced materials*, 12(9):617–628, 2000.

[6] Marian Florescu, Salvatore Torquato, and Paul J Steinhardt. Designer disordered materials with large, complete photonic band gaps. *Proceedings of the National Academy of Sciences*, 106(49):20658–20663, 2009.

[7] Wouter G Ellenbroek, Varda F Hagh, Avishek Kumar, MF Thorpe, and Martin Van Hecke. Rigidity loss in disordered systems: Three scenarios. *Physical review letters*, 114(13):135501, 2015.

[8] Varda F Hagh, Eric I Corwin, Kenneth Stephenson, and MF Thorpe. Jamming in perspective. *arXiv preprint arXiv:1803.03869*, 2018.

[9] Varda F Hagh and MF Thorpe. Auxetic networks with no re-entrant polygons. *arXiv preprint arXiv:1805.03708*, 2018.

[10] H He and Michael F Thorpe. Elastic properties of glasses. *Physical Review Letters*, 54(19):2107, 1985.

[11] PN Sen and MF Thorpe. Phonons in a x 2 glasses: from molecular to band-like modes. *Physical Review B*, 15(8):4030, 1977.

[12] Carl D Meyer. *Matrix analysis and applied linear algebra*, volume 71. Siam, 2000.

[13] Michael F Thorpe. Networks, flexibility and mobility in. In *Encyclopedia of Complexity and Systems Science*, pages 6013–6024. Springer, 2009.

[14] J. C. Maxwell. On the calculation of the equilibrium and stiffness of frames. *Philos. Mag.*, 27:294, 1864.

[15] Joseph Louis Lagrange. *Mécanique analytique*, volume 1. Mallet-Bachelier, 1853.

[16] G. Laman. On graphs and rigidity of plane skeletal structures. *J. Eng. Math.*, 4:331–340, 1970. ISSN 0022-0833. doi: 10.1007/BF01534980.

[17] Bruce Hendrickson. Conditions for unique graph realizations. *SIAM journal on computing*, 21(1):65–84, 1992.

[18] D. J. Jacobs and M. F. Thorpe. Generic rigidity percolation: The pebble game. *Phys. Rev. Lett.*, 75(22):4051–4054, Nov 1995. doi: 10.1103/PhysRevLett.75.4051.

[19] D. J. Jacobs and M. F. Thorpe. Generic rigidity percolation in two dimensions. *Phys. Rev. E*, 53(4):3682–3693, Apr 1996. doi: 10.1103/PhysRevE.53.3682.

[20] Edan Lerner, Eric DeGiuli, Gustavo Düring, and Matthieu Wyart. Breakdown of continuum elasticity in amorphous solids. *Soft Matter*, 10(28):5085–5092, 2014.

[21] Charles Kittel, Paul McEuen, and Paul McEuen. *Introduction to solid state physics*, volume 8. Wiley New York, 1996.

[22] Dapeng Bi, Jie Zhang, Bulbul Chakraborty, and Robert P Behringer. Jamming by shear. *Nature*, 480(7377):355, 2011.

[23] Dietrich Stauffer and Ammon Aharony. *Introduction to percolation theory: revised second edition*. CRC press, 2014.

[24] Vinod KS Shante and Scott Kirkpatrick. An introduction to percolation theory. *Advances in Physics*, 20(85):325–357, 1971.

[25] Muhammad Sahimi. Flow phenomena in rocks: from continuum models to fractals, percolation, cellular automata, and simulated annealing. *Reviews of modern physics*, 65(4):1393, 1993.

[26] AJ Katz and AH Thompson. Quantitative prediction of permeability in porous rock. *Physical review B*, 34(11):8179, 1986.

[27] D Stauffer. Gelation in concentrated critically branched polymer solutions. percolation scaling theory of intramolecular bond cycles. *Journal of the Chemical Society, Faraday Transactions 2: Molecular and Chemical Physics*, 72:1354–1364, 1976.

[28] Antonio Coniglio, H Eugene Stanley, and W Klein. Site-bond correlated-percolation problem: a statistical mechanical model of polymer gelation. *Physical Review Letters*, 42(8):518, 1979.

[29] A Moisala, Q Li, IA Kinloch, and AH Windle. Thermal and electrical conductivity of single-and multi-walled carbon nanotube-epoxy composites. *Composites science and technology*, 66(10):1285–1288, 2006.

[30] Fangming Du, Robert C Scogna, Wei Zhou, Stijn Brand, John E Fischer, and Karen I Winey. Nanotube networks in polymer nanocomposites: rheology and electrical conductivity. *Macromolecules*, 37(24):9048–9055, 2004.

[31] Serge Galam and Alain Mauger. Site percolation thresholds in all dimensions. *Physica A: Statistical Mechanics and its Applications*, 205(4):502–510, 1994.

[32] Peter J Reynolds, HE Stanley, and W Klein. A real-space renormalization group for site and bond percolation. *Journal of Physics C: Solid State Physics*, 10(8): L167, 1977.

[33] Cristopher Moore and Mark EJ Newman. Epidemics and percolation in small-world networks. *Physical Review E*, 61(5):5678, 2000.

[34] Harvey Gould, Jan Tobochnik, and Wolfgang Christian. *An introduction to computer simulation methods*, volume 1. Addison-Wesley New York, 1988.

[35] Mq F Sykes and John W Essam. Exact critical percolation probabilities for site and bond problems in two dimensions. *Journal of Mathematical Physics*, 5(8): 1117–1127, 1964.

[36] Serge Galam and Alain Mauger. Universal formulas for percolation thresholds. *Physical Review E*, 53(3):2177, 1996.

[37] Takehisa Hasegawa, Masataka Sato, and Koji Nemoto. Generating-function approach for bond percolation in hierarchical networks. *Physical Review E*, 82 (4):046101, 2010.

[38] A Brooks Harris, Thomas C Lubensky, William K Holcomb, and Chandan Dasgupta. Renormalization-group approach to percolation problems. *Physical Review Letters*, 35(6):327, 1975.

[39] MF Thorpe and RB Stinchcombe. Two exactly soluble models of rigidity percolation. *Phil. Trans. R. Soc. A*, 372(2008):20120038, 2014.

[40] J Barré. Hierarchical models of rigidity percolation. *Physical Review E*, 80(6): 061108, 2009.

[41] Scott Kirkpatrick. Percolation and conduction. *Reviews of modern physics*, 45 (4):574, 1973.

[42] H Eugene Stanley and Guenter Ahlers. Introduction to phase transitions and critical phenomena. *Physics Today*, 26:71, 1973.

[43] MF Sykes, Maureen Glen, and DS Gaunt. The percolation probability for the site problem on the triangular lattice. *Journal of Physics A: Mathematical, Nuclear and General*, 7(9):L105, 1974.

[44] ME Levinshtein, BI Shklovskii, MS Shur, and AL Efros. The relation between the critical exponents of percolation theory. *Soviet Journal of Experimental and Theoretical Physics*, 42:197, 1976.

[45] Donald J Jacobs and Michael F Thorpe. Generic rigidity percolation: the pebble game. *Physical review letters*, 75(22):4051, 1995.

[46] Donald J Jacobs and Bruce Hendrickson. An algorithm for two-dimensional rigidity percolation: the pebble game. *Journal of Computational Physics*, 137 (2):346–365, 1997.

[47] Chunyu Li and Tsu-Wei Chou. A direct electrifying algorithm for backbone identification. *Journal of Physics A: Mathematical and Theoretical*, 40(49): 14679, 2007.

[48] JT Chayes, L Chayes, Daniel S Fisher, and T Spencer. Finite-size scaling and correlation lengths for disordered systems. *Physical review letters*, 57(24):2999, 1986.

[49] Fumiko Yonezawa, Shoichi Sakamoto, and Motoo Hori. Percolation in two-dimensional lattices. i. a technique for the estimation of thresholds. *Physical Review B*, 40(1):636, 1989.

[50] Nikolaos Tsakiris, Michail Maragakis, Kosmas Kosmidis, and Panos Argyrakis. Percolation of randomly distributed growing clusters: Finite-size scaling and critical exponents for the square lattice. *Physical Review E*, 82(4):041108, 2010.

[51] Cristian F Moukarzel and Phillip M Duxbury. Comparison of connectivity and rigidity percolation. In *Rigidity Theory and Applications*, pages 69–79. Springer, 2002.

[52] C. P. Broedersz and F. C. MacKintosh. Modeling semiflexible polymer networks. *Rev. Mod. Phys.*, 86(3):995–1036, July 2014. URL `http://link.aps.org/doi/10.1103/RevModPhys.86.995`.

[53] Shlomo Alexander. Amorphous solids: their structure, lattice dynamics and elasticity. *Physics Reports*, 296(2–4):65–236, 1998. doi: 10.1016/S0370-1573(97)00069-0.

[54] D. J. Durian. Bubble-scale model of foam mechanics: Melting, nonlinear behavior, and avalanches. *Phys. Rev. E*, 55(2):1739–1751, Feb 1997. doi: 10.1103/PhysRevE.55.1739.

[55] Shechao Feng and Pabitra N. Sen. Percolation on elastic networks: New exponent and threshold. *Phys. Rev. Lett.*, 52(3):216–219, Jan 1984. doi: 10.1103/PhysRevLett.52.216.

[56] Shechao Feng, M. F. Thorpe, and E. Garboczi. Effective-medium theory of percolation on central-force elastic networks. *Phys. Rev. B*, 31(1):276–280, January 1985. URL `http://link.aps.org/doi/10.1103/PhysRevB.31.276`.

[57] Muhammad Sahimi. Non-linear and non-local transport processes in heterogeneous media: from long-range correlated percolation to fracture and materials breakdown. *Physics Reports*, 306(4–6):213–395, December 1998. ISSN 0370-1573. URL `http://www.sciencedirect.com/science/article/pii/S0370157398000246`.

[58] Corey S. O'Hern, Leonardo E. Silbert, Andrea J. Liu, and Sidney R. Nagel. Jamming at zero temperature and zero applied stress: The epitome of disorder. *Phys. Rev. E*, 68(1):011306, Jul 2003. doi: 10.1103/PhysRevE.68.011306.

[59] M van Hecke. Jamming of soft particles: geometry, mechanics, scaling and isostaticity. *J. Phys.: Condens. Matter*, 22(3):033101–, 2010. ISSN 0953-8984.

[60] Andrea J. Liu and Sidney R. Nagel. The jamming transition and the marginally jammed solid. *Annu. Rev. Condens. Matter Phys.*, 1(1):347–369, July 2010. ISSN 1947-5454. doi: 10.1146/annurev-conmatphys-070909-104045. URL `http://dx.doi.org/10.1146/annurev-conmatphys-070909-104045`.

[61] Carl P. Goodrich, Simon Dagois-Bohy, Brian P. Tighe, Martin van Hecke, Andrea J. Liu, and Sidney R. Nagel. Jamming in finite systems: Stability, anisotropy, fluctuations, and scaling. *Phys. Rev. E*, 90(2):022138–, August 2014.

[62] Matthieu Wyart. On the rigidity of amorphous solids. *Ann. Phys. Fr.*, 30, No. 3:1–96, 2005. doi: 10.1051/anphys:2006003.

[63] M. Wyart, H. Liang, A. Kabla, and L. Mahadevan. Elasticity of floppy and stiff random networks. *Phys. Rev. Lett.*, 101(21):215501, 2008. doi: 10.1103/PhysRevLett.101.215501.

[64] Cristian F. Moukarzel. Isostatic phase transition and instability in stiff granular materials. *Phys. Rev. Lett.*, 81(8):1634–1637, August 1998. URL `http://link.aps.org/doi/10.1103/PhysRevLett.81.1634`.

[65] Alexei V. Tkachenko and Thomas A. Witten. Stress propagation through frictionless granular material. *Phys. Rev. E*, 60(1):687–696, Jul 1999. doi: 10.1103/PhysRevE.60.687.

[66] Simon Dagois-Bohy, Brian P. Tighe, Johannes Simon, Silke Henkes, and Martin van Hecke. Soft-sphere packings at finite pressure but unstable to shear. *Phys. Rev. Lett.*, 109(9):095703–, August 2012.

[67] Carl P. Goodrich, Andrea J. Liu, and Sidney R. Nagel. Finite-size scaling at the jamming transition. *Phys. Rev. Lett.*, 109(9):095704–, August 2012.

[68] C.R. Calladine. Buckminster fuller's "tensegrity" structures and clerk maxwell's rules for the construction of stiff frames. *International Journal of Solids and Structures*, 14(2):161–172, 1978. ISSN 0020-7683.

[69] M.F Thorpe, D.J Jacobs, M.V Chubynsky, and J.C Phillips. Self-organization in network glasses. *J. Non-Cryst. Solids*, 266-–269, Part 2(0):859–866, May 2000. ISSN 0022-3093.

[70] Matthieu Wyart, Leonardo E. Silbert, Sidney R. Nagel, and Thomas A. Witten. Effects of compression on the vibrational modes of marginally jammed solids. *Phys. Rev. E*, 72(5):051306, 2005. doi: 10.1103/PhysRevE.72.051306.

[71] Matthieu Wyart, Sidney R Nagel, and Thomas A Witten. Geometric origin of excess low-frequency vibrational modes in weakly connected amorphous solids. *EPL (Europhysics Letters)*, 72(3):486, 2005.

[72] Carl P Goodrich, Wouter G Ellenbroek, and Andrea J Liu. Stability of jammed packings i: the rigidity length scale. *Soft Matter*, 9(46):10993–10999, 2013.

[73] Silke Henkes, Kostya Shundyak, Wim van Saarloos, and Martin van Hecke. Local contact numbers in two-dimensional packings of frictional disks. *Soft Matter*, 6(13):2935–2938, 2010.

[74] F. Leonforte, A. Tanguy, J. P. Wittmer, and J.-L. Barrat. Continuum limit of amorphous elastic bodies II: Linear response to a point source force. *Phys. Rev. B*, 70:014203, 2004.

[75] Wouter G. Ellenbroek, Ellak Somfai, Martin van Hecke, and Wim van Saarloos. Critical scaling in linear response of frictionless granular packings near jamming. *Phys. Rev. Lett.*, 97(25):258001, 2006.

[76] Wouter G. Ellenbroek, Martin van Hecke, and Wim van Saarloos. Jammed frictionless disks: Connecting local and global response. *Phys. Rev. E*, 80(6):061307–, December 2009. URL `http://link.aps.org/doi/10.1103/PhysRevE.80.061307`.

[77] Olaf Stenull and T. C. Lubensky. Penrose tilings as jammed solids. *Phys. Rev. Lett.*, 113(15):158301–, October 2014. URL `http://link.aps.org/doi/10.1103/PhysRevLett.113.158301`.

[78] B. Florijn and M. van Hecke. unpublished.

[79] Le Yan and Matthieu Wyart. Evolution of covalent networks under cooling: Contrasting the rigidity window and jamming scenarios. *Physical review letters*, 113(21):215504, 2014.

[80] Jorge H. Lopez, L. Cao, and J. M. Schwarz. Jamming graphs: A local approach to global mechanical rigidity. *Phys. Rev. E*, 88(6):062130–, Dec 2013. ISSN 1550-2376. doi: 10.1103/physreve.88.062130.

[81] Chase P. Broedersz, Xiaoming Mao, Tom C. Lubensky, and Frederick C. MacKintosh. Criticality and isostaticity in fibre networks. *Nature Phys.*, 7(12):983–988, December 2011. ISSN 1745-2473. URL `http://dx.doi.org/10.1038/nphys2127`.

[82] Kai Sun, Anton Souslov, Xiaoming Mao, and T. C. Lubensky. Surface phonons, elastic response, and conformal invariance in twisted kagome lattices. *Proc. Natl. Acad. Sci. U.S.A.*, 109(31):12369–12374, July 2012.

[83] Xiaoming Mao, Olaf Stenull, and T. C. Lubensky. Elasticity of a filamentous kagome lattice. *Phys. Rev. E*, 87(4):042602–, April 2013. URL `http://link.aps.org/doi/10.1103/PhysRevE.87.042602`.

[84] Leyou Zhang, D Zeb Rocklin, Bryan Gin-ge Chen, and Xiaoming Mao. Rigidity percolation by next-nearest-neighbor bonds on generic and regular isostatic lattices. *Physical Review E*, 91(3):032124, 2015.

[85] Carl P Goodrich, Andrea J Liu, and Sidney R Nagel. The principle of independent bond-level response: Tuning by pruning to exploit disorder for global behavior. *Physical review letters*, 114(22):225501, 2015.

[86] M Van Hecke. Jamming of soft particles: geometry, mechanics, scaling and isostaticity. *Journal of Physics: Condensed Matter*, 22(3):033101, 2009.

[87] F Bolton and D Weaire. Rigidity loss transition in a disordered 2d froth. *Physical review letters*, 65(27):3449, 1990.

[88] James G Puckett, Frédéric Lechenault, and Karen E Daniels. Local origins of volume fraction fluctuations in dense granular materials. *Physical Review E*, 83 (4):041301, 2011.

[89] Carolina Brito and Matthieu Wyart. On the rigidity of a hard-sphere glass near random close packing. *EPL (Europhysics Letters)*, 76(1):149, 2006.

[90] Etienne Guyon, Stéphane Roux, Alex Hansen, D Bideau, J-P Troadec, and H Crapo. Non-local and non-linear problems in the mechanics of disordered systems: application to granular media and rigidity problems. *Reports on Progress in Physics*, 53(4):373, 1990.

[91] Gerard Laman. On graphs and rigidity of plane skeletal structures. *Journal of Engineering mathematics*, 4(4):331–340, 1970.

[92] Louis Theran, Anthony Nixon, Elissa Ross, Mahdi Sadjadi, Brigitte Servatius, and Michael F Thorpe. Anchored boundary conditions for locally isostatic networks. *Physical Review E*, 92(5):053306, 2015.

[93] Corey S. O'Hern, Stephen A. Langer, Andrea J. Liu, and Sidney R. Nagel. Random Packings of Frictionless Particles. *Physical Review Letters*, 88(7): 075507, January 2002. doi: 10.1103/PhysRevLett.88.075507. URL `https://link.aps.org/doi/10.1103/PhysRevLett.88.075507`.

[94] Aleksandar Donev, Salvatore Torquato, and Frank H. Stillinger. Pair correlation function characteristics of nearly jammed disordered and ordered hard-sphere packings. *Physical Review E*, 71(1):011105, January 2005. doi: 10.1103/PhysRevE.71.011105. URL `https://link.aps.org/doi/10.1103/PhysRevE.71.011105`.

[95] Andrea J Liu and Sidney R Nagel. The jamming transition and the marginally jammed solid. *Annu. Rev. Condens. Matter Phys.*, 1(1):347–369, 2010.

[96] S. Torquato and Y. Jiao. Robust algorithm to generate a diverse class of dense disordered and ordered sphere packings via linear programming. *Physical Review E*, 82(6):061302, December 2010. doi: 10.1103/PhysRevE.82.061302. URL `https://link.aps.org/doi/10.1103/PhysRevE.82.061302`.

[97] Carl P. Goodrich, Andrea J. Liu, and Sidney R. Nagel. Finite-Size Scaling at the Jamming Transition. *Physical Review Letters*, 109(9):095704, August 2012. doi: 10.1103/PhysRevLett.109.095704. URL https://link.aps.org/doi/10.1103/PhysRevLett.109.095704.

[98] Edan Lerner, Gustavo Düring, and Matthieu Wyart. Low-energy non-linear excitations in sphere packings. *Soft Matter*, 9(34):8252–8263, August 2013. ISSN 1744-6848. doi: 10.1039/C3SM50515D. URL http://pubs.rsc.org/en/content/articlelanding/2013/sm/c3sm50515d.

[99] Robert Connelly, Evan Solomonides, and Maria Yampolskaya. The isostatic conjecture. *arXiv preprint arXiv:1702.08442*, 2017.

[100] Patrick Charbonneau, Eric I. Corwin, Giorgio Parisi, and Francesco Zamponi. Universal Microstructure and Mechanical Stability of Jammed Packings. *Physical Review Letters*, 109(20):205501, November 2012. doi: 10.1103/PhysRevLett.109.205501. URL https://link.aps.org/doi/10.1103/PhysRevLett.109.205501.

[101] Peter K. Morse and Eric I. Corwin. Geometric Signatures of Jamming in the Mechanical Vacuum. *Physical Review Letters*, 112(11):115701, March 2014. doi: 10.1103/PhysRevLett.112.115701. URL https://link.aps.org/doi/10.1103/PhysRevLett.112.115701.

[102] Patrick Charbonneau, Eric I. Corwin, Giorgio Parisi, and Francesco Zamponi. Jamming Criticality Revealed by Removing Localized Buckling Excitations. *Physical Review Letters*, 114(12):125504, March 2015. doi: 10.1103/PhysRevLett.114.125504. URL https://link.aps.org/doi/10.1103/PhysRevLett.114.125504.

[103] Leonardo E Silbert, Andrea J Liu, and Sidney R Nagel. Vibrations and diverging length scales near the unjamming transition. *Physical review letters*, 95(9):098301, 2005.

[104] Robert Bridson. Fast poisson disk sampling in arbitrary dimensions. In *SIGGRAPH sketches*, page 22, 2007.

[105] Daniel Dunbar and Greg Humphreys. A spatial data structure for fast poisson-disk sample generation. In *ACM Transactions on Graphics (TOG)*, volume 25, pages 503–508. ACM, 2006.

[106] Der-Tsai Lee and Bruce J Schachter. Two algorithms for constructing a delaunay triangulation. *International Journal of Computer & Information Sciences*, 9(3):219–242, 1980.

[107] Daniel Hexner, Andrea J Liu, and Sidney R Nagel. Role of local response in manipulating the elastic properties of disordered solids by bond removal. *Soft matter*, 2018.

[108] Daniel Hexner, Andrea J Liu, and Sidney R Nagel. Linking microscopic and macroscopic response in disordered solids. *arXiv preprint arXiv:1706.06153*, 2017.

[109] JWS Lord Rayleigh. The theory of sound, vol. 1, 1945.

[110] Corey S O'hern, Leonardo E Silbert, Andrea J Liu, and Sidney R Nagel. Jamming at zero temperature and zero applied stress: The epitome of disorder. *Physical Review E*, 68(1):011306, 2003.

[111] Jorge H Lopez, L Cao, and JM Schwarz. Jamming graphs: A local approach to global mechanical rigidity. *Physical Review E*, 88(6):062130, 2013.

[112] William Thurston. *The Geometry and Topology of 3-Manifolds*. Princeton University Notes. preprint.

[113] William Thurston. The finite Riemann mapping theorem, 1985. Invited talk, An International Symposium at Purdue University in celebrations of de Branges' proof of the Bieberbach conjecture, March 1985.

[114] Kenneth Stephenson. *Introduction to Circle Packing: the Theory of Discrete Analytic Functions*. Camb. Univ. Press, New York, 2005. (ISBN 0-521-82356-0, QA640.7.S74).

[115] Kenneth Stephenson. `CirclePack` software, 1992–. http://www.circlepack.com/software.html.

[116] Alan F. Beardon and Kenneth Stephenson. The uniformization theorem for circle packings. *Indiana Univ. Math. J.*, 39:1383–1425, 1990.

[117] Erik Bitzek, Pekka Koskinen, Franz Gähler, Michael Moseler, and Peter Gumbsch. Structural Relaxation Made Simple. *Physical Review Letters*, 97(17): 170201, October 2006. doi: 10.1103/PhysRevLett.97.170201. URL `https://link.aps.org/doi/10.1103/PhysRevLett.97.170201`.

[118] Ling Zhang, Jie Zheng, Yinqiao Wang, Lei Zhang, Zhaohui Jin, Liang Hong, Yujie Wang, and Jie Zhang. Experimental studies of vibrational modes in a two-dimensional amorphous solid. *Nature communications*, 8(1):67, 2017.

[119] Patrick Charbonneau, Eric I Corwin, Giorgio Parisi, Alexis Poncet, and Francesco Zamponi. Universal non-debye scaling in the density of states of amorphous solids. *Physical review letters*, 117(4):045503, 2016.

[120] Silvio Franz and Giorgio Parisi. The simplest model of jamming. *Journal of Physics A: Mathematical and Theoretical*, 49(14):145001, 2016.

[121] Graeme W Milton. Composite materials with poisson's ratios close to -1. *Journal of the Mechanics and Physics of Solids*, 40(5):1105–1137, 1992.

[122] Jean Salençon. *Handbook of continuum mechanics: General concepts thermoelasticity*. Springer Science & Business Media, 2012.

[123] G Neville Greaves. Poisson's ratio over two centuries: challenging hypotheses. *Notes Rec. R. Soc.*, 67(1):37–58, 2013.

[124] Yunan Prawoto. Seeing auxetic materials from the mechanics point of view: a structural review on the negative poisson's ratio. *Computational Materials Science*, 58:140–153, 2012.

[125] Adhémar Jean Claude Barré de Saint et al. *Résumé des leçons données à École des ponts et chaussées sur l'application de la mécanique à l'établissement des constructions et des machines...*, volume 1. Dunod, 1864.

[126] Augustus Edward Hough Love. *A treatise on the mathematical theory of elasticity*. Cambridge university press, 2013.

[127] Lorna J Gibson, Michael Farries Ashby, GS Schajer, and CI Robertson. The mechanics of two-dimensional cellular materials. *Proc. R. Soc. Lond. A*, 382 (1782):25–42, 1982.

[128] Roderic Lakes. Foam structures with a negative poisson's ratio. *Science*, 235: 1038–1041, 1987.

[129] Stephen Burns. Negative poisson's ratio materials. *Science*, 238(4826):551–551, 1987.

[130] BD Caddock and KE Evans. Microporous materials with negative poisson's ratios. i. microstructure and mechanical properties. *Journal of Physics D: Applied Physics*, 22(12):1877, 1989.

[131] KE Evans. The design of doubly curved sandwich panels with honeycomb cores. *Composite Structures*, 17(2):95–111, 1991.

[132] KL Alderson and KE Evans. The fabrication of microporous polyethylene having a negative poisson's ratio. *Polymer*, 33(20):4435–4438, 1992.

[133] KL Alderson, AP Pickles, PJ Neale, and KE Evans. Auxetic polyethylene: the effect of a negative poisson's ratio on hardness. *Acta Metallurgica et Materialia*, 42(7):2261–2266, 1994.

[134] Wei Yang, Zhong-Ming Li, Wei Shi, Bang-Hu Xie, and Ming-Bo Yang. Review on auxetic materials. *Journal of materials science*, 39(10):3269–3279, 2004.

[135] Thomas L Warren. Negative poisson's ratio in a transversely isotropic foam structure. *Journal of applied physics*, 67(12):7591–7594, 1990.

[136] JB Choi and RS Lakes. Nonlinear analysis of the poisson's ratio of negative poisson's ratio foams. *Journal of Composite Materials*, 29(1):113–128, 1995.

[137] Kenneth E Evans, MA Nkansah, and IJ Hutchinson. Auxetic foams: modelling negative poisson's ratios. *Acta metallurgica et materialia*, 42(4):1289–1294, 1994.

[138] N Chan and KE Evans. Fabrication methods for auxetic foams. *Journal of Materials Science*, 32(22):5945–5953, 1997.

[139] Lorna J Gibson and Michael F Ashby. *Cellular solids: structure and properties*. Cambridge university press, 1999.

[140] Chris W Smith, JN Grima, and KenE Evans. A novel mechanism for generating auxetic behaviour in reticulated foams: missing rib foam model. *Acta materialia*, 48(17):4349–4356, 2000.

[141] Joseph N Grima, Ruben Gatt, Naveen Ravirala, Andrew Alderson, and Kenneth E Evans. Negative poisson's ratios in cellular foam materials. *Materials Science and Engineering: A*, 423(1-2):214–218, 2006.

[142] D Prall and RS Lakes. Properties of a chiral honeycomb with a poisson's ratio of -1. *International Journal of Mechanical Sciences*, 39(3):305–314, 1997.

[143] Kenneth E Evans, MA Nkansah, IJ Hutchinson, and SC Rogers. Molecular network design. *Nature*, 353(6340):124, 1991.

[144] Nitin R Keskar and James R Chelikowsky. Negative poisson ratios in crystalline sio2 from first-principles calculations. *Nature*, 358(6383):222, 1992.

[145] Ray H Baughman and Douglas S Galvão. Crystalline networks with unusual predicted mechanical and thermal properties. *Nature*, 365(6448):735, 1993.

[146] Joseph N Grima and Kenneth E Evans. Auxetic behavior from rotating triangles. *Journal of materials science*, 41(10):3193–3196, 2006.

[147] Raphael Blumenfeld and Sam F Edwards. Theory of strains in auxetic materials. *Journal of superconductivity and novel magnetism*, 25(3):565–571, 2012.

[148] Luigi Cabras and Michele Brun. Auxetic two-dimensional lattices with poisson's ratio arbitrarily close to- 1. In *Proceedings of the Royal Society of London A: Mathematical, Physical and Engineering Sciences*, volume 470, page 20140538. The Royal Society, 2014.

[149] Maryam Hanifpour, Charlotte F Petersen, Mikko J Alava, and Stefano Zapperi. Mechanics of disordered auxetic metamaterials. *arXiv preprint arXiv:1704.00943*, 2017.

[150] Daniel R Reid, Nidhi Pashine, Justin M Wozniak, Heinrich M Jaeger, Andrea J Liu, Sidney R Nagel, and Juan J de Pablo. Auxetic metamaterials from disordered networks. *Proceedings of the National Academy of Sciences*, page 201717442, 2018.

[151] AP Pickles, RS Webber, KL Alderson, PJ Neale, and KE Evans. The effect of the processing parameters on the fabrication of auxetic polyethylene. *Journal of materials science*, 30(16):4059–4068, 1995.

[152] AP Pickles, KL Alderson, and KE Evans. The effects of powder morphology on the processing of auxetic polypropylene (pp of negative poisson's ratio). *Polymer Engineering & Science*, 36(5):636–642, 1996.

[153] KL Alderson, A Alderson, and KE Evans. The interpretation of the strain-dependent poisson's ratio in auxetic polyethylene. *The Journal of Strain Analysis for Engineering Design*, 32(3):201–212, 1997.

[154] PJ Hine, RA Duckett, and IM Ward. Modelling the elastic properties of fibre-reinforced composites: Ii theoretical predictions. *Composites science and technology*, 49(1):13–21, 1993.

[155] Naveen Ravirala, Kim L Alderson, Philip J Davies, Virginia R Simkins, and Andrew Alderson. Negative poisson's ratio polyester fibers. *Textile research journal*, 76(7):540–546, 2006.

[156] Ciprian Borcea and Ileana Streinu. Geometric auxetics. *Proc. R. Soc. A*, 471 (2184):20150033, 2015.

[157] Ciprian S Borcea and Ileana Streinu. Periodic auxetics: structure and design. *The Quarterly Journal of Mechanics and Applied Mathematics*, 71(2):125–138, 2017.

[158] Kai Sun, Anton Souslov, Xiaoming Mao, and TC Lubensky. Surface phonons, elastic response, and conformal invariance in twisted kagome lattices. *Proceedings of the National Academy of Sciences*, 109(31):12369–12374, 2012.

[159] Roderic Lakes. Advances in negative poisson's ratio materials. *Advanced Materials*, 5(4):293–296, 1993.

[160] Wouter G Ellenbroek, Zorana Zeravcic, Wim van Saarloos, and Martin van Hecke. Non-affine response: Jammed packings vs. spring networks. *EPL (Europhysics Letters)*, 87(3):34004, 2009.

[161] Jason W Rocks, Nidhi Pashine, Irmgard Bischofberger, Carl P Goodrich, Andrea J Liu, and Sidney R Nagel. Designing allostery-inspired response in mechanical networks. *Proceedings of the National Academy of Sciences*, 114(10): 2520–2525, 2017.

[162] Shechao Feng, MF Thorpe, and E Garboczi. Effective-medium theory of percolation on central-force elastic networks. *Physical Review B*, 31(1):276, 1985.

[163] Mahdi Sadjadi, Bishal Bhattarai, DA Drabold, MF Thorpe, and Mark Wilson. Refining glass structure in two dimensions. *Physical Review B*, 96(20):201405, 2017.

APPENDIX A

COMPUTATIONAL TOOLS

Numerical methods and techniques have been integrated into research in theoretical physics over the past few decades. In the course of my doctoral work, I have extensively used computational tools and have developed many softwares that can be used to reproduce the results reported in this dissertation. Most of the programs used in this dissertation are written in `Python` because of its flexibility and great collection of open source packages such as `Numpy` and `Scipy` which are nowadays fundamental for scientific computing with `Python`.

A.1 Rigidpy

Since this dissertation is written on the rigidity of disordered networks, many of the used programs share the same structure where a framework is built using the connectivity table and coordinates of the vertexes, and then the rigidity and dynamical matrices are calculated. To integrate all the small scripts together, my colleague Mahdi Sadjadi and I have developed a `Python` package named `Rigidpy` that provides a convenient application program interface to study the rigidity and linear response of networks with periodic boundary conditions. The program can be modified to apply to any kind of desired boundary conditions. It is written a generic spatial dimension d with $d = 2$ in the dissertation. The package uses many of the built-in functions in `Numpy`, `Scipy`, and `Networkx`. It is open source and available at `https://github.com/vfaghirh/rigidpy`. The main components of this package include:

1. **Framework rigidity**: A framework is the set of coordinates and connectivity table of a graph. A framework is created by `Rigidpy` using two input files that include the coordinates of N points in pairs $\{x, y\}$:

```
0.67534     0.08986
```

```
0.04657     0.00345
0.11090     0.86786
0.00398     0.03711
...
```

and list of contacts in pairs $\{p_1, p_2\}$ representing points (labeled from 0 to $N-1$) that are mutually in contact. The edge list has the form:

```
0 1
0 2
2 5
3 8
...
```

Once the framework is created, this submodule uses the two repeat vectors $\{a_1, a_2\}$ to calculate the rigidity matrix, the stress matrix, Hessian matrix, dynamical matrix, and the eigenvalues and eigenvectors of dynamical matrix.

2. **Geometrical optimization**: This submodule finds the closest local energy minimum for a given set of edge lengths by optimizing the graph geometry using a conjugate gradient algorithm.

3. **Modulus**: This submodule uses the built framework to calculate the bulk and shear moduli of the network. The inputs include the coordinates of the graph vertexes, the edge list, and the lattice repeat vectors. The lattice vectors are multiplied by appropriate strains and the changes in the lengths of the edges are calculated. Then the moduli are calculated using methods introduced in Chapter one.